UNIVERSITÀ DELLA CALABRIA

Dipartimento di CHIMICA

School "BERNARDINO TELESIO"

Department of Chemistry
Department of Physics

UNIVERSITY OF CALABRIA

DEPARTMENT OF CHEMISTRY

BERNARDINO TELESIO – DOCTORATE SCHOOL OF SCIENCE AND TECHNIQUE

CURRICULUM: MESOPHASES AND MOLECULAR MATERIALS (CHIM-02)

XXV CYCLE

NOVEL ORGANIC OPTOELECTRONIC MATERIALS

Submitted in partial fulfillment of requirements for the Degree of Doctor of Philosophy in Science and Technique.

Supervisor
Dr. Bruna Clara De Simone

Coordinator
Prof. Carlo VERSACE

Chairman
Prof. Roberto BARTOLINO

Candidate
Dr. Sante COSPITO

Academic Year 2011/2012

To My Family

ABSTRACT

Il presente lavoro di Tesi di Dottorato di Ricerca (Scuola di Dottorato in Scienza e Tecnica "Bernardino Telesio") dal titolo "*Novel Organic Optoelectronic Materials*" è stato svolto all'interno dei laboratori di "Organic Optoelectronic Materials" e "New Syntheses via Organometallic Catalysis" del Dipartimento di Chimica dell'Università della Calabria.

Nuovi semiconduttori organici potenzialmente impiegabili in dispositivi optoelettronici quali OLEDs, celle solari, transitors ed elettrocromici sono state progettate, sintetizzate e caratterizzate.

La prima parte del lavoro ha riguardato la sintesi e la caratterizzazione di derivati di triarilammine, molecole elettron-donatrici (anodiche), da impiegare in dispositivi elettrocromici ("smart windows") per l'attenuazione della radiazione solare nel vicino infrarosso (NIR). L'intensa ed estesa banda di assorbimento nel NIR prodotta delle specie mono-ossidate ha suggerito l'impiego di queste triarilammine in dispositivi "complementari" in cui vengono utilizzate insieme a molecole elettron-accetrici (catodiche) elettrocromiche nel visibile, per un'ampia modulazione dello spettro solare. Tali sistemi sono stati dispersi all'interno di matrici polimeriche al fine di realizzare dei gel elettrocromici le cui prestazioni sono state ampiamente studiate. La risposta elettrocromica del gel è stata inoltre provata in un dispositivo plastico, dimostrandone le potenziali applicazioni campo dell'elettronica flessibile.

La seconda parte del lavoro invece, ha riguardato la sintesi e lo studio delle proprietà di cristalli liquidi semiconduttori di tipo "n" (elettron-accetori) da impiegare in celle solari organiche "bulk heterojunction". Tali molecole, appartenenti alla famiglia dei viologeni estesi, hanno mostrato interessantissime proprietà mesomorfiche fortemente influenzate dalla lunghezza delle catene alchiliche (a 9, 10 e 11 atomi di carbonio) e dell'anione utilizzato, la bis(triflimmide). Le proprietà elettrochimiche di questi composti sono state investigate sia in soluzione che nelle mesofasi. Un'efficace elettrocromismo dovuta (*i*) al doppio strato elettrico creato all'elettrodo degli anioni presenti e (*ii*)

all'elevata sovrapposizione degli orbitali di frontiera dell'esteso sistema π-coniugato è stato osservato nelle fasi colonnari e smettiche in cui le molecole si sono auto-assemblate.

Infine, le proprietà elettrocromiche di questi composti sono state studiate all'interno di film plastici utilizzabili in dispositivi quali i displays.

ACKNOWLADGMENTS

I sincerely thank to my supervisors, Dr. Bruna Clara De Simone for providing both general and technical advice, direction and support throughout the course of my thesis. I will always remember with great pleasure the long time that we spent together during my experiments.

I am very grateful to my colleague and friend Dr. Amerigo Beneduci. He worked with me during the last part of my PhD project, with joy and enthusiasm

that were contagious and motivational for me.

For her contribution to my interest in electrochemical methods, I thank Dr. Daniela Imbardelli.

The studies on the thienoviologen liquid crystals discussed in this dissertation would not have been possible without the compounds synthesized by Dr. Lucia Veltri. Moreover, under her superivision I synthesized my first organic semiconductor molecule. I am also grateful to Prof. Giuseppe Salerno for welcoming me to his Lab and for his kind advise during my experience as Organic Chemist.

Finally, I would like to extend my deepest gratitude to Prof. Giuseppe Chidichimo. I appreciate all his contributions of time, ideas, and funding to make my Ph.D. experience productive and stimulating.

PUBLICATIONS

1. B. C. De Simone, A. Quartarolo, S. Cospito, L. Veltri, G. Chidichimo, N. Russo, "Theoretical and experimental investigation on the near-infraredand UV–vis spectral regions of a newly synthesized triarylamine electrochromic system". *Theoretical Chemistry Accounts*, 2012, Vol. 131, pp. 1225-1228.

2. M. E. Alberto, B. C. De Simone, S. Cospito, D. Imbardelli, L. Veltri, G. Chidichimo, N. Russo, "Experimental and Theoretical Characterization of a New Synthesized Extended Viologen", *Chemical Physics Letters*, 2012, Vol. 552, pp. 141-145.

3. S. Cospito, B. C. De Simone, D. Imbardelli, A. Beneduci, G. Chidichimo, "Visible and near-infrared electrochromic devices containing triphenylamine derivatives", submitted to *Materials Chemistry and Physics*.

4. S. Cospito, B. C. De Simone, D. Imbardelli, A. Beneduci, G. Chidichimo, "Plastic electrochromic film with high optical contrast in the visible and near-infrared light regions", submitted to *Materials Letters*.

CONTENTS

ABSTRACT i

ACKNOWLEDGEMENTS iii

PUBLICATIONS iv

INTRODUCTION 1

CHAPTER 1

OPTOELECTRONIC MATERIALS

1.1. Introduction 4

1.2. Electrochromism 5

1.2.1. Electrochromic Contrast 5

1.2.2. Coloration Efficiency 6

1.2.3. Switching Speed 6

1.2.4. Stability 7

1.2.5. Optical Memory 7

1.3. Organic Electrochromic Materials 8

1.3.1. Triarylamine derivatives 8

1.3.2 Viologens and Extended Viologens 13

1.4. Semiconducting Liquid Crystals 16

1.4.1. Electrochromic Liquid Crystals 22

1.4.2. Viologen Liquid Crystals 24

CHAPTER 2

Near-infrared electrochromic materials based on Triarylamine moieties

2.1. Introduction 27

2.2. Experimental and theoretical details 28
2.2.1. Materials 28
2.2.2. Synthesis 28
2.2.3. Methods 31
2.2.4. Computational details 32
2.3. Results and discussion 33
2.3.1. Electrochemistry 33
2.3.2. Spectroelectrochemistry and Theoretical studies 35
2.4. Conclusions 41

CHAPTER 3

Visible and Near-Infrared Electrochromic Devices containing Triphenylamine derivatives

3.1. Introduction 43
3.2. Experimental 44
3.2.1. Materials 44
3.2.2. Methods 44
3.3. Results and discussion 45
3.3.1. Solution-phase electrochromic devices 45
3.3.2. Electrochromic gel 49
3.4. Conclusions 52

CHAPTER 4

Structural characterization of new thienoviologen mesogens

4.1. Introduction 54
4.2. Experimental 55
4.2.1. Materials 55
4.2.2. Methods 58
4.3. Results and discussion 59

4.4. Conclusions 67

CHAPTER 5

Redox and spectroscopic properties of the thienoviologen mesogens

5.1. Introduction 68

5.2. Experimental and theoretical details 69

5.2.1. Materials 69

5.2.2. Methods 69

5.2.3. Computational details 71

5.3. Results and discussion 72

5.3.1. Redox and spectroelectrochemical properties in solution state 72

5.3.2. Redox and spectroscopic properties in the bulk state 76

5.4. Conclusions 80

CHAPTER 6

Novel electrochromic plastic film containing a thienoviologen derivative

6.1. Introduction 81

6.2. Experimental 82

6.2.1. Materials 82

6.2.2. Methods 82

6.3. Results and discussion 83

6.3.1. Cyclic voltammetry 83

6.3.2. Spectroelectrochromic behavior 84

6.3.3. Electrochromic switching studies 85

6.4. Conclusions 87

SUMMARY AND OUTLOOK 88

REFERENCES 92

INTRODUCTION

Organic optoelectronic materials have attracted particular attention since the discovery of conducting polymers in the 1970s [1]. Conceptually, organic materials allow chemical engineering of optoelectronic properties by molecular design, taking advantage of low cost, flexibility, low temperature processing and roll-to-roll large area producing ability. Moreover, organic optoelectronic devices exhibit high sensitivity to electrical and optical stimulus and can realize the integration of light detection, energy conversion and signal magnification, and hence have attracted the world's attention for decades [2]. The organic semiconducting materials used in electronic and optoelectronic devices are based on π-conjugated systems and generally are split into two groups: small molecules and polymers [3]. Compared to polymer materials, small molecules possess defined molecular structure and molecular weight for convenient synthesis and purification, which greatly improves the synthetic reproducibility as well as exhibiting a greater tendency to form ordered domains, affording higher charge carrier (holes and electrons) mobilities [4]. Charge transport in organic semiconductors typically, depends on the ability of the charge carriers to move from one molecule to another, which depends on the energy gap between highest occupied molecular orbital (HOMO) and lowest unoccupied molecular orbital (LUMO) levels. The physical properties (such as optical, charge carrier mobility, HOMO/LUMO energy levels, and structural ordering) of these organic semiconductors can be easily fine-tuned by various chemical functionalizations [5].

This thesis focuses on the synthesis, characterization and device exploitation of novel organic materials for optoelectronics. In particular, one aim of this thesis has been to explore the properties of compound based on triarylamine derivatives. These have attracted great interest for their good electron donating and hole-transporting capabilities that have made them widely applied in various electro-optical devices such as organic light emitting diodes (OLEDs) [6],

organic field-effect transistors [7] and more recently as dyes in organic solar cell [8,9].

The electrochromic (EC) properties of triarylamines with multiple redox centres, mainly arising from the intervalence charge transfer (IV-CT) bands produced by their radical cation species, have been widely investigated (see Chapter 1). Usually, these IV-CT bands are very intense and are centered in the near-infrared (NIR) region of the solar spectrum [10-15]. Thus, EC materials able to absorb in the NIR could be exploitable for thermal control devices, for this reason in the last years a great number of molecules [16,17] and polymers [18-22] based on triarylamine unit were designed and synthesized.

With the purpose to extend the solar control toward the NIR region, we synthesized and characterized the new triarylamine molecule *N*,*N'*-Bis(4-heptanoylamidophenyl)-*N*,*N'*-di(4-methoxyphenyl)-1,4-phenylendiamine (TPPAHM). Its electrochemical and spectroelectrochemical behavior has been studied either experimentally or theoretically (time-dependent–density functional theory, TD-DFT, spectral simulation) and has been compared with those of the unsubstituted analogue *N*,*N*,*N'*,*N'*-Tetraphenyl-1,4-phenylendiamine (TPPA) (Chapter 2). These two anodic NIR electroactive molecules were then used in complementary EC devices (ECDs). Highly transparent EC solutions composed of TPPA or TPPAHM coupled to an electron-acceptor molecule such as the ethyl viologen (EV) were prepared and fully characterized (Chapter 3). The most stable and performing system was then mixed with a thermoplastic polymeric matrix in order to prepare a gel-based ECD. Moreover, a flexible EC device was also assembled and its electrochromic response has been successfully achieved, thus showing the potentialities of this EC gel for a wide range of applications.

The second aim of this thesis has been focused on the synthesis and characterization of semiconducting liquid crystals with electron-acceptor character potentially useful for bulk heterojunction solar cells. This device architecture have attracted significant attention because p-type and n-type organic semiconductors form nanosegregated structures [23], allowing an easy control of the morphology of the photoactive layers [5]. However, most of liquid crystalline semiconductors studied up to now are of p-type [24]. Thus, with the aim to contribute significantly

to the advancement of efficient electron-transporting (n-type) materials, we designed and synthesized a new class of n-type semiconducting mesogens. Our strategies was to functionalize with flexible alkyl chains, the "rod-like" core of a strong electron-acceptor molecule such as the extended viologen.

The synthesis and the self-assembling nature (mesomorphism) of these compounds (thienoviologen mesogens) have been widely discussed in Chapter 4. Instead, Chapter 5 has been devoted to the investigation of the redox properties of these mesogens. A fast and reversible electrochromism in the liquid crystalline state of these compounds was demonstrated. The differences in the response times between the nanostructured phases in which the molecule self-organize can be explained by the difference in the electronic conduction *via* π-conjugated system.

Finally, in the Chapter 6 we have shown the potential applicability of these molecules in plastic films that could be used for display technologies.

CHAPTER 1

Organic Materials for Optolectronics

1.1. Introduction

Recently, the search for new materials has been greatly extended into the field of organic (semiconducting) molecules and polymers, which offer the advantage of wide chemical functionalities by which their optical, electrochemical, solubility, morphological, and electrical properties can be tuned [5]. Compared to classical inorganic semiconductors, organic materials offer facile solution processability into flexible films at low temperatures, which makes them attractive for novel electronic devices [25] (Fig. 1.1). New efficient and potentially low-cost methods for fabricating useful, and, in some cases, complicated structures that are inaccessible by conventional methods using conventional semiconductors, can be employed using organic compounds as active materials of electronic and optoelectronic devices [3].

Although the organic optoelectronic materials studied in this thesis (triarylamines and semiconducting liquid crystals) appear chemically very different, they are however unites by a particular property: the electrochromism. Thus, in this chapter we are going to discuss the fundamentals of this property and then we will talk about other related properties such as the electronic conduction in the ordered semiconducting materials.

Fig. 1.1. Flexible Electrochromic Display [167].

1.2. Electrochromism

Electrochromism is defined as a reversible change in color when a material is oxidized or reduced as a result of changes in the band-gap of the material [26]. This phenomenon was suggested theoretically by J. R. Platt [27] in 1961 and discovered by Deb in 1969 [28]. Many chemical species can be switched between redox states that have distinct electronic absorption spectra [29]. Such spectra arise from either a moderate energy internal electronic excitation or an intervalence optical charge transfer where the chemical species has two centers of differing valence or oxidation state [26, 29–38].

While materials are considered to be electrochromic (EC) when marked visible color changes are shown under illumination, recent interest in electrochromic devices (ECDs) for multispectral energy modulation by reflectance and absorbance has extended the definition [39]. Chemical species are now being studied for modulation of radiation in the near infrared (NIR) [34,35], thermal infrared [36], and microwave regions, and "color" can mean response of detectors to these electromagnetic regions, not just the human eye [40]. Before switching to a more detailed discussion of EC organic materials some of the important parameters in identifying and characterizing the electrochromic materials are outlined.

1.2.1. Electrochromic Contrast

Electrochromic contrast is probably the most important factor in evaluating an electrochromic material. It is often reported as a percent transmittance change (Δ%T) at a specified wavelength where the electrochromic material has the highest optical contrast.

For some applications, it is more useful to report a contrast over a specified range rather than a single wavelength. To obtain an overall electrochromic contrast, measuring the relative luminance change provides more realistic contrast values since it offers a perspective on the transmissivity of a

material as it relates to the human eye perception of transmittance over the entire visible spectrum [41,42]. The light source used is calibrated taking into account the sensitivity of the human eye to different wavelengths.

1.2.2. Coloration Efficiency

The coloration efficiency (also referred to as electrochromic efficiency) is a practical tool to measure the power requirements of an electrochromic material. In essence, it determines the amount of optical density change (ΔOD) induced as a function of the injected/ejected electronic charge (Q_d), i.e., the amount of charge necessary to produce the optical change. It is given by the equation

$$\eta = \frac{\Delta \mathrm{OD}}{Q_d} = \log\left[T_b/T_c\right]/Q_d$$

where η (cm^2/C) is the coloration efficiency at a given λ and T_b and T_c are the bleached and colored transmittance values, respectively. The relationship between η and the charge injected to the EC material can be used to evaluate the reaction coordinate of the coloration process, or the η values can be reported at a specific degree of coloration for practical purposes [43,44].

1.2.3. Switching Speed

Switching speed is often reported as the time required for the coloring/bleaching process of an EC material. It is important especially for applications such as dynamic displays and switchable mirrors. The switching speed of electrochromic materials is dependent on several factors such as the ionic conductivity of the electrolyte, accessibility of the ions to the electroactive sites (ion diffusion in thin films), magnitude of the applied potential, film thickness, and morphology of the thin film. Today subsecond switching rates are easily attained using polymers and composites containing small organic electrochromes [43,44].

1.2.4. Stability

Electrochromic stability is usually associated with electrochemical stability since the degradation of the active redox couple results in the loss of electrochromic contrast and hence the performance of the EC material. Common degradation paths include irreversible oxidation or reduction at extreme potentials, *iR* loss of the electrode or the electrolyte, side reactions due to the presence of water or oxygen in the cell, and heat release due to the resistive parts in the system. Although current reports include switching stabilities of up to 10^6 cycles without significance performance loss, the lack of durability (especially compared to LCDs) is still an important drawback for commercialization of ECDs. Defect-free processing of thin films, careful charge balance of the electroactive components, and air-free sealing of devices are important factors for long-term operation of ECDs [19].

1.2.5. Optical Memory

One of the benefits of using an EC material in a display as opposed to a light-emitting material is its optical memory (also called open-circuit memory), which is defined as the time the material retains its absorption state after the electric field is removed. In solution-based electrochromic systems such as viologens, the colored state quickly bleaches upon termination of current due to the diffusion of soluble electrochromes away from the electrodes (a phenomenon called self-erasing). In solid-state ECDs, where the electrochromes are adhered to electrodes, the electrochromic memory can be as long as days or weeks with no further current required. In reality, however, ECDs may require small refreshing charges to maintain the charge state because side reactions or short circuits change the desired color [43,44].

1.3. Organic Electrochromic Materials

Electrochromic organic materials can be classified in three main types in terms of their electronically accessible optical states. The first type includes materials with at least one colored and one bleached state. These materials are especially useful for absorption/transmission-type device applications such as smart windows and optical shutters. Typical examples of this area are viologens and polymers such as poly(3,4-ethylenedioxythiophene) (PEDOT). A second class of materials consists of electrochromes with two distinctive colored states. These EC materials lack a transmissive state but are useful for display-type applications where different colors are desired in different redox states. Polythiophene is a good example of this type, where the thin films of this polymer switch from red to blue upon oxidation. A third class includes the growing interest in the electrochromic field, where more than two color states are accessible depending on the redox state of the material. This is the area where conjugated polymers have found the most interest due to their versatility for making blends, laminates, and copolymers. Additionally, there are inherently multicolor EC polymers such as PANI or poly(3,4-propylenedioxypyrrole) (PProDOP) [43, 44].

In this work we studied the properties of some anodic and cathodic EC organic molecules. In particular, we focused our interest on triarylamine derivatives as anodic species, whereas viologens and extended viologens as cathodic molecules.

1.3.1. Triarylamine derivatives

The general interest in triarylamines stems from the fact that they are widely used not only as hole transport material in multilayer organic light-emitting diodes (OLEDs) [45] and as organic thin layer in a large variety of optoelectronics [46-48]. A series of triphenylamine molecules (Fig. 1.2) with varied oxidation potentials were synthesized by Yeh and coworkers [16] as active components for OLEDs and display, in order to evaluate the effects of electron-

donating groups (amino) and electron-withdrawing groups (nitro, cyano and carboxylic acid) on the electron moiety of *p*-phenylenediamine.

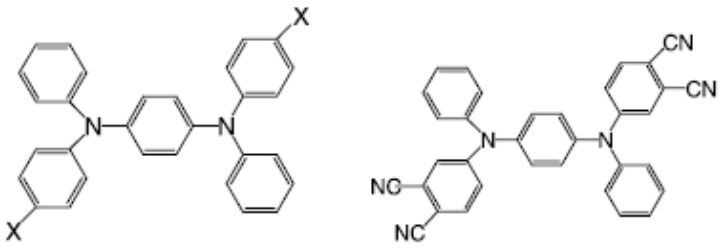

APD, X = NH_2

NPD, X = NO_2

CPD, X = CN

CAPD, X = COOH

DCPD

Fig. 1.2. Chemical structures of *p*-phenylendiamines [16].

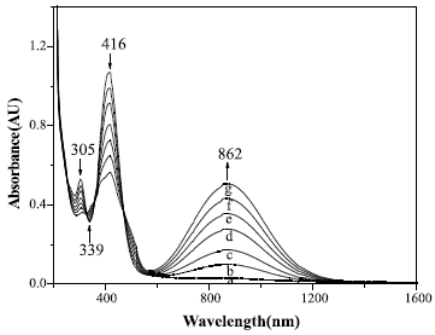

Fig. 1.3. Absorption spectral change of 1.91 x 10^{-4} M NPD in CH_2Cl_2 containing 0.1 M TBAP. E_{appl} =(a) 0.90 (b) 0.96 (c) 0.98 (d) 1.00 (e) 1.02 (f) 1.04 and (g) 1.10 V [16].

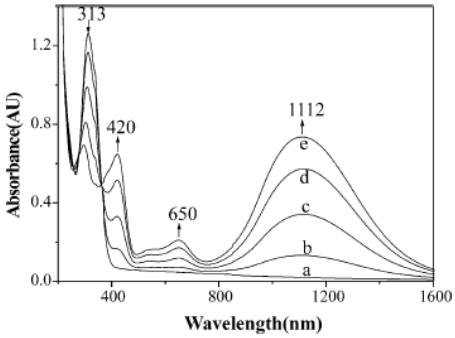

Fig. 1.4. Absorption spectral change of 3.01 x 10^{-4} M APD in CH_2Cl_2 containing 0.1 M TBAP. E_{appl} = (a) 0.20 (b) 0.36 (c) 0.40 (d) 0.44 and (e) 0.52 V [16].

In another work, Chiu et al. [17] designed the structurally isomeric *N*,*N*,*N'*,*N'*-tetraaryl-*p*-phenylenediamine derivatives (PDs) by introduction suitable substituents at the outer-phenyl positions (Fig. 1.5). They investigated the electrochemical and spectroscopic properties of the molecules in order to observe the substituent effects on the electronic structure and the molecular delocalization and thus clarify intramolecular electron transfer (ET) processes.

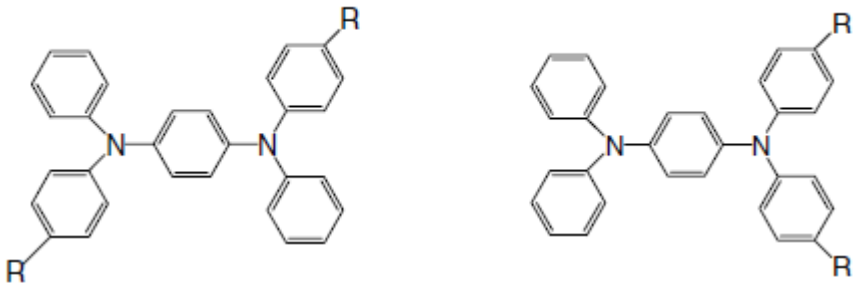

Series 1 PDs
NPD1, R = NO_2
CPD1, R = CN
MPD1, R = OCH_3
APD1, R = NH_2

Series 2 PDs
NPD2, R = NO_2
CPD2, R= CN
MPD2, R = OCH_3
APD2, R = NH_2

Fig. 1.5. Chemical structures of PDs [17].

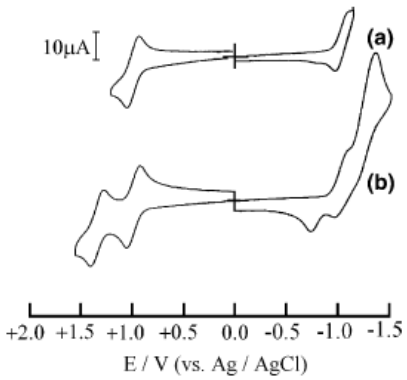

Fig. 1.6. Cyclic voltammogram of NPD2 in CH_2Cl_2 containing 0.1 M TBAP. Scan rate = 0.1 V/s [17]

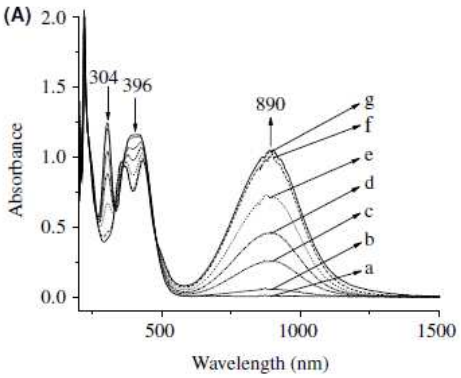

Fig. 1.7. Absorption spectral change of 1 x 10^{-3} M NPD2 in CH_2Cl_2 containing 0.1 M TBAP. E_{appl} =(a) 0.76 (b) 0.85 (c) 0.91 (d) 0.94 (e) 0.97 (f) 1.03 (g) 1.10 V [17].

The strong absorption band in the near-infrared (NIR) region of the solar spectrum, due to the radical cation species formed upon electrochemical oxidation was extensively studied [11-15]. Triarylamines are mixed-valence (MV) compounds and are extensively studied for the comprehension of the intramolecular ET [11]. For example, Nelsen and coworkers [49] studied a number of *p*-phenylenediamine cation radicals using both the time-dependent theory and spectroscopic measurements. The properties of MV systems depend

strongly on the extent of electronic interaction between the redox centers. In accordance with the Robin–Day classification [50], *N*,*N*,*N*′,*N*′-tetraphenyl-*p*-phenylenediamine (TPPA) cation radical has been proposed as a symmetrical delocalized class III structure with a strong electronic coupling (the electron is delocalized over the two redox centers) [15].

Because their significantly NIR attenuation, the Triarylamines seems to be potential candidates for thermal control devices.

Novel NIR electroactive materials, for technological application, was obtained from polyamide films containing tetraphenyl-*p*-phenylendiamine units (Fig. 1.8) and their electronic spectra are reported in Fig. 1.9 [20].

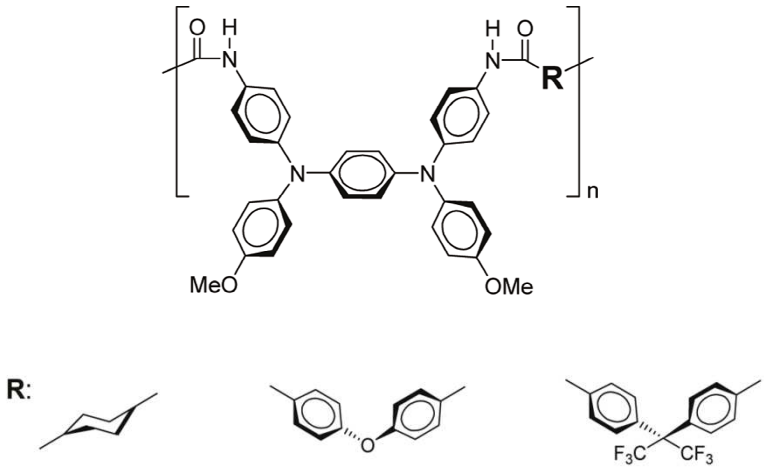

Fig. 1.8. Aromatic Polyamides [20].

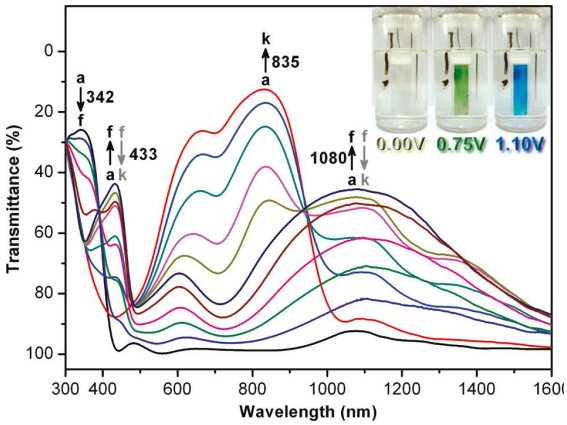

Fig. 1.9. Electrochromic behavior of polyamide **Ib** thin film (λ=65 nm in thickness) on the ITO-coated glass substrate in 0.1 M TBAP/CH_3CN at applied potentials of (a) 0, (b) 0.40, (c) 0.50, (d) 0.60, (e) 0.70, (f) 0.75, (g) 0.80, (h) 0.85, (i) 0.93, (j) 1.00, (k) 1.10 (V vs Ag/AgCl). $\mathbf{Ib}^{+\cdot}$, black solid arrow; $\mathbf{Ib}^{2+}$, gray solid arrow [20].

New polymeric films with improved NIR electrochromic response was proposed by Liou et al. [21]. They synthesized aromatic polyamides with strarburst triarylamine groups in the backbone (Fig. 1.10). Their spectra are shown in Fig. 1.11.

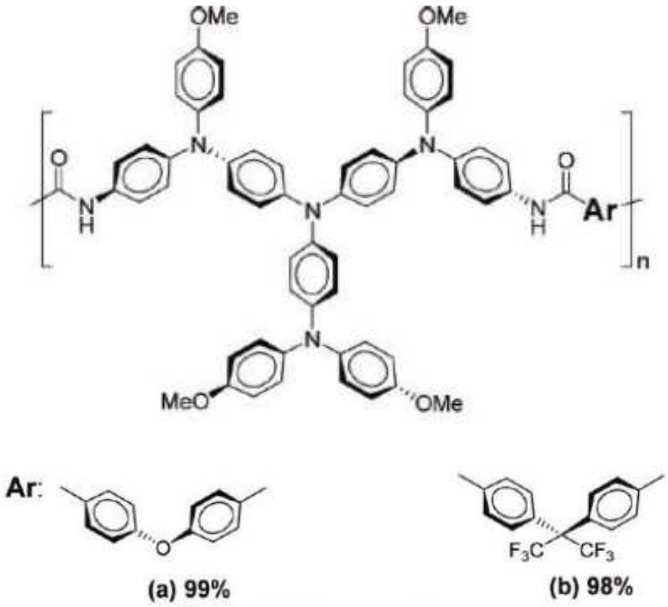

Fig. 1.10. Starburst Triarylamine-containing electroactive aramids [21].

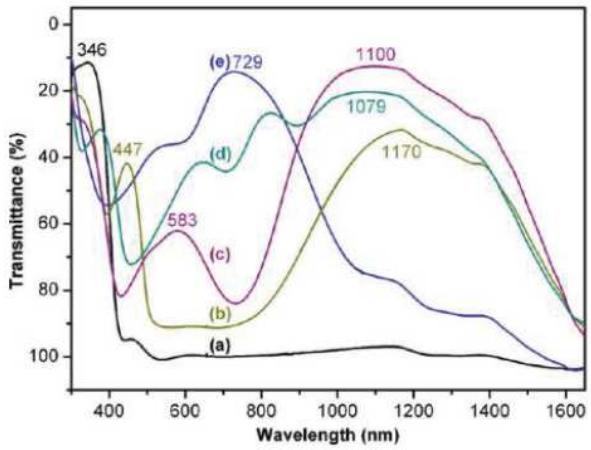

Figure 1.11. Electrochromic behavior at applied potentials of (a) 0.00, (b) 0.55, (c) 0.80, (d) 1.10, (e) 1.45 (V vs Ag/AgCl) of polyamide Ia thin film (~120 nm in thickness) on the ITO-coated glass substrate in 0.1 M TBAP/CH_3CN [21].

1.3.2 Viologens and Extended Viologens

Viologen species, formally named as salts of 1,1'-disubstituent-4,4'-bipyridinium [51], are classic organic building blocks that have been utilized in a variety of fields, such as photochemistry [52], electrochemistry [53], solar energy conversion [54], and as bridging ligands in metallosupramolecular assemblies, or molecular wires [55]. Viologens can undergo two successive electron-transfer reactions from the dication (the most stable form) to produce a radical cation, and then form a neutral species (figure 1.12).

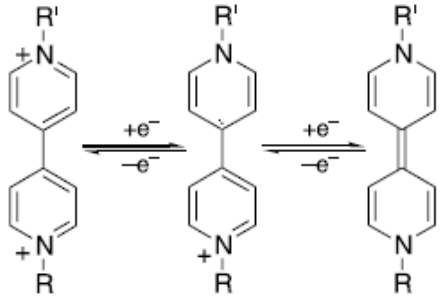

Fig. 1.12. The three common redox states of viologens, showing the two successive electron transfer reactions. R and R' can be the same aliphatic or aromatic substituents.

The bipyridinium dication has a relatively high electron affinity [56] so a stable and colored radical cation species is formed after the reversible single electron reduction [57]. Its stability is attributable to the delocalisation of the radical electron throughout the π-framework of the bipyridyl nucleus, the 1 and 1' substituents commonly bearing some of the charge. The radical cation in particular is highly colored because of an intense optical charge transfer between the (formally) +1 and zero valent nitrogens. A suitable choice of nitrogen substituents in viologens to attain the appropriate molecular orbital energy levels can, in principle, allow colour choice of the radical cation. Short alkyl chains for example, are blue/violet whereas aryl groups such as 4-cyanophenyl in 1,1'-bis(4-cyanophenyl)-4,4'-bipyridilium generally impart a green hue to the radical cation [35]. The neutral species show a weak color intensity instead, since no optical charge transfer or internal transition corresponding to visible wavelength is accessible [34,57].

So far, various viologen systems have been proposed and much effort has been made to develop industrially applicable EC displays [36] and electronic papers [58-59] with high coloration efficiency and good cyclability of the coloration–decoloration process. Recently, much attention has been paid to the viologen incorporating bridging phosphoryl group [60] or π-conjugated fragment [61] that dramatically enhances the electron-acceptor features of the molecule. These new viologens, called "extended viologens" having different skeletal structures from traditional ones and that give stable radical cations are of current interest for organic electronics. The extended viologens known are dications that have phenylene [62-64], thiophene [62, 65-66], furan [62], and polyene [67-69] units between the pyridylium rings (Fig. 1.13).

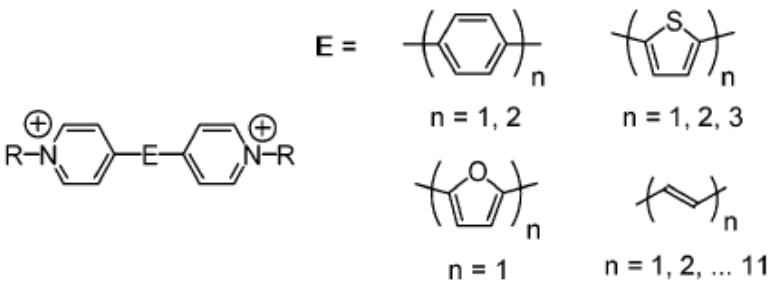

Fig. 1.13. Known extended viologens [61]

Viologens containing the butadienylene- and higher polyethenylene-extended ones tend to be reduced to the unstable radical cations [70], so that they are not good EC materials. Takahashi et al. [62] have demonstrated that viologens in which the two pyridylium rings are connected by two or more ethylene moieties undergo one-stage two-electron reduction while those including one thiophene or a furan group undergo reversible two-stage one-electron reduction, detected in cyclic voltammetry experiments (Fig. 1.14), indicating the formation of stable and intensely coloured radical cations (Fig. 1.15) as well as the corresponding neutral species. In addition, viologens containing a single thiophene, furan or phenyl group, have showed fluorescence emission spectra upon photoexcitation at room temperature [62].

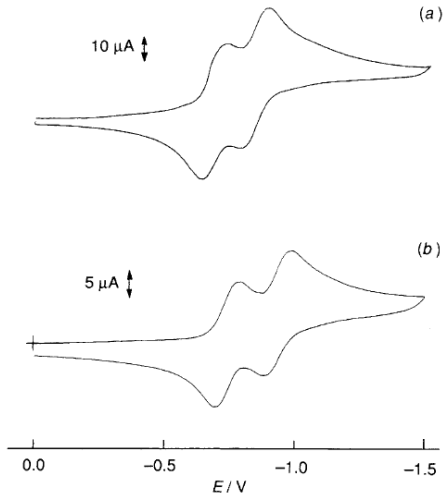

Fig. 1.14 Cyclic voltammograms of extended viologen containing (a) thiophene and (b) furan unit, 0.1 mmol dm^{-3} in MeCN with 0.1 mol dm^{-3} Et_4NC10_4 at room temperature [scan rate: 50 mVs^{-1}; reference electrode: saturated calomel electrode (SCE)] [62].

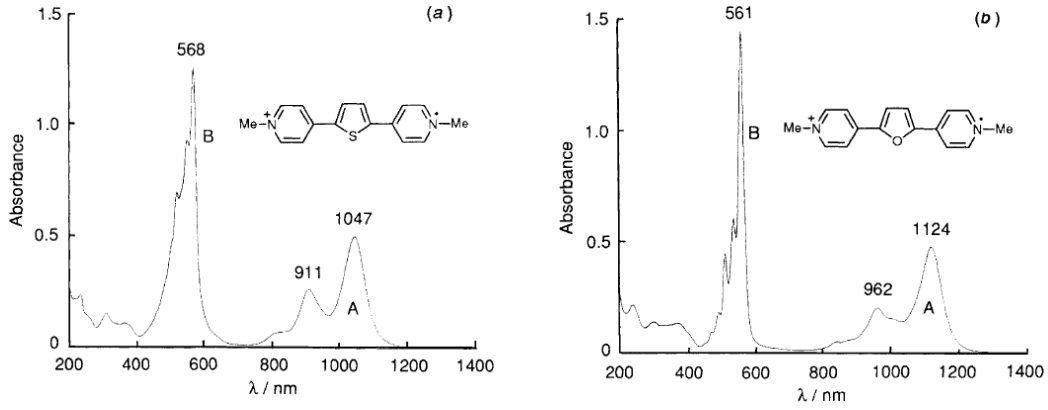

Fig. 1.15. Electronic spectra of radical cations of conjugation-extended viologens containing (a) thiophene and (b) furan unit, in MeCN [62].

Interestingly, viologens incorporating thiophene units of variable length, "thienoviologens" are described as promising candidates for molecular wires in biosensor applications [71].

1.4. Semiconducting Liquid Crystals

Amongst the various new materials for organic electronics, conjugated liquid crystals (LCs) are currently viewed as a new generation of organic semiconductors because they bring *order* and *dynamics* [72]. Order is likely the most important parameter that governs the performances of organic semiconductors in devices. Conjugated LCs offer the decisive advantage of controlling order in the bulk and at interfaces, and at all length scales from molecular to macroscopic distances. The role of dynamics in organic semiconductors is also important but less explored. The most striking example of the effect of dynamics is the ability of conjugated liquid crystals to self-heal structural defects such as grain boundaries due to their liquid-like character [73]. Upon simple thermal annealing, it is common to observe the spontaneous formation of large single domains that extend over several square mm, for films up to several μm thick [74,75]. Molecules with liquid crystalline ordering [76,77], the so called mesogens, are usually composed of two parts: a rigid form anisotropic inner part, of rod- or disc-like shape (the core of the mesogen), and flexible chains linked to this rigid core [78]. In the case of semiconducting materials, the core of the mesogen consists of a larger π-conjugated system and allows charge carrier transport. In more highly oriented low temperature phases, the pronounced order between the aromatic cores is facilitated by strong π-π interactions, while the disordered flexible side-chains prevent a "true long-range order" and distinguish these ordered liquid crystalline phases from true crystals [78]. The flexible parts of molecules play an important role for the self-assembling nature as well as for the solubility. On the basis of the requirement for ‘"wet processing" in thin film device fabrication, the alkyl tails in the terminal/peripheral positions have made such π-electronic conjugation systems much more attractive due to their better solubility in common organic solvents [79].

The ease of alignment into single domains arises from the fact that conjugated LCs are composed of small organic molecules that form phases of low inherent viscosity. The low molecular weight of conjugated LCs associated with

discrete mass allows the synthesis of defect-free chemical structure that are amenable to a higher purity level than most conjugated polymers [80].

Columnar, smectic and, more recently, nematic liquid crystals are widely recognized as very promising charge-transporting organic semiconductors due to their ability to spontaneously self-assemble into highly ordered domains in uniform thin films over large areas [81]. Typical structures of mesogenic molecules are of ‘rod-like’ and ‘disk-like’ types which are known as calamitic and discotic liquid crystals, respectively (Fig. 1.16) [24]. They differ in their molecular shape, their phase symmetry, the dimensionality of their charge transport and exciton migration and in the extent of their orbital overlap (Fig. 1.17) [73].

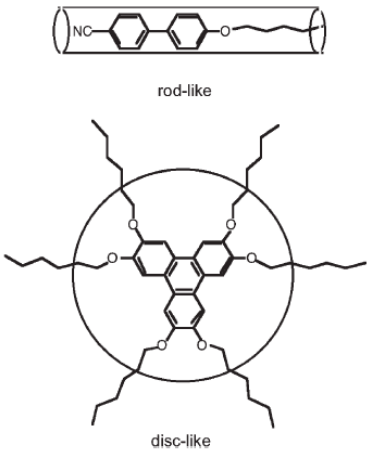

Fig. 1.16. Typical shapes of molecules for discotic and calamitic liquid crystals [24].

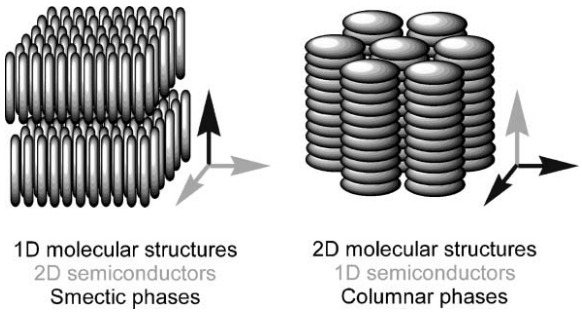

Fig. 1.17. Schematic drawing of calamitic (left) and discotic (right) semiconductors [73].

The π-electronic systems being core parts of the mesogenic molecules play an important role for electronic conduction [81]. In an organic semiconductor, holes and electrons are transported *via* the highest occupied molecular orbital (HOMO) and the lowest unoccupied molecular orbital (LUMO), respectively, of closely-packed, highly conjugated aromatic molecules [78].

Smectic planes demonstrate a two-dimensional charge transport, whereas columns of discotic mesogens exhibit one-dimensional charge transport that is rather sensitive to the structural defects [72]. As a result of the assembly of

discotic aromatic mesogens into columnar stacks with typical intercore distances of about 3.5Å, an overlap of the π^*–π^* LUMOs should be possible, which would lead to a conduction band for charge transport along the column axis (Fig. 1.18) [82]. Within the columns adjacent disc-like molecules experience a much larger orbital overlap than calamitics. The band width reaches values as high as 1.1 eV, close to that of graphite (*ca.* 1.0–1.4 eV) [83]. In the smectic mesophases instead, the extent of frontier orbital overlap is rather moderate. Typically, the band width of calamitics is expected to be below the corresponding value for pentacene, a well-studied low molecular weight organic crystalline semiconductor (*ca.* 0.5–0.6 eV) [84].

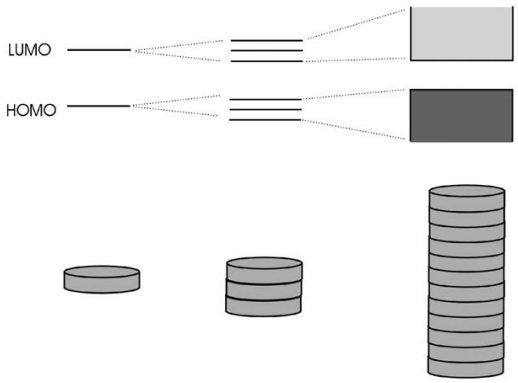

Fig. 1.18. Electronic band formation from a single molecule (left) to the column (right) [82].

Liquid crystals are relatively disordered compared to molecular crystals, so a coherent band-like description of charge-carrier transport in liquid crystals is inappropriate. Theoretical predictions indicated a thermally activated hopping mechanism of the charge carriers via π-π interactions between single molecules [85]. At the molecular level, transport is mostly governed by two key parameters: (*i*) the transfer integral which is a function of the overlap of HOMO (LUMO) orbitals of adjacent molecules for hole (electron) transport, and (*ii*) the internal reorganization energy associated with the energy difference between charged and neutral species [86].

Disorder-based empirical models, e.g., that derived from the Monte-Carlo simulations of charge transport by Bässler [87], describe mobility as a function of

temperature and electric field taking into account positional and electronic disorder [88-91]. The electronic density of states is broadened by disorder (Fig. 1.19), and is often represented by a Gaussian distribution, whose width depends on variations in the local conformation of the molecule, structural defects, dipolar disorder due to random orientation of polar groups, etc. Higher temperatures improve charge transport by providing the energy required to overcome the barriers for hopping between neighbouring states created by energetic disorder. Positional disorder is caused by variations in the relative positions and orientations of molecules and results in a distribution of electronic couplings within the material. Polaron theories require a strong electron-phonon coupling, with the disorder being of secondary importance, and relate the activation energy of the mobility to the polaron binding energy [92].

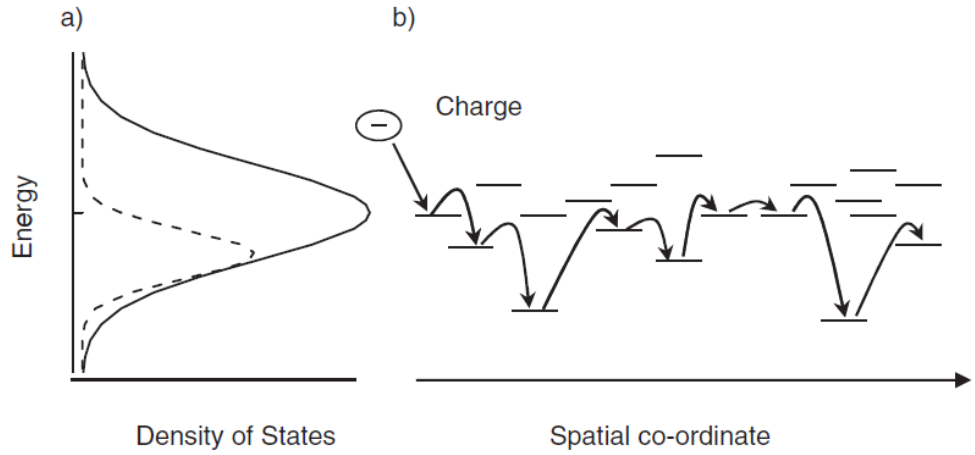

Fig. 1.19. a) The density of LUMO states (solid line) and occupied LUMO states (dashed line) for a disordered, liquid crystalline semiconductor. b) The horizontal lines indicate energy levels of individual molecules in a disordered ensemble of molecules. The sequence of arrows show an arbitrary pathway for an electron through the molecular ensemble. Hopping to a higher energy state requires activation energy and so is less likely than hopping to a lower energy state [81].

In the hopping model the mobility is correlated with the mesophase structure using molecular dynamics, which simulate the structural organization of a liquid crystal ensemble, in combination with kinetic Monte Carlo or master-equation descriptions of charge dynamics, based on the Marcus polaronic model. This considers that the charge carriers are localized at high temperatures and that transport occurs by a thermally-activated hopping mechanism, i.e., an electron or hole transfers from a charged molecule to an adjacent, neutral molecule.

The rate of charge transfer (k_{CT}) between two molecules in a given geometric arrangement can be expressed in the limit of weak electronic coupling via semiclassical Marcus theory as [93, 94]:

$$k_{CT} = \frac{4\pi^2}{h} t^2 \frac{1}{\sqrt{4\pi\lambda k T}} \exp\left[-\frac{(\lambda+\Delta E)^2}{4\lambda k T}\right]$$

where t denotes the transfer integral, ΔE the free energy gained or lost by the system upon charge transfer, and λ the total reorganization energy, which has internal (λ_i) and external (λ_s) components. A high charge-transfer rate, and hence a high mobility value, requires the transfer integrals to be large and the ΔE and λ terms to compensate one another (because a charge transfer between two molecules of the same nature corresponds to a self-exchange reaction, ΔE is generally small, which means that the reorganization energies need to be minimized). ΔE is different from zero upon application of an electric field [90] and when disorder is present, that is, when the geometry or environment (i.e., the relative positions of the neighboring neutral molecules) of the molecules are different in the initial and final states. These two contributions are expected to be generally similar for hole and electron transport [85]; this might not hold true in cases where the negative and positive charge carriers have a very different spatial extent (e.g., in conjugated block copolymers when one type of carrier is confined into a co-monomeric unit while the other is fully delocalized over the conjugated backbone).

The external reorganization (λ_s) accounts for the changes in the relative positions of the surrounding molecules upon charge transfer. In contrast to electron-transfer processes in solution, this nuclear polarization term is expected to be rather small in the bulk of organic thin films, up to *ca*. 0.1 eV [91]; again, it appears to be similar for holes and electrons.

The internal reorganization part (λ_i) reflects the changes in the geometry of the two molecules when going from the initial to the final state. This term originates from the fact that the geometry of a charged π-conjugated molecule differs significantly from that of the corresponding neutral molecule, owing to a marked redistribution of the π-electron bond densities. A smaller internal reorganization is the suggested explanation for the very high hole mobility of a calamitic thioalkyl

substituted aromatic compound compared to the equivalent alkoxy-substituted triphenylene (Fig. 1.20a), which exhibits a columnar discotic phase of flat disk-shaped aromatic molecules [86]. Simulations of charge transport have highlighted the role that defects play in slowing down charge transport in discotic columnar liquid crystals. For example, self-organization and charge transport was modelled for an ensemble of semi-triangular shaped, graphene-like, molecules, with three pairs of 4-alkylphenyl substituents (Fig. 1.20b) and a self-assembled columnar organization [95].

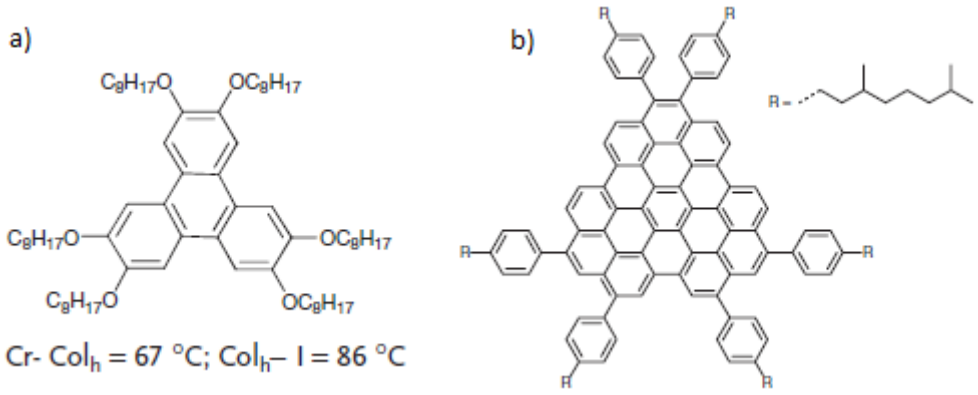

Fig. 1.20. Chemical structure of (a) compound 1 and their transition temperatures. Cr =Crystal; Col_h =Columnar hexagonal; I =Isotropic; (b) compound 2 [81].

One promising approach to the preparation of functional liquid crystals is to form anisotropic electron-, ion- conducting materials by using nano-segregation [96]. In this context, nanostructures of LCs that combine an ion-conductive group and a π-conjugated moiety transporting electronic charges for the construction of redox-active anisotropic materials have been developed [97,98]. In the redox activity of these systems, the mobile ions in the nanostructure play a crucial role [99, 100]. The enhancement of electronic functions by the combination with ions has been studied in conjugated polyelectrolytes, where the disordered structures of the polymers limits the charge carrier transport [10]. Their ionic conductivities are also low because of the large viscosity. In contrast, the efficient ion and electron (hole) transports are possible for example, in the nanosegregated smectic liquid crystals where the structure of ion- and electron-transporting layers is well-defined on the scale of nanometer. The combination of the ionic and electronic functions in the nanostructured LC phases should be effective in applications to

various electronic devices such as electrochromic devices and light-emitting electrochemical cells [97, 98].

1.4.1. Electrochromic Liquid Crystals

For efficient electrochromism, fast formation of an electrical double layer at an electrode surface is essential moreover, fast electronic charge transfer from the electrode is also required [93]. Usually, the electrochromism of the electroactive liquid crystal materials has been observed only in solutions or in thin films dipped in electrolyte solutions or combined with solid electrolytes [102-104]. Recently Kato et al. [97] have reported the first example of reversible electrochromism in the bulk of the liquid-crystalline state without an electrolytes. They proposed a series of ionic liquid crystals (Fig. 1.21), consisting of π-conjugated mesogens and ionic units, designed to induce smectic A (SmA) phases where the ion and hole transport layers are alternately formed through the nanosegregation (Fig. 1.22).

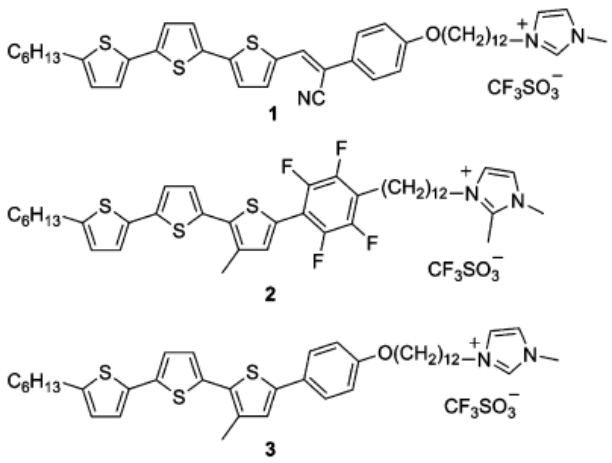

Fig. 1.21. Molecular structures of liquid crystals **1**-**3** [98].

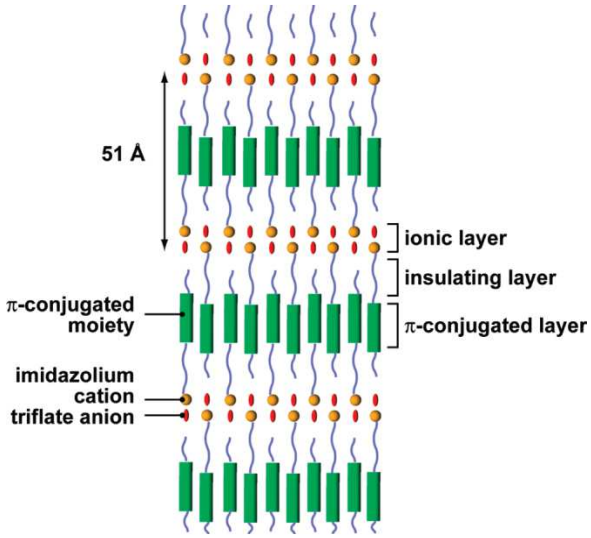

Fig. 1.22. Schematic illustration of a possible structure in the SmA phases for liquid crystals **1**-**3**. Green cylinders, red ellipsoids, and orange spheres represent π-conjugated moieties, triflate anions, and imidazolium cations, respectively. The ionic and π-conjugated moieties are organized into segregated layers [98].

As shown in Fig. 1.23, the ions would be accumulated on the surface of the electrode forming an electrical double layer when an electric field is applied to the liquid crystal. Subsequently, electronic charges should be injected from the electrode into the π-conjugated systems of the liquid-crystalline molecules and transported between them [98]. Monitoring the response of the trasmittance at 632.8 nm as a function of time of LCs **1**-**3** in the bulk state, the most efficient electrochromic response was observed for compound **1** (Fig. 1.24.).

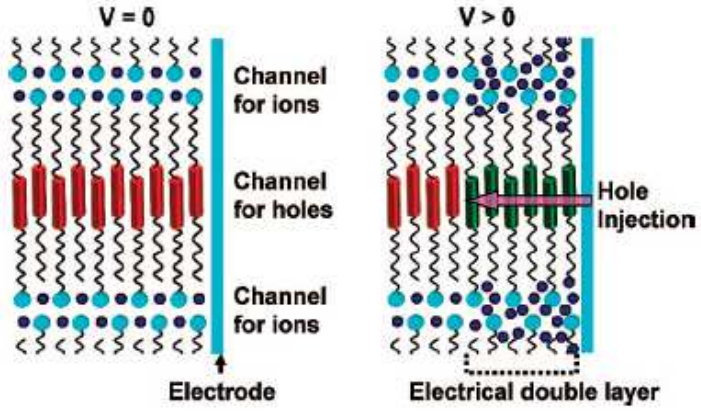

Fig. 1.23. Schematic image of a nanostructured liquid crystal consisting of ionic and moieties. Red cylinders are neutral π-conjugated units. Dark green cylinders are the oxidized ones. Dark blue spheres and light blue plates are triflate anions and imidazolium moieties, respectively [97].

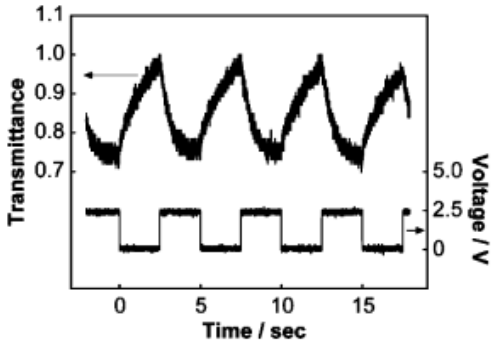

Fig. 1.24. Responses of transmittance of the cell with compound **1** in the SmA phase at 160 °C on the application of double-potential steps between 0 V (2.5 s) and 2.5 V (2.5 s). The sample thickness is 4 μm. [98]

Ionic liquid crystals based on viologen-like core, are very interesting electroactive self-assembled materials. It was observed that the viologens in the liquid-crystalline state are electric semiconductors and that they could be transformed into a state with a much higher electric conductivity by applying a voltage above a certain threshold over two ITO electrodes in a sandwich cell filled with the liquid crystal. An increase in electric conductivity by a factor of 10^4 was observed by applying a voltage of 30 V over the electrodes. The liquid-crystalline viologen kept this high electric conductivity, even when the voltage was no longer applied [105].

1.4.2. Viologen Liquid Crystals

The synthesis of liquid-crystal "viologens" makes it possible to expand the field of application of viologens [106]. Kominami and coworkers [105] described the first thermotropic liquid crystalline viologen compounds with electrochromic properties. Viologens with long alkyl chains are liquid-crystalline and the mesophase behavior depends on the type of anion [105,107-111]. 1,1'-Diheptyl-4,4'-bipyridinium dibromide and 1,1'-dioctyl-4,4'-bipyridinium dibromide decompose without melting, whereas the corresponding bis(triflimide) salts

exhibit a smectic A phase (Fig. 1.25a) [110, 112]. In another work [111] was demonstrated that 1,1'-Dipentyl-4,4'-bipyridinium bis(triflimide) is a ionic liquid crystal at room temperature (smectic A phase), but both 1,1'-dibutyl-4,4'-bipyridinium bis(triflimide) and 1,1'-dihexyl-4,4'-bipyridinium bis(triflimide) have melting points well above room temperature. No mesophase was observed for the tetrafluoroborate salts. By replacement of the alkyl chain by an oligoethyleneoxide chain, compounds with a large mesophase stability range could be obtained [105-107]. 1,1'-Di(3,6,9-trioxatridecyl)-4,4'-bipyridinium diiodide (Fig 1.25b) is liquid-crystalline between 63 and 216 °C [105].

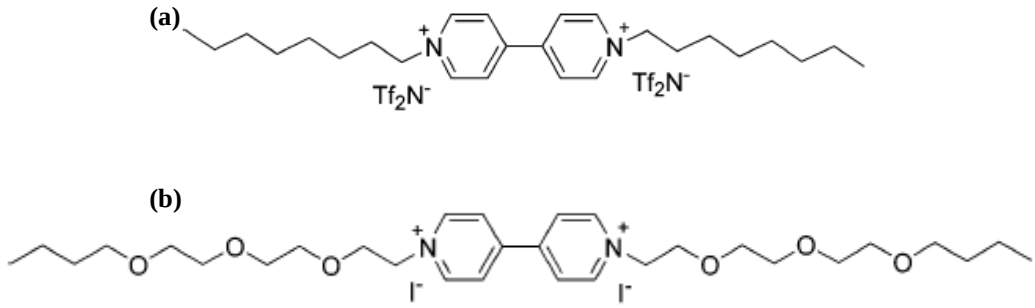

Figure 1.25. Molecular structures of viologen liquid-crystals: (a) 1,1'-dioctyl-4,4'-bipyridinium bis(triflimide) and (b) 1,1'-Di(3,6,9-trioxatridecyl)-4,4'-bipyridinium diiodide [113]

Discotic molecules such as ‘‘viologens’’ usually form columnar mesophases, the molecules are stacked on top of each other into columns, which are arranged in either hexagonal Colh or rectangular Colr order [113,114]. Kato et al. [102] reported the first example of columnar liquid crystals incorporating a redox-active viologen unit (Fig. 1.26). They exhibit rectangular or hexagonal columnar phases, which are stable up to 160 °C.

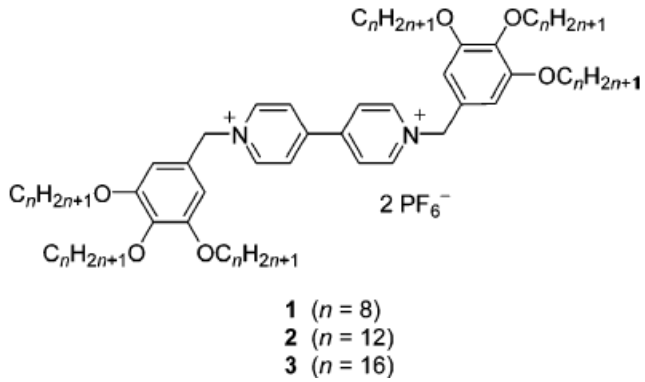

Fig. 1.26. Molecular structures of liquid-crystalline viologens 1-3 [102].

The group of Saielli [115] showed that the symmetrically substituted viologen salts with sufficiently long alkyl chains exhibit a smectic mesophase of type B (SmB) over a wide temperature range from 0 °C to 140 °C. Because of a rigid anisotropic molecular core no nematic mesophase is known for such systems [109]. More specifically, by the induction of asymmetry in molecular structure by changes in the alkyl sidechains attached to the viologen core, the solid–liquid crystal transition temperatures can be lowered more than in a symmetrical structure [115].

CHAPTER 2

Near-infrared electrochromic materials based on Triarylamine moieties

2.1. Introduction

Triphenylamines with multiple redox centres have attracted many interest as anodic electrochromic (EC) system and hole-transporting materials for optoelectronic devices [16,17]. The one-electron oxidation product, triphenylamine radical cation, shows a strong electronic coupling (the electron is delocalized over the two or more redox centers), leading an intervalence charge transfer (IV-CT) absorption band in the near infrared (NIR) region [11-15]. This property could be potentially used in devices for thermal control. Herein we present the electrochemical and spectroelectrochemical properties of a new synthesized triarylamine molecule, *N*,*N'*-Bis(4-heptanoylamidophenyl)-*N*,*N'*-di(4-methoxyphenyl)-1,4-phenylenediamine (TPPAHM) incorporating electron donating substituents at the *para* position of the phenyl groups in order to greatly prevent the coupling reactions by affording stable cation radical [20]. For comparison we have investigated the electrochemical and spectroelectrochemical properties of the triarylamine molecule without substituents, *N*,*N*,*N'*,*N'*-Tetraphenyl-1,4-phenylendiamine (TPPA) (scheme 1). Moreover, in order to contribute to the clarification of the electron-transfer process occurring in this systems, the experimental results were supported by theoretical studies (time-dependent–density functional theory, TD-DFT, spectral simulation) [117].

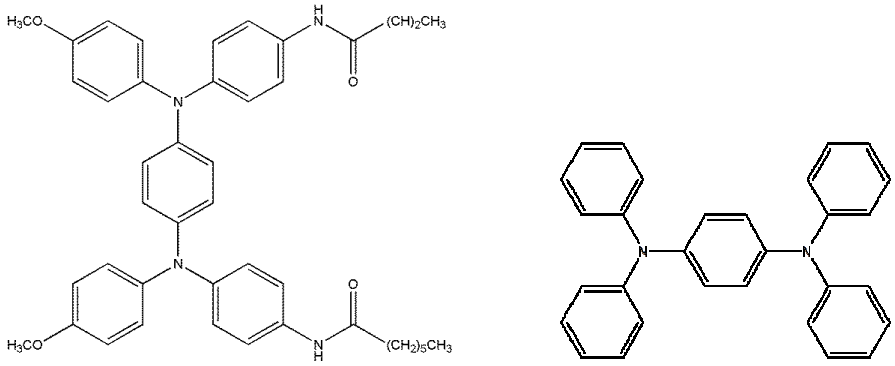

Scheme 1. Molecular structures of TPPAHM (left) and TPPA (right)

2.2. Experimental and theoretical details

2.2.1. Materials

N,N,N',N'-Tetraphenyl-1,4-phenylendiamine (TPPA) were purchased from Sigma-Aldrich and were not further purified before use. Dichlomethane was purchased from Carlo Erba. *N*-methyl-2-pyrrolidinone (NMP) was purchased from Pancreac. The solvents were used after removing water by molecular sieves. Tetra-*n*-butylammonium perchlorate, TBAP (Fluka Chemika) was used as an electrolyte without further purification.

2.2.2. Synthesis

The synthesis of the target molecule TPPAHM is depicted in Scheme 2. *N,N'*-Bis(4-nitrophenyl)-*N,N'*-di(4-methoxyphenyl)-1,4-phenylendiamine (**2**) that was prepared by Ullmann coupling between 1,4-diiodobenzene and 4-methoxy-4'-nitrodiphenylamine (**1**) according to a previous published procedures [20]. TPPAHM was prepared in two steps procedure as described below. In a 250 mL three-neck round-bottomed flask equipped with a stirring bar under nitrogen atmosphere, *N,N'*-Bis(4-nitrophenyl)-*N,N'*-di(4-methoxyphenyl)-1,4-phenylen-diamine (1.01g, 1.79 mmol) was dissolved in 10 mL of ethanol and 60 mL of tetrahydrofurane (THF). To the stirred solution was slowly added hydrazine monohydrate (1g, 20.0 mmol) and the mixture was refluxed. Just it began to reflux, a small amount of Raney Ni was added. The solution frothed and as the

reaction proceeded the color changed from yellow to almost colorless. After further 6 h of heating, the hot solution was filtered under nitrogen to remove Raney Ni and the filtrate was washed with THF. The THF was removed by distillation at 65-70 °C under nitrogen atmosphere. The remaining ethanol solution was cooled to 0 °C under nitrogen in order to have the precipitation of crude *N,N'*-Bis(4-aminophenyl)-*N,N'*-di(4-methoxyphenyl)-1,4-phenylendiamine that was recovered by filtration, washed with cold ethanol and dried in vacuum. The *N,N'*-Bis(4-aminophenyl)-*N,N'*-di(4-methoxyphenyl)-1,4-phenylendiamine (**3**) was instable and was immediately used in the next step without further purification. To a stirred solution of crude *N,N'*-Bis(4-aminophenyl)-*N,N'*-di(4-methoxyphenyl)-1,4-phenylendiamine, prepared as described above, in 16 mL of dry THF, was added under nitrogen 0.9 mL of Net_3. To the resulting mixture was dropped a solution of heptanoyl chloride (0.46 mL, 2.98 mmol) in 11 mL of dry THF and the mixture was stirred at room temperature. After 20 h, a colorless precipitate was formed. The precipitate was collected by filtration, washed with cold ethanol and dried in vacuum to give 0.58 g (45% based on starting *N,N'*-Bis(4-nitrophenyl)-*N,N'*-di(4-methoxyphenyl)-1,4-phenylendiamine) of crude *N,N'*-Bis(4-heptanoylamidophenyl)-*N,N'*-di(4-methoxyphenyl)-1,4-phenylen-diamine, TPPAHM (**4**), that was sufficiently pure by TLC (silica gel 60 F_{254}; 1:1 Hexane-AcOEt) and NMR analysis and was used without further purification. Mp 218-221 °C; IR (KBr): ν = 3303 (m), 2976 (m), 2938 (m), 2756 (m), 2758 (m), 2677 (m), 2491 (m), 1657 (s), 1505 (s), 1398 (m), 1171 (m), 1036 (m), 805 (m) cm^{-1}; ^1H NMR (300 MHz, DMSO-d_6): δ = 0.86 (d, *J* = 6.4, 6 H), 1.24 – 1.40 (m, 8 H), 1.48 – 1.62 (m, 4 H), 2.21 – 2.34 (m, 8 H), 3.73 (s, 6 H), 6.80 (s, 4 H), 6.88 (d, *J* = 9.1, 4 H), 6.89 (d, *J* = 9.1, 4 H), 6.98 (d, *J* = 9.1, 4 H), 7.46 (d, *J* = 9.1, 4 H), 9.77 (s br, 2 H); MS (ESI^+, direct infusion): *m/z* = 749 [$(M+Na)^+$]; Anal. Calcd for $C_{46}H_{54}N_4O_4$ (726.95): C 76.00, H 7.49, N 7.71; found C 76.19, H, 7.47, N 7.73.

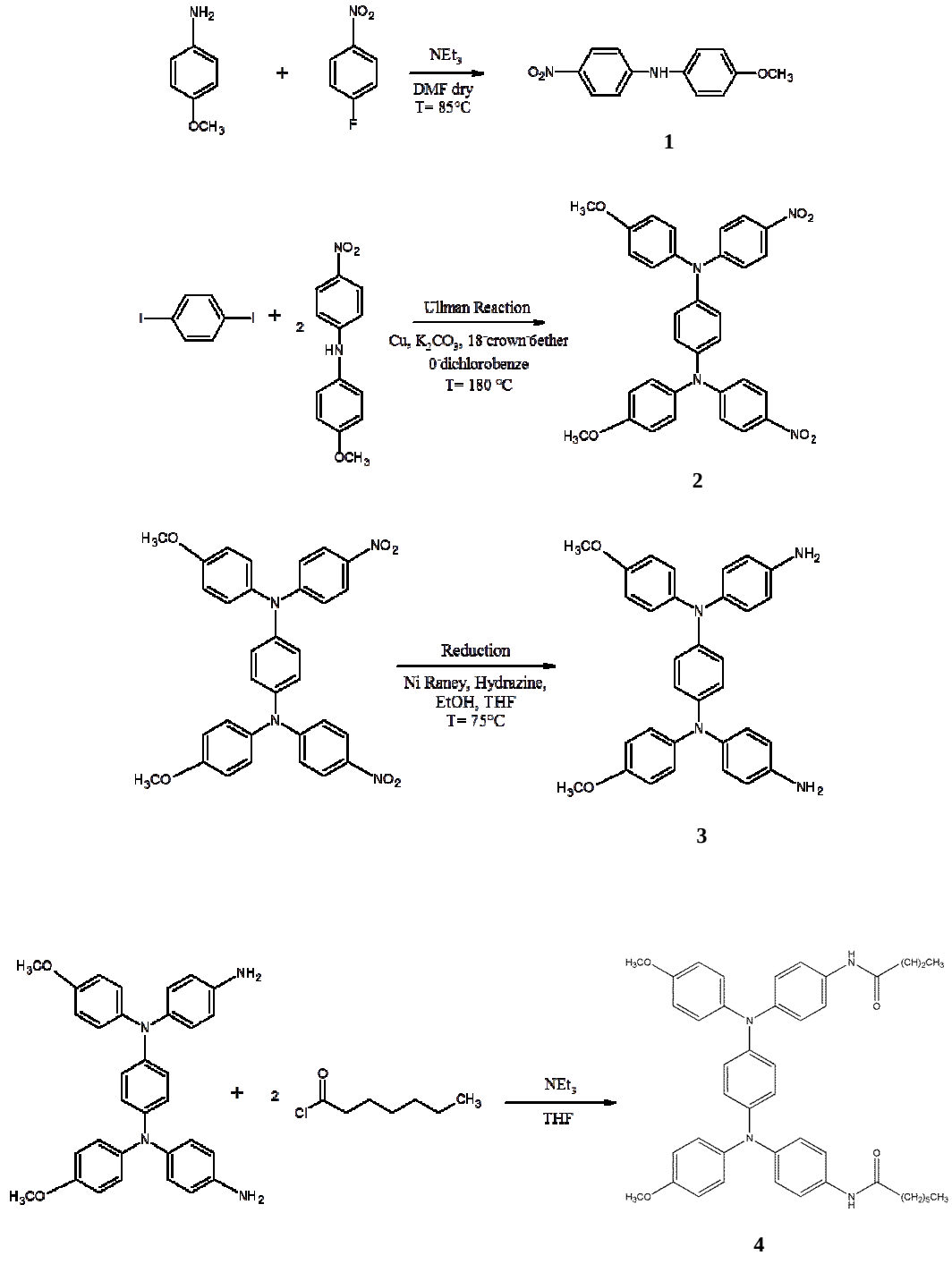

Scheme 2 Synthetic route to TPPAHM

2.2.3. Methods

Melting point analyses were performed on a Linkam (LTS350 stage, TP94 System Controller) at scan rate of 10 °C/min. ^{1}H NMR spectra were recorded at 25 °C on a Bruker DPX Avance 300 Spectrometer in DMSO-d_6 solutions at 300 MHz with Me_4Si as internal standard. IR spectra were taken with a JASCO FT-IR 4200 spectrometer and microanalyses were carried out with a Carlo Erba Elemental Analyzed Mod. 1106. The electrospray ionization mass spectra were acquired by direct infusion on an ABSciex API 2000 mass spectrometer equipped with a turbo ion spray ionization source. The spectra in the positive ion mode were obtained under the following conditions: ionspray voltage (IS) 4500 V; curtain gas 10 psi; temperature 25 °C; ion source gas (1) 20 psi; declustering and focusing potentials 50 and 400 V, respectively.

Cyclic Voltammetry (CV) was done in NMP with 0.1 M TBAP as the supporting electrolyte and with 5 mM of molecule under a nitrogen inert gas atmosphere. CV was conducted with the use of a three–electrode cell equipped with a graphite working electrode a Pt auxiliary electrode and an Ag/AgCl, KCl (sat.) reference electrode. The measurements were performed with an Amel Instruments 7050 model potentiostat.

Spectroelectrochemical experiments were conducted in a electrolytic cell (BioLogic Science Instruments) which was composed of a 1 mm cuvette, where a platinum gauze thin layer and a platinum wire were used as working electrode and auxiliary electrode, respectively and a Ag wire as pseudo-reference electrode that was calibrated against the Ag/AgCl using the redox couple Ferroce/Ferrocenium as internal standard [$E_{1/2}$ (Fc/Fc^+ vs Ag) ≈ 0.42 V, $E_{1/2}$ (Fc/Fc^+ vs Ag/AgCl) ≈ 0.57 V].

The spectroelectrochemical cell was filled with a solution containing 1 mM of molecule and TBAP (0.1 M). The UV-vis-NIR spectra were recorded with a Thermo Scientific GENESYS 10S UV–vis spectrophotometer. The potential was supplied by means of an Amel 2049 model potentiostat. Measurements were performed at 25 °C.

2.2.4. Computational details

All calculations were performed with the TURBOMOLE V-6.0 software package [120]. Due to the medium–high molecular size of TPPAHM that requires high computational costs, the computation has been performed in a model system in which the $–(CH_2)_5CH_3$ moiety is substituted with the $–CH_3$ one. This substitution does not affect the spectral properties that are essentially due to the aromatic core. Geometry optimizations, without imposing symmetry constraints, as well as vibrational frequency analysis were carried out at the density functional level of theory in conjunction with the non-empirical PBE0 hybrid functional [121, 122] that adds up a fixed amount of Hartree-Fock exchange energy (25%) to the gradient corrected PBE exchange-correlation functional.

The SV(P) double-ζ quality basis set containing polarization functions on C, N and O atoms ([3s2p1d]/[2s]) of Ahlrichs et al. [123,124] was used for all the computations. Vibrational frequency analysis confirmed each optimized structure as absolute energy minimum on the relative energy potential surfaces. The closed-shell systems (neutral species) were treated with the restricted Kohn-Sham (RKS) formalism while for the open-shell systems (cation and di-cation species) unrestricted (UKS) calculations were performed. For the open-shell compounds the $<S^2>$ values of the ground-state Kohn-Sham determinant computed at PBE0/SV(P) level of theory were found in the range 0.76-0.77 (for the cation) and 2.02-2.05 (for the dication) indicating a small effect of spin-contamination. The lowest twenty vertical excitation energies were calculated from time-dependent density functional linear response theory [125,126] (TD-DFT) on the PBE0/SV(P) optimized geometries. The reliability of excitation energies obtained from the combination of SV(P) basis set and hybrid functional (PBE0) has been previously tested for a series of molecular systems, giving a mean absolute deviation from experimental within 0.2-0.3 eV [127-131]. Solvent effects on geometries and excitation energies, due to electrostatic interaction in polar solvent, were taken into account with the conductor-like screening model [132-133] assuming the dielectric constant value of 32.2 for NMP and default parameters for the cavity generation. The simulation of the electronic spectra band profile was obtained by a sum of Gaussian shape functions centred at each excitation energy and with a

constant full width at half maximum of 0.3 eV. On the other hand, the used protocol is very similar to that suggested by Renz et al. [134] for the study of mixed-valence radical cations.

2.3. Results and discussion

2.3.1. Electrochemistry

The electrochemical properties of the triphenylamines were investigated at room temperature by cyclic voltammetry (CV) and their voltammograms are shown in Fig. 2.1. Results are summarized in Table 2.1. The voltammograms of TPPA in NMP/0.1M TBAP (Fig. 2.1a) showed a rather complex behavior. In the first oxidation scan, one peak at 0.75 V was observed. This can be attributed to the formation of the stable monocationic radical $TPPA^{+}\cdot$. Upon further increase of the potential up to 1.4 V another peak at 1.13 V occurred due to the formation of the dication species $TPPA^{2+}$. This oxidation process is irreversible and no half-wave potential could be measured for it. This irreversibility is evidenced by the fact that the i_c/i_a ratio relative to the first redox process is smaller than 1 as well as by the appearance of an irreversible peak at 0.4 V in the reductive scan and an additional irreversible oxidation peak at 0.58 V in the subsequent oxidative scans. This suggest that the species $TPPA^{2+}$ is very reactive and undergoes a follow-up chemical reaction. The unknown follow-up product is unstable after reduction and undergoes a reversible transformation into their precursors, i.e., the TPPA molecules. This is evidenced by the fact that the overall cycle from 0 up to 1.4 V is essentially reversible since both the TPPA oxidation peaks did not exhibit significant decrease within the first few redox cycles. A possible hypothesis that takes into account the above behavior is that the dication $TPPA^{2+}$ undergoes a reversible coupling reaction leading to a σ-dimer. This hypothesis is suggested by a similar behavior of the *N,N',N''-p*-trimethylphenylamine (*p*-TTA), even if, in such a case, the reaction pathway leading to the reversible σ-dimer species from the $p\text{-}TTA^{2+}$, become favored over other pathways only at low temperature (-40°C) in CH_2Cl_2 [135]. CV of the TPPA was also performed in more common solvents for this technique such as CH_2Cl_2 and its voltammograms are depicted in Fig. 2.1b. It appears more simple with only two reversible oxidation peaks at 0.72

and at 1.20 V. These results suggest that the electrochemical behavior of the molecule is strongly affected by the solvent. Probably, the CH_2Cl_2 which is much less polar than NMP, inhibits the dimerization reaction of the TPPA, and the reasons are unknown at the moment, but are object of future studies.

On the contrary, the electrochemical behavior of the TPPAHM was completely reversible and in agreement with literature data on *para*-substituted triarylamines [16,17,20]. In the oxidative scan the TPPAHM exhibited two sequential reversible peaks at 0.6 V, which leads to the stable $TPPAHM^{+}\cdot$, and at 0.96 V which leads to its stable dication (Fig. 2.1c). In the TPPAHM the oxidative coupling was avoided because the electron donating substituents (*i*) stabilize the radical cations [17,161-163] and (*ii*) block the reactive *para* sites to the nitrogen centers with the highest spin electron density [161,164,165].

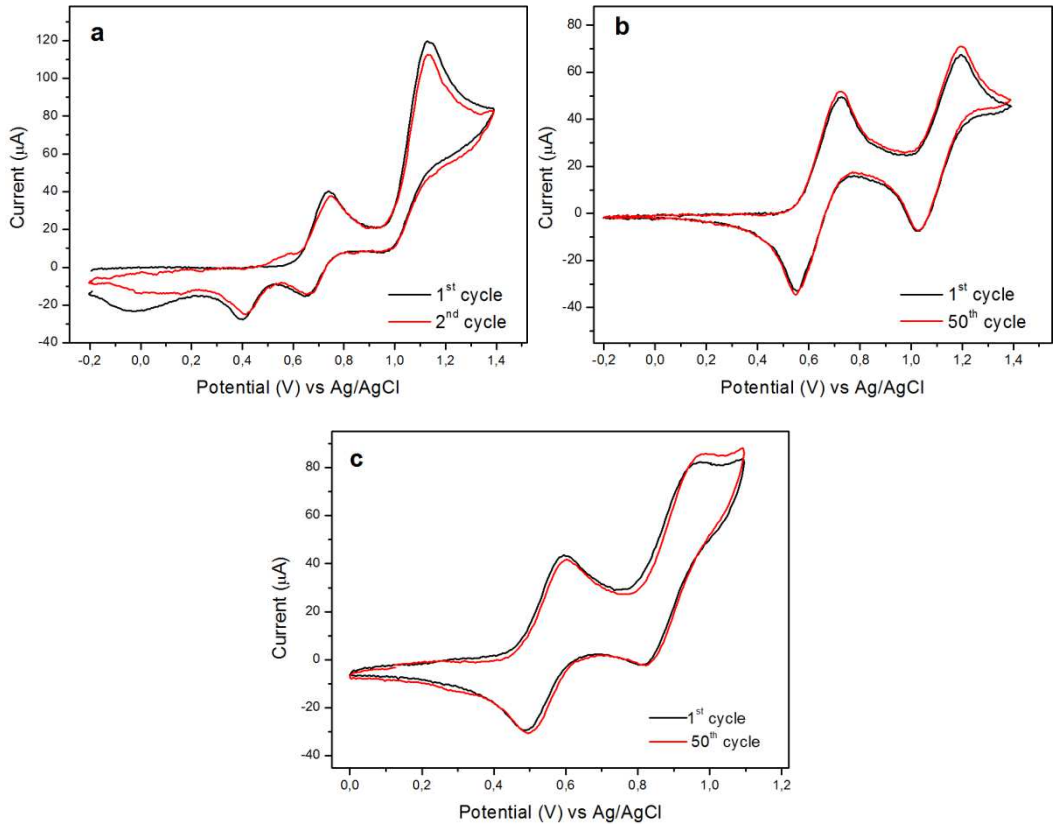

Fig. 2.1. Cyclic voltammograms of TPPAHM (a) in an electrolyte solution of NMP/0.1 M TBAP. Cyclic voltammograms of TPPA in electrolyte solution of NMP/0.1M TBAP (b) and CH_2Cl_2/0.1 M TBAP (c). Scan rate = 50 mV/s

Table 2.1 reports the values of the redox couple separation ΔE (the difference of the first and the second oxidation potentials) for the triarylamines. The ΔE values calculated for TPPAHM and for TPPA (only in CH_2Cl_2/0.1M TBAP solution) are about one order of magnitude larger than the statistical ΔE value for non-interacting centers [136]. This suggests that the triarylamine centers of these molecules are strongly coupled and that both $TPPAHM^{+\cdot}$ and $TPPA^{+\cdot}$ can be classified as a symmetrical delocalized class III structure, according to Robin and Day [50]. The energy of the HOMO and LUMO levels of the investigated molecules (Table 2.1) were determined from the half-wave potentials and the onset absorption wavelength, assuming that the HOMO energy for the Ferrocene/Ferrocenium standard is 4.80 eV below the zero vacuum level [137].

Table 2.1. Optical and Electrochemical data for TPPA and TPPAHM.

Compound	Solvent	λ_{max} (nm)	λ_{onset} (nm)	Oxidation (V) 1^{th} $E_{1/2}$ (V)	Oxidation (V) 2^{nd} $E_{1/2}$ (V)	Oxidation (V) ΔE^a (V)	HOMO[b] (eV)	LUMO[c] (eV)	E_g[d] (eV)
TPPAHM	NMP	360	398	0.54	0.90	0.36	-4.77	- 1.65	3.12
TPPA	NMP	348	374	0.70	-	-	-5.36	- 2.01	3.35
	CH_2Cl_2	344	374	0.63	1.11	0.48	-4.86	- 1.51	3.35

Scan rate = 0.05V/s; [a] $\Delta E = 2^{nd} E_{1/2} - 1^{st} E_{1/2}$; [b] The HOMO energy levels were calculated from cyclic voltammograms and were referenced to ferrocene (- 4.8 eV); [c] LUMO = HOMO + E_g; [d] $Eg = 1240/ \lambda_{onset}$

2.3.2 Spectroelectrochemistry and Theoretical studies

The solutions of the triphenylamines in polar aprotic solvents such as NMP are completely transparent in the visible region and exhibited strong UV absorption bands at 348 (TPPA) and 360 nm (TPPAHM) (Fig. 2.2), assignable to the π-π* transition resulting from the conjugation between the aromatic rings and nitrogen atoms. From this band we extrapolated the energy band gap (E_g) that as reported in Table 2.1, for TPPAHM is smaller than that for TPPA and this difference can be attributed to the effect of the electron-donating groups.

The electrochromic behavior of the TPPA dissolved in a electrolyte solution of NMP/0.1M TBAP, is depicted in Fig. 2.2a. When the first oxidation potential is reached (+ 0.95V vs Ag/Cl) the IV-CT band due to the $TPPA^{+\cdot}$ appears in the spectrum at 820 nm. This band cover a large part of the visible where is possible to observe also another band at 400 nm. The resulting

coloration of the solution is green. Applying a voltage of + 1.10 V the band at 400 nm slightly increases, while the maximum wavelength of the IV-CT band shifts to 750 nm. Increasing the potential to + 1.35 V the IV-CT band disappears and the entire visible range is covered by an intense and broad band having two maximum at 410 nm and 650 nm. According to the theoretical studies, the electronic transitions of the bi-oxidized species ($TPPA^{2+}$) reported in Table 2.2, are concentrated in the wavelengths range between 541 and 658 nm. So it is clear that all these transitions contribute to the large band of the $TPPA^{2+}$ that appears in the experimental spectrum. The coloration of the solution containing the TPPA dication is deep-blue.

The electronic spectrum of the TPPAHM, shows that, under an applied potential of + 0.75 V vs Ag/AgCl, a strong absorption band at about 1000 nm appears (Fig. 2.2b). This is the typical IV-CT band due to the radical cation species $TPPAHM^{+\cdot}$ formed when the first oxidation potential is reached. The solution containing the radical cation triarylamine became green and in addition to NIR band, two new bands at 424 nm and at 594 nm appear in the spectrum. Increasing the voltage up to +1.15 V vs Ag/AgCl, the second oxidation of the triarylamine occurs and the color of the solution switches to blue. In the electronic spectrum, the NIR band and the band at 424 nm decrease in intensity, while a broad band with a maximum at 580 nm and another at about 800 nm appear. These results are in very good agreement with the predicted spectra by theoretical calculation as reported in Fig. 2.3 and Table 2.2.

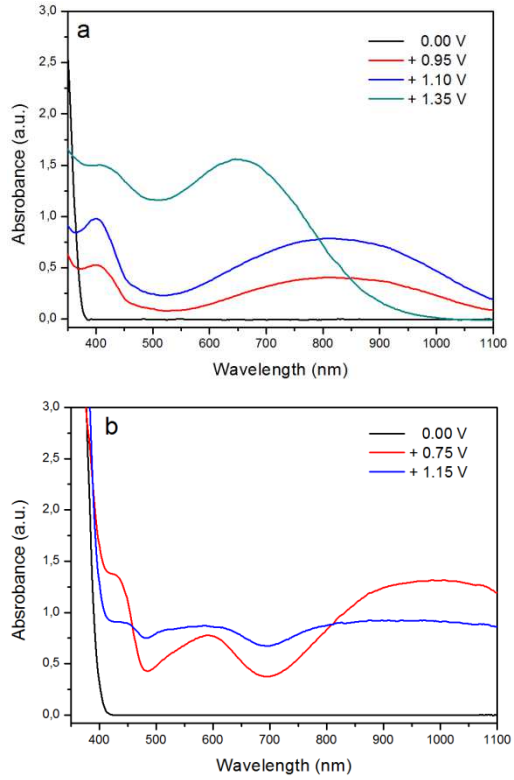

Fig. 2.2. Electronic spectra of 5 mM of TPPAHM (a) and 5 mM of TPPA (b) in NMP/0.1M TBAP.

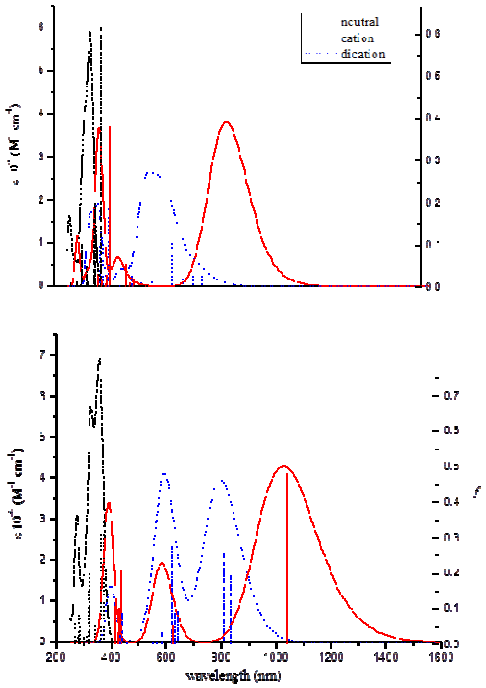

Fig. 2.3. TDDFT simulated spectra of TPPA (top) and TPPAHM (bottom).

Table 2.2. Computed vertical excitation energies, main configuration, and oscillator strenghts *f* for TPPA and TPPAHM in *N*-methyl-2-pyrrolidinone (ε = 32.2).

TPPA				TPPAHM			*Exptl.*
state	ΔE (eV, nm)	Main configuration (%)	*f*	ΔE (eV, nm)	Main configuration (%)	*f*	
1	3.65, 338	H → L	0.0102	3.40, 365	H → L (95.6)	0.0046	318 (1.9257)
2	3.70, 335	H → L + 1 (97.6)	0.6169	3.48, 356	H → L + 1 (93.7)	0.7344	
3	3.97, 312	H → L + 2 (93.7)	0.1988	3.71, 335	H → L + 2 (84.0)	0.0192	
4	3.99, 311	H → L + 3 (56.5)	0.0385	3.78, 328	H → L + 2 (94.0)	0.3432	
5	4.04, 307	H → L + 4 (50.9)	0.1608	3.88, 319	H → L + 3 (90.4)	0.3094	
cation							
1	1.47, 842	H-1 → L *β* (96.8)	0.4247	1.21, 1025	H-1 → L *β* (97.9)	0.4812	848 (0.1983)
2	2.42, 513	H-6 → L *β* (69.6)	0.0038	2.09, 593	H-3 → L *β* (97.5)	0.0520	
3	2.46, 504	H-3 → L *β* (97.6)	0.0000	2.14, 580	H-4 → L *β* (97.8)	0.1668	
4	2.66, 466	H-9 → L *β* (97.7)	0.0176	2.63,471	H-17 → L *β* (63.2)	0.0004	
5	3.37, 368	H → L + 1 α (74.3)	0.3800	3.14, 395	H → L + 1 α(43.7)	0.2058	
dication							
1	1.69, 733	H-3 → L *β* (83.6)	0.0272	1.53, 810	H-2 → L *β* (95.0)	0.1916	
2	1.72, 721	H-4 → L +1 *β* (81.8)	0.0000	1.58, 786	H-3 → L *β* (93.9)	0.2547	
3	1.77, 699	H-2 → L *β* (66.7)	0.0262	2.03, 611	H-2 → L +1 *β* (92.9)	0.0927	
4	1.88, 658	H-10 → L *β* (59.3)	0.1911	2.07, 599	H-3 → L +1 *β* (94.3)	0.0823	
5	2.02, 615	H-8 → L *β* (58.8)	0.1022	2.11, 588	H-6 → L *β* (87.1)	0.2745	
6	2.05, 605	H-5 → L *β* (64.8)	0.1276	2.23, 556	H-11 → L *β* (71.3)	0.0003	
7	2.29, 541	H-14 → L *β* (86.1)	0.2404	2.24, 553	H-12 → L *β* (67.3)	0.0333	

Looking at the orbital energy diagram reported in Fig. 2.4, in both molecules, the appearance of the NIR transition can be correlated with the lowering of the orbital energies in going from the neutral to the cation radical species. The oxidation

mechanism of triarylamine derivatives has been the subject of many previous publications [45,138-140]. In the major part of these works, it is supposed that the first oxidation is due to the removal of an electron from the nitrogen atom with the larger electron density, while the second one derives from the removal of a second electron from the other nitrogen atom. Recently, Wu et al. [141], in order to explain the spectrochemical behavior of a series of fluorine-based conjugated polymers containing propeller-shape di-triarylamine, have proposed a other mechanism for which the first electron must be removed by the HOMO orbital instead from the nitrogen lone pair and the second from the SOMO orbital. This proposal is based on coupling the spectrochemical data by the net charges of neutral and oxidized states calculated at the B3LYP/6-31G* level of theory. Following this strategy, we have computed, by using our computational protocol, the natural bond charges and the spin density (Fig. 2.5) for the neutral, cation radical, and di-cation of the TPPA and TPPAHM studied systems. From our data, it is evident that in both systems, although the N atom loss 0.11|e| (TPPA) and 0.10|e| (TPPAHM) in going from the neutral to the cation radical, these quantities are not sufficient to assert that the oxidation is mainly generated by this atom. Looking at the other net charges of the atoms surrounding the nitrogen, we note other loss of charge especially in the carbon located in the phenyl moiety that links the two nitrogen centers. Furthermore, from the orbital composition of the LUMO orbital in the neutral species (Fig. 2.6), we note, in both molecules, a strong involvement of the nitrogen in the formation of the phenyl π system. Similar results are obtained from the analysis of the spin density distribution as shown in Fig. 2.5. On the basis of these data, we can conclude that the first oxidation involves the entire HOMO π systems and not only the nitrogen atom. Concerning the second oxidation, the analysis of Table 2.2, as well as that of Figs. 2.4 and 2.5, suggests that the electron must be removed from the SOMO orbital created in the first oxidation process.

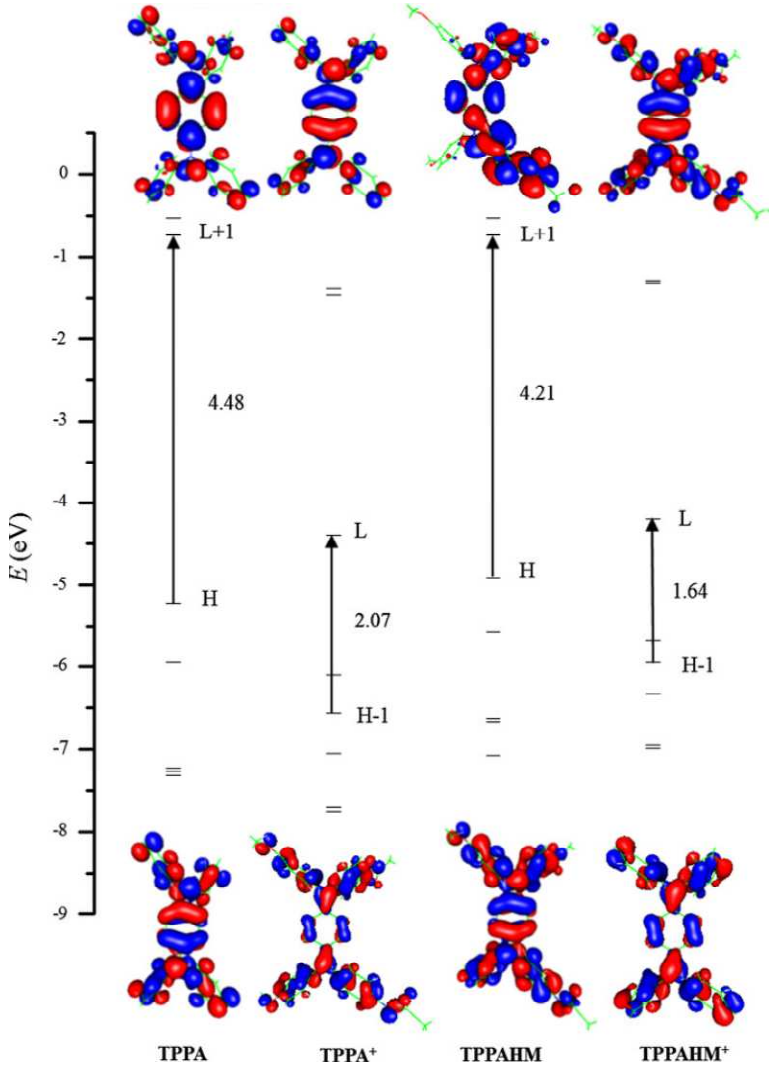

Fig. 2.4. Partial energetic diagram (eV) for the highest occupied and lowest virtual unoccupied molecular orbitals of molecules TPPA and TPPAHM (neutral and cationic forms). The orbital compositions are reported for the most intense transitions.

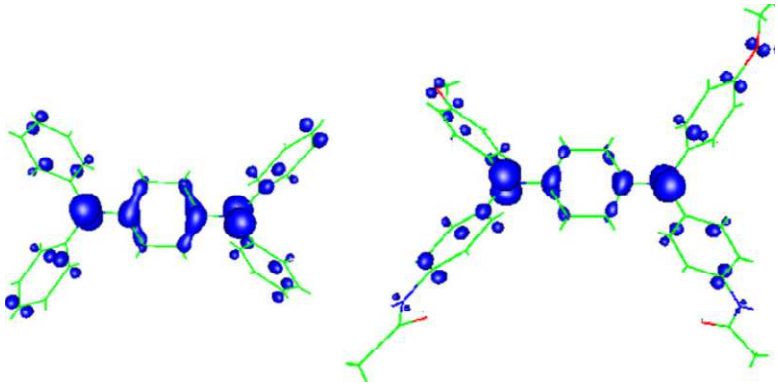

Fig. 2.5. Spin density contour plot for $TPPA^{\bullet+}$ (left) and $TPPAHM^{\bullet+}$ (right) (isodensity value of 0.005 a.u.)

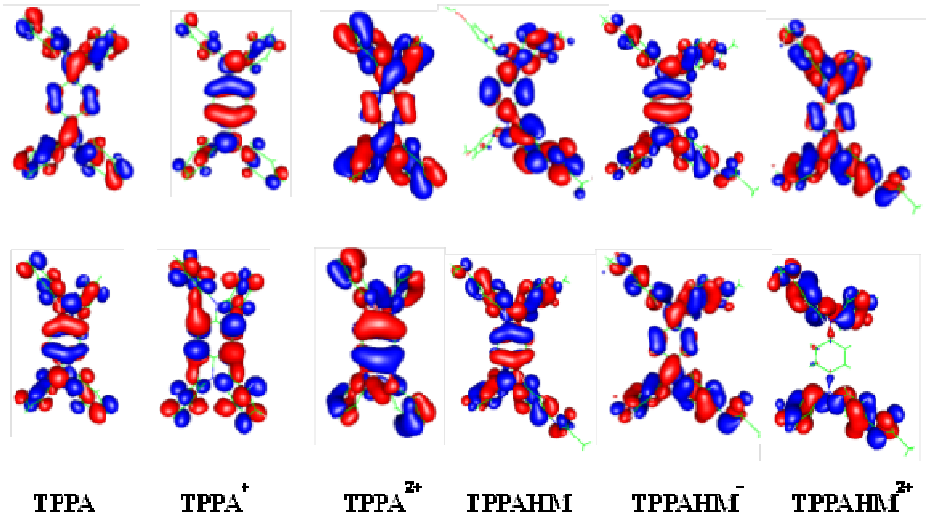

Fig. 2.6. HOMO and LUMO molecular orbitals for **TPPA** and **TPPAHM** (neutral and cationic forms).

2.4. Conclusions

A new triarylamine molecule, TPPAHM was synthesized and its electrochemical and spectroelectrochemical properties were investigated. We compared these properties with that of its unsubstituted analogous, TPPA, that revealed a very complex electrochemical behavior in NMP solvent. The irreversibility of the second oxidation peak in the cyclic voltammograms of TPPA indicates clearly that the reactive TPPA dications undergo dimerization reaction. But this oxidative coupling seems to be inhibited in dichloromethane. The electron donating substitutents incorporating in the TPPAHM prevent the coupling reaction and shift the IV-CT absorption band to higher wavelength with respect to the TPPA. In addition, DFT first principles computations were used revealing very interesting results:

• Both radical cations have a delocalized intervalence (IV) state in which the unpaired electron is fully delocalized over the whole molecules;

• The two oxidation processes occur with the involvement of the delocalized HOMO orbital that releases an electron in the first ionization, while in the second, the electron is given by the SOMO orbital;

• Although the used hybrid exchange–correlation functional can give an overestimation of the charge delocalization, the agreement between the calculated and experimental UV–vis–NIR spectral behavior is very satisfactory.

CHAPTER 3

Visible and Near-Infrared Electrochromic Devices containing Triphenylamine derivatives

3.1. Introduction

Triphenylamine derivatives presented in Chapter 2 seem to be very promising candidate as anodic molecules in electrochromic devices (ECDs) devoted to thermal control applications, because their strong NIR absorption bands [11-15]. In addition, the high transparence in the visible region of the TPPA and TPPAHM is a great advantage for their potential employment in smart windows application. Herein, we present two new complementary solution-phase ECDs able to absorb wither in the visible or in the NIR region thus allowing the control over a wide range of the solar spectrum. Our strategies was to create two transparent EC systems containing anodic NIR electroactive molecules based on tetraphenylphenylendiamine (TPPD) unit mixed to ethyl viologen dication (EV^{2+}) as cathodic molecule. This viologen completely transparent in the dicationic state, became deep blue colored in its mono-reduced form, so we can expect to obtain high optical contrast (Δ%T) devices. The electrochemical and spectroelectrochromic properties of the devices were investigated, moreover their stability was evaluated by EC switching studies.

The most performing EC system was then dissolved into a thermoplastic polymeric matrix in order to prepare a gel-based ECD. In this gel that for technological applications is much more interesting than EC solution, the mobility of the redox species is reduced but not suppressed and depends strongly by the cross-linking degree of the preformed polymer and by the molecular dimensions. This new EC system was fully characterized and its potential application for flexible electronics was also demonstrated.

3.2. Experimental

3.2.1. Materials

Ethyl viologen diperclorate ($EV(ClO_4)_2$) and *N*,*N*,*N'*,*N'*-Tetraphenyl-benzene-1,4-diamine (TPPA) were purchased from Sigma-Aldrich and were not further purified before use. *N*,*N'*-Bis(4-heptanoylamidophenyl)-*N*,*N'*-di(4-methoxyphenyl)-1,4-phenylendiamine (TPPAHM) was synthesized following the procedure previously described (Chapter 2). *N*-methyl-2-pyrrolidinone, NMP (Pancreac) was used as the solvent after removing water by molecular sieves. Tetra-*n*-butylammonium perchlorate, TBAP (Fluka Chemika) was used as an electrolyte without further purification.

3.2.2. Methods

The home-made two electrodes cells were assembled sandwiching two glass supports coated by indium tin oxide (ITO) (supplied by Visiontek Systems Ltd. with a sheet resistance of 27 ohm/sq and a thickness of 1 mm) creating an active area of 2 x 2 cm^2, with a thickness set at 60 µm by means of glass spheres. The cells were filled by a syringe with the two EC liquid solutions containing 5 mM of $EV(ClO_4)_2$) and 5 mM of triphenylamine (TPPA or TPPAHM) in NMP/ 0.1 M TBAP.

The EC gel was prepared dissolving $EV(ClO_4)_2$) (1 wt %), TPPAHM (1.8 wt %), TBAP (2.2 wt %) and PVF (25 wt %) in NMP (70 wt %) at 150 °C.

A two-electrodes cell was assembled by drop casting of the hot EC mixture sandwiched between two parallel ITO-coated glass supports (supplied by Visiontek Systems Ltd. with a sheet resistance of 27 ohm/sq and a thickness of 1 mm) creating an active area of 2 x 2 cm^2. The thickness was set at 60 µm by a plastic spacer of epoxy tape. Finally, the device was sealed with an epoxy resin.

Cyclic Voltammetry (CV) was done on the EC solutions using a three–electrode cell equipped with a graphite working electrode, a Pt auxiliary electrode and an Ag/AgCl, KCl (sat.) reference electrode. The measurements were performed with an Amel Instruments 7050 model potentiostat.

UV-Vis-NIR spectra were recorded with a Thermo Scientific GENESYS 10S UV-Vis spectrophotometer. Electrochromic Switching Studies were

performed with a Jasco V-550 UV-Vis spectrophotometer. The potential difference was supplied by means of an Amel 2049 model potentiostat and an Amel 568 model programmable function generator. Measurements were performed at 25 °C.

3.3. Results and discussion

3.3.1. Solution-phase electrochromic devices

The electrochemical behavior of the complementary EC systems was performed in a three-electrodes cell. In the voltammograms reported in Fig. 3.1., both the reductive and the oxidative character of the EV^{2+} and triphenylamines, respectively, can be observed. Indeed, in addition to the peaks of the triarylamines already observed in Chapter 2, two reversible redox couples at -0.47 and -0.89 V appeared, ascribable to the sequential one electron gain of the EV bipyridilium units [26,29,57].

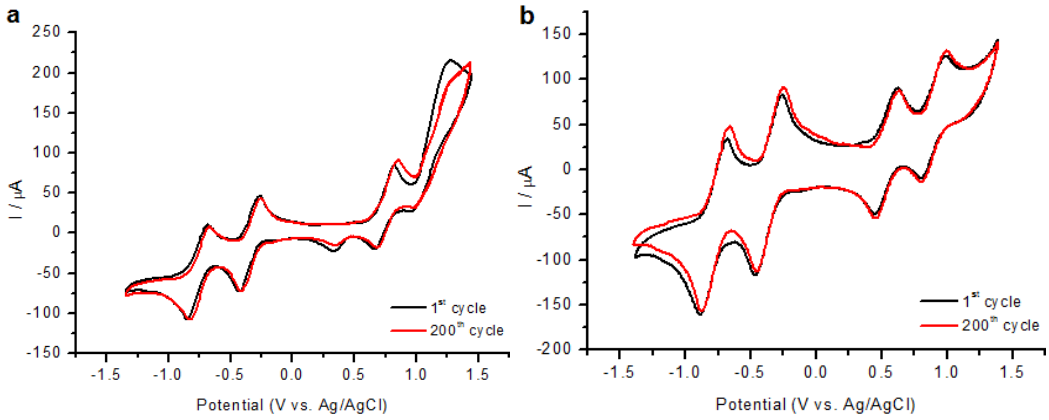

Fig. 3.1. Cyclic voltammograms of EV^{2+}/TPPA (a) and EV^{2+}/TPPAHM (b) in NMP/0.1 M TBAP. Scan rate = 50 mV/s

The electrochromic response of the complementary systems was investigated by UV-Vis-NIR spectroscopy under increasing applied voltages in a home-made two-electrode ITO sandwich-type cells.

When the device is switched on, the species will move by electrical migration to their respective electrodes to generate an intense composite green-blue colour. After the dual electrochromic colouration process is initiated, the

products will diffuse away from their respective electrodes and meet in the intervening solution where a mutual reaction regenerating the original uncoloured species takes place (Scheme 3.1).

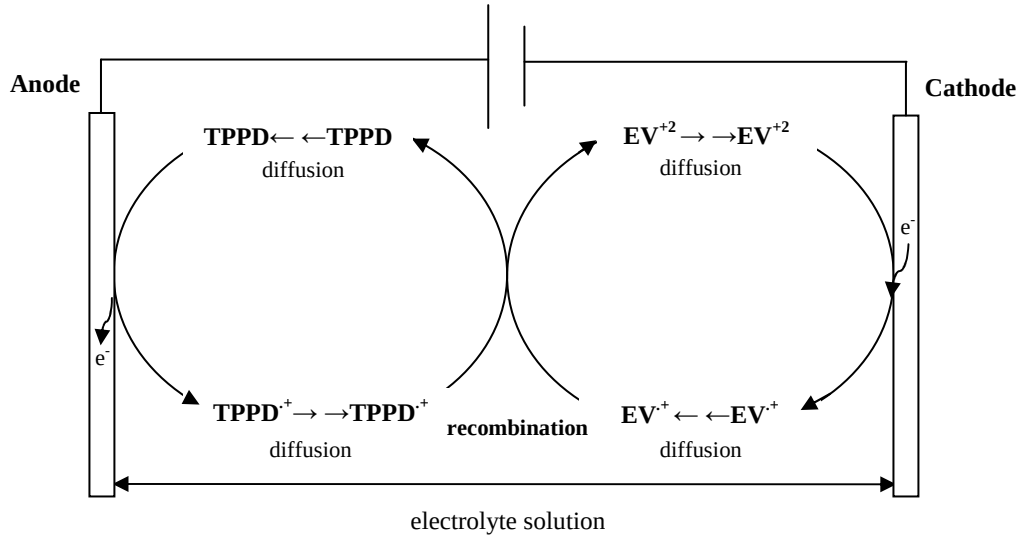

Scheme 3.1. Working principle of the all-solution ECD

As depicted in Fig. 3.2, in the switch off state both the ECDs are transparent in the vis-NIR region. Upon the application of 1.1 V two broad bands, in the visible and in the NIR regions, appeared simultaneously in each EDCs (Fig. 3.2.a and 3.2.b). The first band centered at 606 nm is ascribed to the radical cation $EV^{+\cdot}$ [142,143], which caused a deep blue coloration of the solution. The NIR band can be attributed to the formation of the radical cations of the triphenylamines, and arises from an intervalence charge-transfer (IV-CT) excitation [20]. As far as the electrochromic response of the TPPAHM is highlighted, it can be seen that, at increasing voltage, the intensity of the absorption bands, either in the visible or in the NIR, increased until a plateau was reached, at about 1.3 V. Upon further increase of the applied potential, the intensities of the above bands started to decrease, while another new band at 834 nm appeared. This behavior can be explained by the fact that the seconde oxidation of the TPPAHM gradually occures, as demonstrated by the spectroelectrochemical studies (Chapter 2).

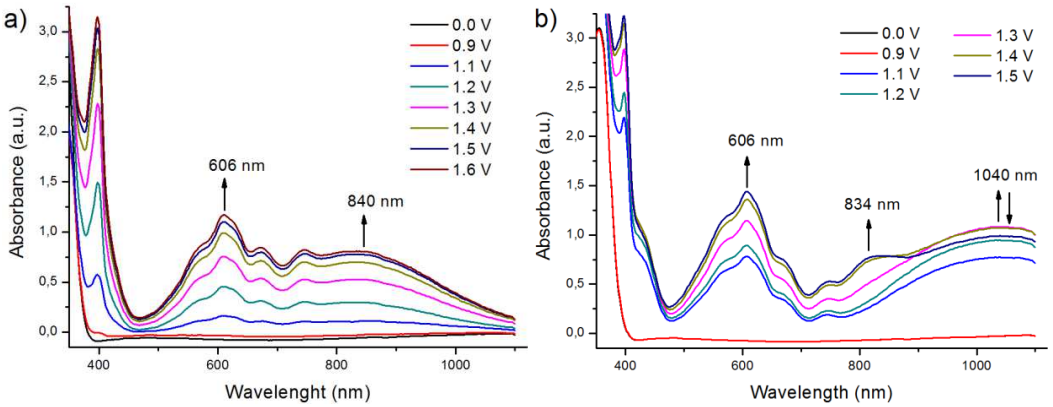

Fig. 3.2. Electrochromic behavior at difference voltages of the solution-phase (NMP/0.1 M TBAP) ECDs EV^{2+}/TPPA (a) and EV^{2+}/TPPAHM (b).

To probe the electrochromic stability of the complementary ECDs, we investigated the switching characteristics of thin layer (60 µm) two-ITO electrodes cells by monitoring the transmittance at 606 nm, 840 nm and 1040 nm during repeated redox stepping experiments between the highly transmissive state (0 V) and the darkening state achieved at 1.3 V for 5 s followed by 55 s delays between each redox switch.

From the insets of Fig. 3.3, where a few cycles are shown, it can be seen that the transmittance decreased during the dc pulse application since the population of the radical cations $EV^{\bullet+}$ and $TPPAHM^{+\bullet}$ ($TPPA^{+\bullet}$) gradually increased. Once the pulse had been removed the device returned rapidly to the bleached state because the recombination processes between the $EV^{\bullet+}$ and radical cations $TPPD^{\bullet+}$ took place (Scheme 3.1). The bleaching kinetic mainly depends on the cell gap-dependant diffusion of the above species from the electrodes surface to the bulk solution, provided if a sufficient concentration of supporting electrolyte is added, as is indeed the case here [144].

The electrochromic stability of both the devices was monitored by running 8000 cycles (Fig. 3.3.). In general, a systematic loss of the optical contrast occurred in both the devices as the number of darkening/bleaching cycles increased. However, independently on the wavelength used for the measurement, this phenomenon was faster in the EV^{2+}/TPPA device than in the other one containing the substituted triarylamine. In particular, within the first 2000 switching cycles a loss as large as 50% of the initial contrast was observed in the

EV^{2+}/TPPA device either at 606 nm (Fig. 3.3a) or at 840 nm (Fig. 3.3b). In the EV^{2+}/TPPAHM case, after the same number of cycles, the contrast loss was restricted to less than 17% at both the wavelengths monitored (Fig. 3.3a and b).

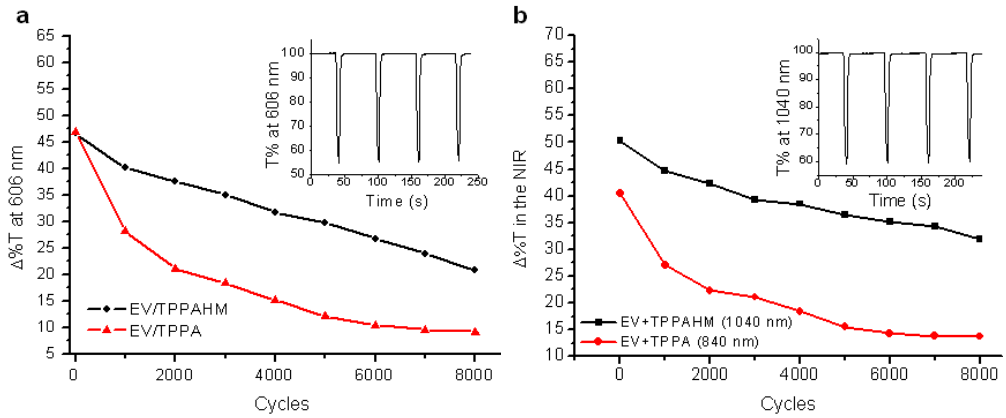

Fig. 3.3. Variation of the optical contrast (Δ%T) of both ECDs during 8000 switching cycles at 606 nm (a) and in the NIR at 840 nm (TPPA) and 1040 nm (TPPAHM) (b). Insets: first switching cycles at 606 nm (a) and 1040 nm (b).

It is clear that the instability of the EV^{2+}/TPPA device is not due the viologen radical cation known to be very stable [26,29,30, 34-37] but, rather, it should be attributed to the instability of the anodic component. It is likely that at the potential used in the switching experiment, a fraction of the TPPA is oxidized to its dication species. As already discussed in Chapter 2, $TPPA^{2+}$ is unstable and transforms into an adduct that is stable in its highly oxidized state. Therefore, the marked decrease of the transmittance during the switching cycles should be caused by a decrease of the concentration of the anodic components with increasing cycles. It is worth to recall that the anodic and the cathodic components within the complementary device work in a coupled way (Scheme 3.1) so that the reversibility and, consequently, the cyclability of the device is strongly affected by the stability of each component. In the EV^{2+}/TPPAHM device an improved electrochromic stability was observed. This should reflects the higher stability of the TPPAHM anodic system in which the electron-donating *para* substitutions decrease the reactivity of the oxidized radical species preventing potential coupling reaction involving the phenyl groups [20].

The higher performance of EV^{2+}/TPPAHM system and the better solubility of the TPPAHM due to its polar substituents, suggested us to

incorporate the viologen and TPPAHM in a thermoplastic polymeric matrix, using the NMP as plasticizer. The EC gel prepared (Scheme 3.2) were fully studies as reported in the following paragraphs.

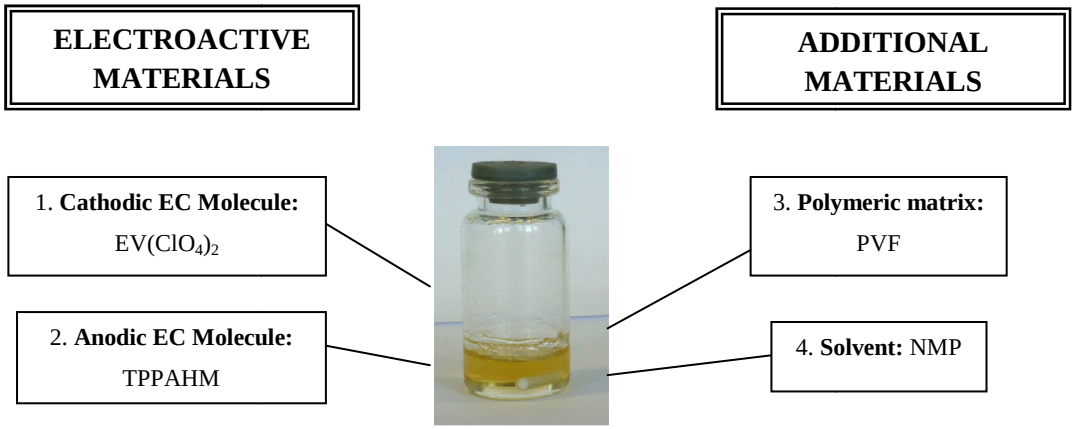

Scheme 3.2.

3.3.2. Electrochromic gel

Cyclic voltammetry (CV) on the EC gel were performed in a three-electrode cell. A silver wire (Ag wire) was used as pseudo-reference electrode and was located in between ITO glass electrodes. The Ag wire was coated by a thin film to prevent the electrical contact with the ITO electrodes. The CV of the EV/TPPAHM/PVF gel system is shown in Fig. 3.4. Both the reductive (triarylamine) and the oxidative (viologen) character of the system, can be observed. The two reversible reduction peaks at -0.95 and -1.34 V vs Fc/Fc^+ can be ascribed to the sequential one electron reduction steps of the viologen [26,29,30,34-37]. The two reversible peaks occurring at +1.17 V and +1.56 V vs Fc/Fc^+ have been assigned to the one electron step oxidation of the TPPAHM molecule.

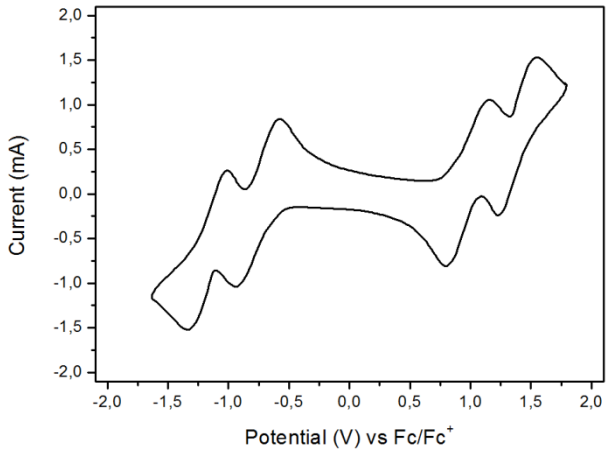

Fig. 3.4. Cyclic voltammogram of EV/TPPAHM system in PVF matrix (scan rate: 50 mV/s).

The electro-optical properties of the EC gel were exploited into a two-electrodes cell. Fig. 3.5a shows the three-dimensional absorbance-wavelength-applied potential correlation plot of this sample from 400 nm up to 1100 nm. In the switch off state (0 V), the ECD is completely transparent in this wavelength range. Upon increasing applied voltages two absorption bands centered at 606 nm and at 1000 nm appear in the spectrum, indicating that the one electron reduction of the EV^{+2} and the first oxidation of TPPAHM occur simultaneously. The ECD switches to a blue coloration because the radical cation $EV^{+\cdot}$ (absorbing at 606 nm) formed at the cathode, diffuses throughout the film. The NIR band is due to the IV-CT transition of the radical cation $TPPAHM^{+\cdot}$ as previously described. The intensity of this band gradually increases up to 1.2 V and starts to decrease at higher potentials when the second oxidation of the triarylamine takes place. The dication formed $TPPAHM^{++}$ does not exhibit the IV-CT transition, while it absorbs at about 800 nm [25]. At the same time, the band at 606 nm of the mono-reduced species $EV^{+\cdot}$ grows in intensity because evidently the second reduction has not yet occurred.

The switching kinetics of the ECD were calculated by chronoabsorptometry either at 606 nm (the wavelength of maximum absorption in the visible region), or at 880 nm in the NIR region (Fig. 3.5b).

Although the band of the maximum absorption in the NIR is centered at 1000 nm, we could not perform the switching measurements at this wavelength

because the acquisition time of the GENESYS 10S UV-Vis spectrophotometer was too long with respect to the response time of the device. Therefore, the chronoabsorptometry measurements in the NIR were performed with the JASCO V-550 UV-visible spectrophotometer, at 880 nm, a wavelength value close to the edge of its spectral window. In order to have the highest optical contrast at the two wavelengths chosen, the ECD was switched between the transparent (0 V) and the colored states obtained, respectively, at 1.2 V for the NIR and 1.6 V for the visible. The coloration time (τ_c) was calculated as the time needed to achieve 90% of the maximum transmittance change (Δ%T) in a single switching cycle. As reported in Table 3.1., and evidenced in Fig. 3.5.b, fast coloration times (τ_c) were observed either in the visible or in the NIR. In particular, the τ_c to obtain the blue coloration is comparable to other viologen-based EC gel with similar optical contrast [145]. The measured bleaching times (τ_b) were around 18 s. They were faster than those of analogous ECDs were an optical memory effect were observed with memory time higher than 5 min [145,146]. Notably, the ECD exhibits high optical contrasts at both the wavelengths monitored.

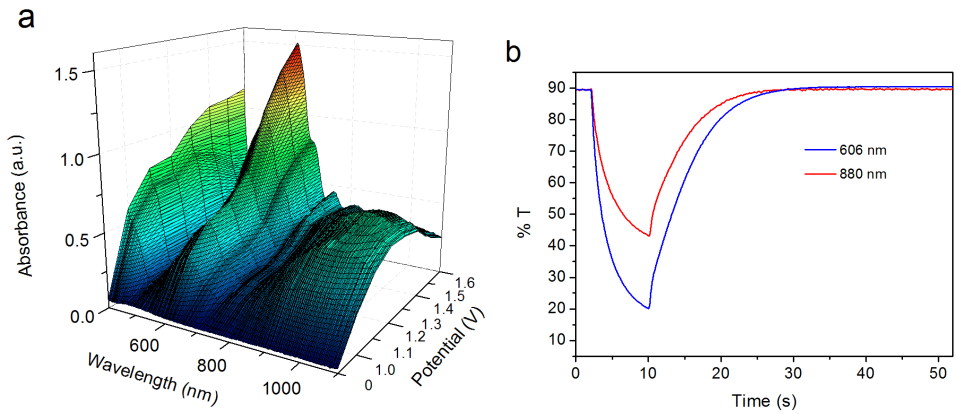

Fig. 3.5. 3D spectroelectrochemical behavior of the gel-based ECD from 0.0 V to 1.6 V and kinetic curves of the ECD obtained at 606 nm and 808 nm (b).

At the same wavelengths we calculated, the coloration efficiency, CE (η) by the equation described in Chapter 1:

$$\eta = \frac{\Delta \mathrm{OD}}{Q_i} = \log\left[T_b/T_c\right]/Q_i$$

Table 3.1 reports the CE values for the ECD with an area of 2 x 2 cm^2. The CE value exhibited by this device at 606 nm is one of the highest ever reported in the literature for similar viologen-based EC gel device [145]. Also, the CE value measured at 880 nm was rather good despite the fact that it was not determined at the wavelength of maximum absorption in the NIR region.

Table 3.1. Response times for the coloration and bleaching state and CE of the EC film measured at 606 and 880 nm.

Wavelength (nm)	Operating Voltage (V)	Δ%T	τ_c (s)	τ_b (s)	CE (cm^2/C)
606	1.6	69.4	4.8	18.4	118.65
880	1.2	46.5	5.3	18.7	47.08

Finally, the applicability of the EC gel was also tested in a flexible device made of two conductive PET electrodes. As shown in Fig. 3.6., the device become uniformly colored upon the application of 1.6 V and the color was identical to that of the glass-electrode EC cell, indicating that the EC gel works well even in the flexible device.

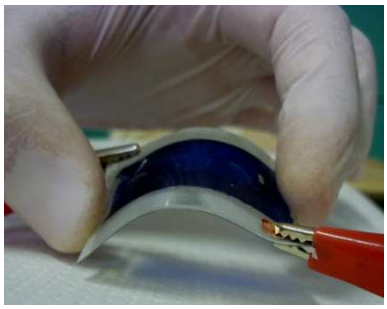

Fig. 3.6. Electrochromic behavior of the flexible EC device at 1.6 V.

3.4. Conclusions

We presented two new solution-phase complementary ECDs based on NIR electroactive triphenylamines (TPPA and TPPAHM) and EV^{2+} as cathodic molecule that was used to improve the optical contrast in the visible. The application of voltages as low as 1.3 V allowed to switch the devices between the highly transmissive state (0 V) and the darkening state with high transmittance

change in the NIR region too. The electrochemical investigation and the EC switching study revealed that, in contrast to its unsubstituted analogue (TPPA) the TPPAHM is rather stable, due to the *para* substitution of the phenyl moieties that prevent the coupling reaction of the radical cations. In addition because the high polarity of the substituents the TPPAHM showed a better solubility than the TPPA in polar aprotic solvent such as NMP that can be also used as plasticizer in EC gel. The potentialities of EV^{+2}/TPPAHM system were tested in a gel-based EC device. A new transparent EC gel with dual electrochromic behavior in the visible and in the NIR was prepared and studied by cyclic voltammetry, UV-vis-NIR spectroscopy and EC switching studies. The cyclic voltammetry experiment revealed a good electrochemical behavior of the cathodic and anodic materials dispersed into a polymeric matrix. The switching studies indicated that low operating voltages are enough to obtain high optical contrasts in the visible and in the NIR regions with fast response times. The EC gel has shown very good coloration efficiency values and also a uniform coloration when it was tested in a flexible device. It is expected that the present ECD has high potentialities as candidate for smart windows applications.

CHAPTER 4

Structural characterization of new thienoviologen mesogens

4.1. Introduction

Extended viologens have been presented in Chapter 1 as a very interesting class of electron-acceptor compounds for organic electronics. Viologens incorporating oligothiophene conducting spacer between the pyridinium rings (thienoviologens) provide very interesting electrochromic properties [71, 147]. In addition, high photoluminescence (fluorescence) was observed in these materials [61-69]. The field of application of these compounds can be expanded through the synthesis of viologens with liquid-crystalline properties [106]. In this way, the resultant materials might exhibit functional order in the bulk that is expected to enhance the performances of electronic devices [96]. The few examples of π-conjugated ionic liquid-crystals reported in the literature demonstrate that such materials can combine relevant anisotropic electron and ion transport properties [97, 98]. Liquid-crystal extended viologens seems to be very promising candidate to obtain new ordered functional materials exhibiting redox-active supramolecular assemblies useful for various electronic and optoelectronic devices. Therefore, the strategy aimed at the design and synthesis of this new class of n-type semiconducting materials is worth to be pursued. To this aim, an appropriate choice of the substituent on the nitrogen atoms of the pyridinium rings as well as the introduction of mobile substituents in the bridging unit, can be used to confer mesomorphic properties to these compounds. However, to date, no such materials have been yet reported in the literature. Herein we present the study of the mesomorphic properties of a newly synthesised class of π-extended viologens dications, 4,4'-(2,2'-bithiophene-5,5'-diyl)bis(1-alkylpyridinium)$^{2+}$ (***m*V^{2+}s**), that bears a bithiophene bridging unit and alkyl-chains of different length (*m* = 9-11)

on the nitrogen atoms. Differential scanning calorimeter (DSC) analysis, polarizing optical microscopy observations (POM) and X-ray diffraction pattern (XRD) revealed that the choice of the anion is crucial for disclosing the liquid crystalline properties of the viologen dications.

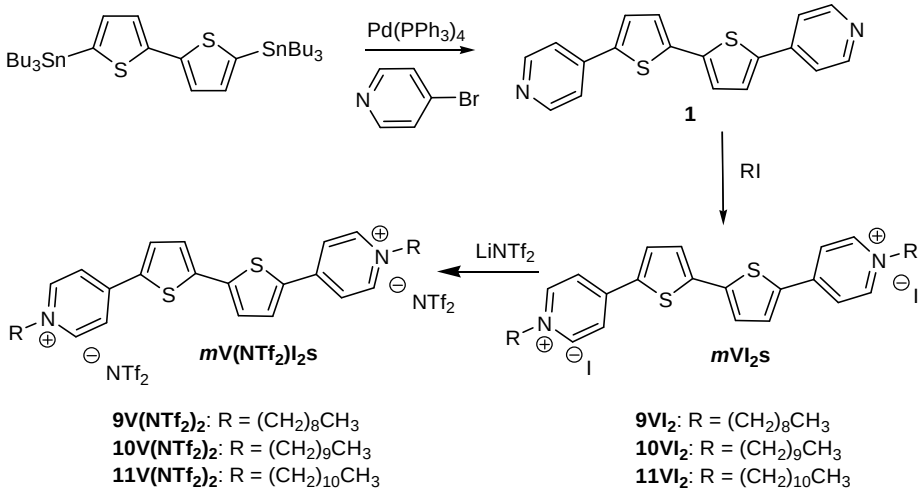

Scheme 4.1 Synthetic route to thienoviologen mesogens

4.2. Experimental

4.2.1. Materials

The thienoviologen mesogens were synthesized as reported in the Scheme 4.1. 5,5'-Bis(4-pyridyl)-2,2'-bithiophene (**1**) was prepared by Stille coupling between 4-bromopyridine and 5,5'-bis(tri-*n*-butylstannyl)-2,2'-bithiophene according to a reported literature procedure [148]. The thienoviologens bis(triflimide) **mV(NTf$_2$)$_2$** was prepared in two steps procedure as described below. All other materials were commercially available and were used without further purification.

In a Schlenk flask, 5,5'-Bis(4-pyridyl)-2,2'-bithiophene **1** (1g, 3.12 mmol) was suspended under nitrogen atmosphere in 70 mL of anhydrous chloroform. To the stirred suspension was added the appropriate iodoalcane (31.2 mmol) [iodononane: 7.9 g; iododecane: 8.4 g; iodoundecane: 8.8 g] and the mixture was heated at 80 °C for 24 h. After cooling, the solvent was removed under vacuum and to the resulting mixture was added diethyl ether (50 mL). The suspension was

filtered, and the solid residue was washed several times with diethyl ether (6×10 mL) to give pure thienoviologens bis(iodide) **mVI$_2$s**.

4,4'-(2,2'-bithiophene-5,5'-diyl)bis(1-nonylpyridinium) iodide (**9VI$_2$**). Yield: 1.4 g, starting from 1 g of **1** (54%). Orange solid, mp 230-232°C. IR (KBr): ν = 2921(m), 1633(s), 1529 (m), 1433 (m), 1226 (m), 1115 (m), 803 (m), 617 (m) cm^{-1}; ^{1}H NMR (300 MHz, $CDCl_3$): δ = 9.07 (d, J = 7.0, 4 H, H-2 + H-2' + H-6 + H-6'on pyridine rings), 8.26 (d, J = 7.0, 4 H, H-3 + H-3'+ H-5 + H-5' on pyridine rings), 8.05 (d, J = 4.0, 2 H, H-3 + H-3'on thiophene rings), 7.28 (d, J = 4.0, 2 H, H-4 + H-4'on thiophene rings), 4.73 (t, J = 7.3, 4 H, 2 $^+$NCH_2CH$_2$(CH$_2$)$_6$CH$_3$), 2.07-1.96 (m, 4 H, 2 $^+$NCH$_2$CH_2(CH$_2$)$_6$CH$_3$), 1.45-1.20 (m, 24 H, 2 $^+$NCH$_2$CH$_2$(CH_2)$_6$CH$_3$), 0.87 (t, J = 6.9, 6 H, 2 $^+$NCH$_2$CH$_2$(CH$_2$)$_6$CH_3); anal. calcd for $C_{36}H_{50}I_2N_2S_2$ (828.73): C 52.17, H 6.08, I 30.63, N 3.38, S 7.74; found C 52.21, H 6.06, I 30.58, N 3.39, S 7.76.

4,4'-(2,2'-bithiophene-5,5'-diyl)bis(1-decylpyridinium) iodide (**10VI$_2$**). Yield: 1.3 g, starting from 1 g of **1** (49%). Orange solid, mp 213-216°C. IR (KBr): ν = 2923 (m), 1633 (m), 1525 (m), 1434 (m), 1224 (m), 1111 (m), 796 (m), 616 (m) cm^{-1}; ; ^{1}H NMR (300 MHz, DMSO-d_6): δ = 9.02 (d, J = 6.4, 4 H, H-2 + H-2' + H-6 + H-6'on pyridine rings), 8.40 (d, J = 6.4, 4 H, H-3 + H-3'+ H-5 + H-5' on pyridine rings), 7.87 (d, J = 4.1, 2 H, H-3 + H-3'on thiophene rings), 7.70 (d, J = 4.1, 2 H, H-4 + H-4'on thiophene rings), 4.53 (t, J = 6.8, 4 H, 2 $^+$NCH_2CH$_2$(CH$_2$)$_7$CH$_3$), 1.98-1.83 (m, 4 H, 2 $^+$NCH$_2$CH_2(CH$_2$)$_7$CH$_3$), 1.40-1.10 (m, 28 H, 2 $^+$NCH$_2$CH$_2$(CH_2)$_7$CH$_3$), 0.85 (t, J = 6.9, 6 H, 2 $^+$NCH$_2$CH$_2$(CH$_2$)$_7$CH_3); anal. calcd for $C_{38}H_{54}I_2N_2S_2$ (856.79): C 53.27, H 6.35, I 29.62, N 3.27, S 7.48; found C 53.21, H 6.37, I 29.66, N 3.26, S 7.50.

4,4'-(2,2'-bithiophene-5,5'-diyl)bis(1-undecylpyridinium) iodide (**11VI$_2$**). Yield: 1.3 g, starting from 1 g of **1** (47%). Orange solid, mp 226-229 °C. IR (KBr): ν = 2921(m), 1633(s), 1529 (m), 1433 (m), 1226 (m), 1115 (m), 803 (m), 617 (m) cm^{-1}; ^{1}H NMR (300 MHz, $CDCl_3$): δ = 9.03 (d, J = 6.7, 4 H, H-2 + H-2' + H-6 + H-6'on pyridine rings), 8.25 (d, J = 6.7, 4 H, H-3 + H-3'+ H-5 + H-5' on pyridine rings), 8.01 (d, J = 4.1, 2 H, H-3 + H-3'on thiophene rings), 7.25 (d, J = 4.1, 2 H, H-4 + H-4'on thiophene rings), 4.72 (t, J = 7.1, 4 H, 2 $^+$NCH_2CH$_2$(CH$_2$)$_8$CH$_3$), 2.10-1.96 (m, 4 H, 2 $^+$NCH$_2$CH_2(CH$_2$)$_8$CH$_3$), 1.47-1.19 (m, 32 H, 2

$^{+}NCH_2CH_2(CH_2)_8CH_3$), 0.87 (t, *J* = 7.0, 6 H, 2 $^{+}NCH_2CH_2(CH_2)_8CH_3$); anal. calcd for $C_{40}H_{58}I_2N_2S_2$ (884.84): C 54.30, H 6.61, I 28.68, N 3.17, S 7.25; found C 54.33, H 6.60, I 28.65, N 3.16, S 7.26.

To a stirred solution of thienviologen bis(iodide) **2** (1 mmol) [**9VI$_2$**:0.83 g **10VI$_2$**: 0.85 g; **11VI$_2$**: 0.88 g] in 300 mL of methanol, was added lithium triflimide (1.15 g; 4 mmol). The mixture was stirred at room temperature for 15 h. The solvent was removed under vacuum and to the resulting mixture was added water (50 mL). The suspension was filtered, and the solid residue was washed several times with water (4×10 mL) to give pure thienoviologens bis(triflimide) **mV(NTf$_2$)$_2$** .

4,4'-(2,2'-bithiophene-5,5'-diyl)bis(1-nonylpyridinium) triflimide [**9V(NTf$_2$)$_2$**]. Yield: 0.54 g, starting from 0.83 g of **9VI$_2$** (48%). Yellow solid, mp 132-135°C. IR (KBr): *v* = 2925 (m), 1634 (m), 1530 (m), 1434 (m), 1358 (s), 1333 (m), 1193 (s), 1138 (m), 1055 (m), 810 (m), 611 (m) cm^{-1}; ^1H NMR (500 MHz, DMSO-d_6): δ = 9.02 (d, *J* = 6.5, 4 H, H-2 + H-2' + H-6 + H-6'on pyridine rings), 8.41 (d, *J* = 6.4, 4 H, H-3 + H-3'+ H-5 + H-5' on pyridine rings), 8.34 (d, *J* = 4.0, 2 H, H-3 + H-3'on thiophene rings), 7.87 (d, *J* = 4.0, 2 H, H-4 + H-4'on thiophene rings), 4.53 (t, *J* = 7.2, 4 H, 2 $^{+}NCH_2CH_2(CH_2)_6CH_3$), 1.98-1.86 (m, 4 H, 2 $^{+}NCH_2CH_2(CH_2)_6CH_3$), 1.36-1.20 (m, 12 H, 2 $^{+}NCH_2CH_2(CH_2)_6CH_3$), 0.86 (t, *J* = 6.2, 6 H, 2 $^{+}NCH_2CH_2(CH_2)_7CH_3$); ^{19}F NMR (471MHz, DMSO-d_6): δ = –74.0 (s, 3 F, CF_3); MS (ESI^+, direct infusion): *m/z* = 1158 [$(M+Na)^+$]; anal. calcd for $C_{40}H_{50}F_{12}N_4O_8S_6$ (1135.22): C 42.32.17, H 4.44, F 20.08, N 4.94, S 16.95; found C 42.36, H 4.45, F 20.10, N 4.93, S 16.99.

4,4'-(2,2'-bithiophene-5,5'-diyl)bis(1-decylpyridinium) triflimide [**10V(NTf$_2$)$_2$**]. Yield: 0.66 g, starting from 0.85 g of **10VI$_2$** (57%). Yellow solid, mp 138-141°C. IR (KBr): = 2925 (m), 1634 (m), 1527 (m), 1435 (m), 1359 (s), 1334 (m), 1193 (s), 1135 (m), 1052 (m), 804 (m), 614 (m) cm^{-1}; ^1H NMR (500 MHz, DMSO-d_6): δ = 9.02 (d, *J* = 6.4, 4 H, H-2 + H-2' + H-6 + H-6'on pyridine rings), 8.40 (d, *J* = 6.4, 4 H, H-3 + H-3'+ H-5 + H-5' on pyridine rings), 8.35 (d, *J* = 4.0, 2 H, H-3 + H-3'on thiophene rings), 7.87 (d, *J* = 4.0, 2 H, H-4 + H-4'on thiophene rings), 4.53 (t, *J* = 7.1, 4 H, 2 $^{+}NCH_2CH_2(CH_2)_7CH_3$), 1.97-1.86 (m, 4 H, 2 $^{+}NCH_2CH_2(CH_2)_7CH_3$), 1.36-1.19 (m, 14 H, 2 $^{+}NCH_2CH_2(CH_2)_7CH_3$), 0.86 (t, *J* = 6.5, 6 H, 2 $^{+}NCH_2CH_2(CH_2)_7CH_3$); ^{19}F NMR (471MHz, DMSO-d_6): δ = –73.9 (s,

3 F, CF_3); MS (ESI^+, direct infusion): *m/z* = 1186 [(M+Na]; anal. calcd for $C_{42}H_{54}F_{12}N_4O_8S_6$ (1163.27): C 43.36, H 4.68, F 19.60, N 4.82, S 16.54; found C 43.42, H 4.68, F 19.63, N 4.83, S 16.50.

4,4'-(2,2'-bithiophene-5,5'-diyl)bis(1-undecylpyridinium) triflimide [**11V(NTf$_2$)$_2$**]. Yield: 0.56 g, starting from 0.88 g of **11VI**$_2$ (47%). Yellow solid, mp 155-157°C. IR (KBr): *v* = 2922 (m), 1634 (m), 1529 (m), 1435 (m), 1348 (m), 1184 (s), 1137 (m), 1057 (m), 809 (m), 650 (m) cm^{-1}; ^1H NMR (300 MHz, $CDCl_3$): δ = 8.24 (d, *J* = 2.0, 1 H, H-4), 7.46-7.38 (m, 3 H, aromatic), 7.37-7.31 (m, 2 H, aromatic), 7.26-7.20 (m, 3 H, aromatic), 7.17 (distorted dd, *J* = 8.5, 2.0, 1 H, H-6), 7.11 (distorted d, *J* = 8.9, 1 H, H-7), 5.17 (s, 2 H, C*H*$_2$Ph), 3.77 (s, 3 H, CO_2Me); ^{19}F NMR (471MHz, DMSO-d_6): δ = –73.9 (s, 3 F, CF_3); MS (ESI^+, direct infusion): *m/z* = 1214 [$(M+Na)^+$]; anal. calcd for $C_{44}H_{58}F_{12}N_4O_8S_6$ (1191.32): C 44.36, H 4.91, F 19.14, N 4.70, S 16.15; found C 44.40, H 4.92, F 19.11, N 4.71, S 16.11.

4.2.2. Methods

Melting point analyses were performed on a Linkam (LTS350 stage, TP94 System Controller) at scan rate of 10 °C/min. ^1H NMR spectra were recorded at 25 °C in $CDCl_3$ or DMSO-d_6 on a Avance 300 Bruker NMR spectrometer at 300 MHz or on a Avance 500 Bruker NMR spectrometer at 500 MHz with Me_4Si as internal standard. ^{19}F NMR spectra were recorded at 25 °C in DMSO-d_6 on a Avance 500 Bruker NMR spectrometer at 471 MHz with CF_2Br_2 as internal standard. Chemical shifts (δ) and coupling constants (*J*) are given in ppm and in Hz, respectively. IR spectra were taken with a JASCO FT-IR 4200 spectrometer. Microanalyses were carried out with a Carlo Erba Elemental Analyzed Mod. 1106. Mass spectra were obtained using a ABSciex API 2000 mass spectrometer equipped with a turbo ion spray ionization source in the positive mode [ion spray voltage (IS) 4500 V; curtain gas 10 psi; temperature 25 °C; ion source gas (1) 20 psi; declustering and focusing potentials 50 and 400 V, respectively].

The transition temperatures and enthalpy changes of compounds were determined by differential scanning calorimetry (DSC) using a DSC-NETZSCH 200 calorimeter. The heating and cooling rate was 5 °C min^{-1} and the sample mass was around 4.0 mg. A Leitz, Laborlux 12 POL polarizing optical microscopy

equipped with Linkam LTS350 heating stage was used for visual observation of optical textures. The powder X-Ray diffraction patterns were obtained by using a Bruker AXS General Area Detector Diffraction System (D8 Discover with GADDS) with Cu-Ka radiation; the area detector was placed at a distance of 20 cm from the sample and at an angle $2\theta_D$ of 14°. Measurements were performed by charging samples in Lindemann capillary tubes with inner diameters of 0.5 mm. A CalCTec (Italy) heating stage was used to heat the samples at a rate of 5°C min^{-1} to the appropriate temperature.

4.3. Results and discussion

The mesophases of these compounds were studied by POM, DSC and XRD. Notably, it was found that, while the compounds of the homologous series **mV(NTf$_2$)$_2$** exhibit a rich and complex mesomorphism (Table 4.1) none of those of the ***m*VI$_2$s** series is liquid crystalline. This profound difference reflects the strong influence of the anion in disclosing the liquid crystalline nature of the thienoviologens dication mV^{2+}.

Table 4.1. Transition temperature (T /°C) and transition enthalpy values (kJ mol^{-1}, in brackets) for ***m*V(NTf$_2$)$_2$s** [a]

Compound		phase $\xrightarrow{\text{T / °C [}\Delta\text{H / kJ mol}^{-1}\text{]}}$ phase
9V(NTf$_2$)$_2$	1st heating cooling	$K \xrightarrow{67.8[15.4]} K' \underset{Col_{2ro} \xleftarrow{109.2[3.4]}}{\xrightarrow{113.5[1.3]}} Col_{1ro} \underset{\xleftarrow{128.8\,[14.9]}}{\xrightarrow{131.9\,[17.1]}} IL$
10V(NTf$_2$)$_2$	1st heating cooling	$K \xrightarrow{114.8\,[3.0]} Col_{rd} \underset{\text{freezed SmA} \xleftarrow{117.5\,[0.8]} SmA}{\xrightarrow{135.4\,[3.6]}} IL \xleftarrow{126.2\,[5.0]}$
11V(NTf$_2$)$_2$	1st heating cooling	$K \xrightarrow{117.3\,[14.2]} Col_{rd} \underset{\text{freezed SmA} \xleftarrow{124.3\,[18.1]} SmA}{\xrightarrow{151.5\,[4.5]}} IL \xleftarrow{159.2\,[5.8]}$

[a]Determined by DSC at a scan rate of 5 °C/min; abbreviations: K = crystalline solid, Col_{ro} and Col_{rd} = respectively, ordered and disordered columnar rectangular phases, SmA = smectic A phase, IL = isotropic liquid state.

The DSC traces relative of compounds mV(NTf$_2$)$_2$ in the first heating and cooling scans are shown in Fig. 4.1. For the compound **9V(NTf$_2$)$_2$** a first transition at low temperature with a large enthalpy change was observed followed by a transition at about 115 °C exhibiting a very low ΔH (Table 4.1). Upon further heating, the isotropic liquid state was reached. When cooled from the melt, the growth of dendritic aggregates was observed (Fig. 4.2a). These transformed into a mosaic structure (Fig. 4.2b) typical of columnar mesophases [149] below 120 °C. Upon further cooling across the second transition found by DSC (Fig. 4.1a), a striated mosaic texture appeared (Fig. 4.2c). This optical texture was almost entirely kept on further cooling down to room temperature (Fig. 4.2d) indicating that no additional transitions took place, in agreement with the DSC analysis that did not detect any enthalpy change below 110 °C.

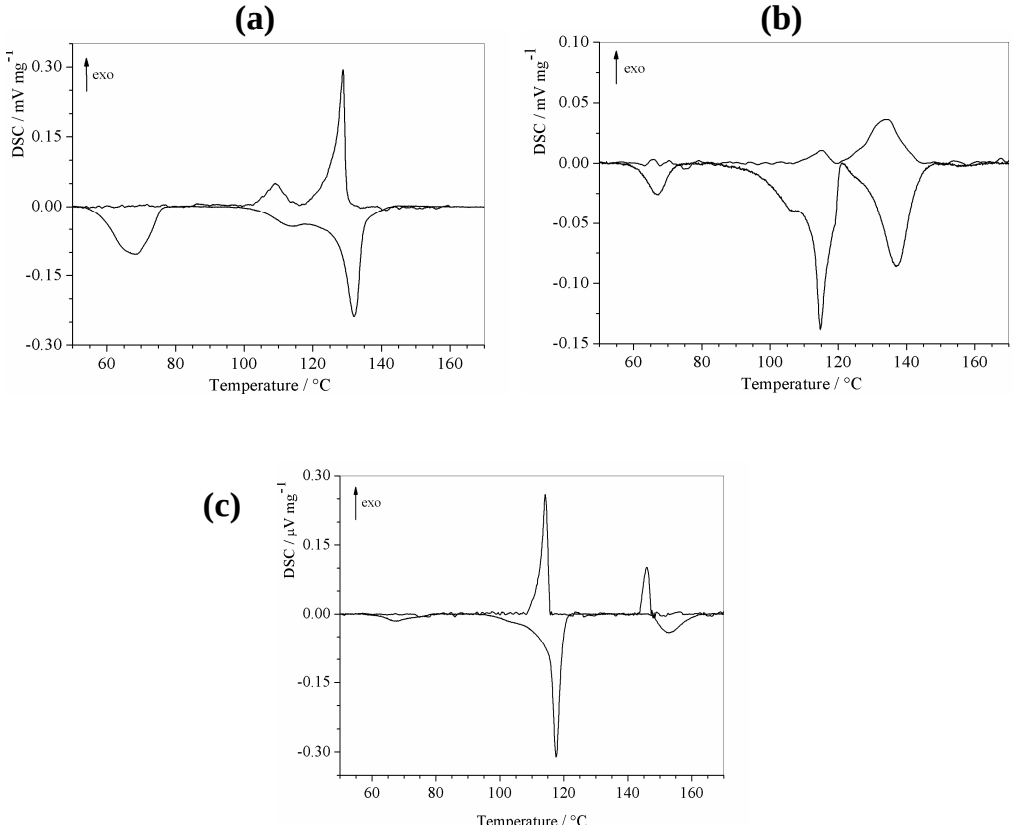

Fig. 4.1. DSC traces of *m*V(NTf$_2$)$_2$s with m = 9 (a), m = 10 (b), m = 11 (c) for the 1st heating and cooling scan at a rate of 5 °C/min.

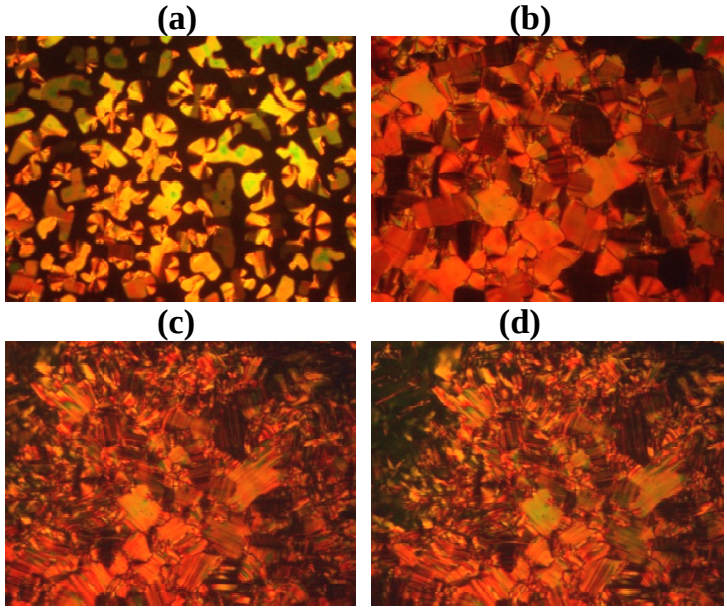

Fig. 4.2. Representative optical textures for the mesophase behaviour of compound **9V(NTf$_2$)$_2$** upon cooling from the IL state. (a) Dendritic aggregates growth of the Col$_{rd}$ phase (T = 133 °C) separating from the isotropic melt that transform into (b) a mosaic texture on further cooling (T=118 °C). Striated mosaic texture of the Col$_{ro}$ phase at 100 °C (c). Paramorphic behaviour of the Col$_{ro}$ phases at 30 °C (d) with very subtle differences compared to plate (c).

The mesophase behaviour of the other two compounds of the series with *m* = 10-11 was different. Before reaching the isotropic liquid state, they shared a main transition at about 115-120 °C with large ΔH values (Fig. 4.1 b-c; Table 4.1), that led to a liquid crystalline phase. POM observation of dendritic aggregates on thin films of these materials, suggested that this should be a columnar mesophase (Fig. 4.3.a). The range of existence of these phases was very narrow for **10V(NTf$_2$)$_2$** and relatively wide (~30°C) for **11V(NTf$_2$)$_2$**. Upon cooling from the IL state of both **10V(NTf$_2$)$_2$** and **11V(NTf$_2$)$_2$**, the growth of bâtonnetes was observed that, on cooling, transformed into the typical fan-shaped texture of a smectic phases (Fig. 4.3b). Upon further cooling below 115 °C, striated fan-shaped textures with striations across the fans were observed (Fig. 4.3c). These textures were maintained during the cooling down to room temperature (Fig. 4.3d) indicating that no further transition occurred. Interestingly, the thermal analysis showed that the melting point (m.p.) of *m*V(NTf$_2$)$_2$s monotonically increases with the alkyl-chain length (*m*) in the temperature range 130-175 °C. In contrast, we did not find any similar trend in the iodide homologous series for which, comparatively higher m.p. values were measured.

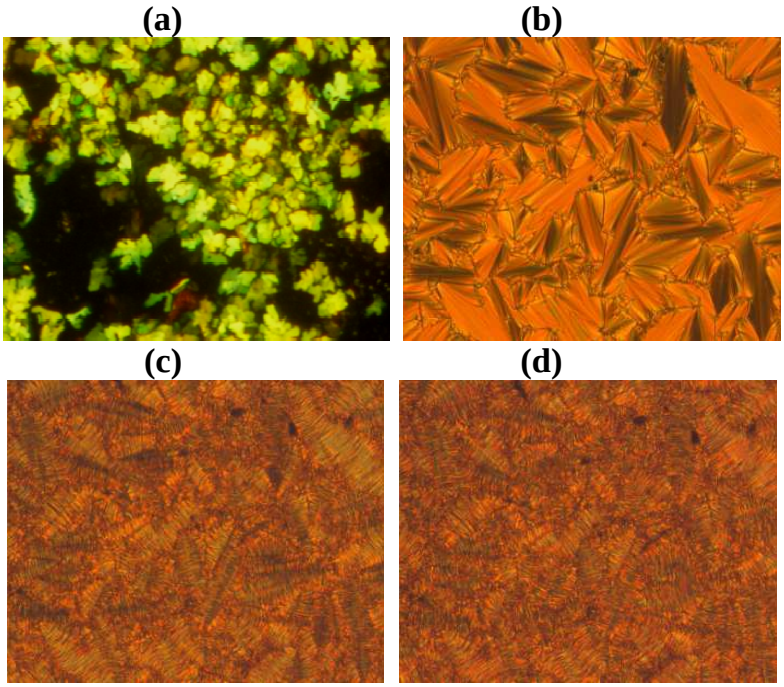

Fig. 4.3. Representative optical textures for the mesophase behaviour of compound **11V(NTf$_2$)$_2$** during (a) the 1st heating scan (123 °C) and on cooling from the IL state at (b) 140 °C, (c) 100 °C and (d) 30 °C. Plate (a) illustrates the typical dendritic aggregates of the columnar phase. On cooling from the isotropic melt (b) the typical fan-shaped texture of a SmA phase appeared that transformed into (c) a striated fan-shaped texture on further cooling. (d) This structure was maintained during the cooling down to room temperature.

To confirm the phase identification, the mesophase of compounds *m*V(NTf$_2$)$_2$s was investigated by XRD.

In the case of compound **9V(NTf$_2$)$_2$** the X-ray pattern recorded at 120 °C on cooling shows two reflections in the small angle region which, together with the other peaks in the middle angle range, can be indexed on the basis of a rectangular columnar structure, with the first intense peaks assigned as (20) and (11) reflections. This diffraction pattern (Fig. 4.4) corresponded to rectangular lattice constants: a = 55.8 Å and b = 22.6 Å.

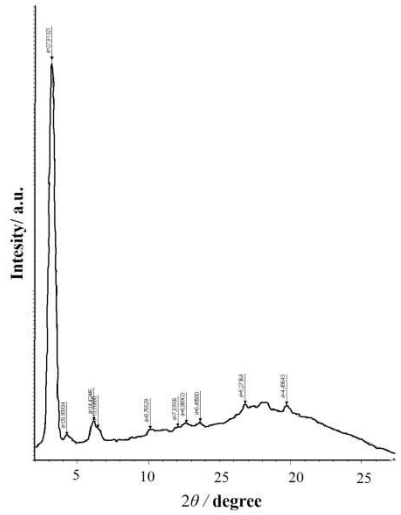

Fig. 4.4. Powder pattern of $9V(NTf_2)_2$ recorded at 120 °C on cooling

The extinction rules for the rectangular lattice indicates a Col_r phase with $P2_1/a$ symmetry. Other weak diffraction lines were observed in the wide angle region, underneath the broad halo typical of the liquid-like disorder of the aliphatic chains centred at about 4.6 Å. In particular, the line corresponding to d = 4.5 Å can be considered the diffraction due to the columnar stacking of the core parts of the molecules. This value is significantly higher than the expected value of 3.4/3.5 Å for π-π stacking with face-to-face interactions of aromatic moieties, suggesting the association of cations into dimers through bridging interacting anions. Most probably, we can hypothesize that hydrogen bonds between the pyridinium moieties and the anions occur. Indeed, the Z value can be calculated as about 4, assuming a density ρ equal to unity, which corresponds to 2 molecules included in each disk. The association of molecules of **$9V(NTf_2)_2$** into dimers as shown in Fig. 4.5 a gives rise to a disk-like structure, with an elliptic columnar cross section typical of rectangular columnar organizations, consisting of central cores, (interacting through electrostatic forces and hydrogen bonds) and peripheral alkyl chains. Decreasing the temperature, the columnar phase is kept until room temperature, with a slight variation of the lattice parameters (a = 54.2 Å and b= 22.0 Å) and the appearance of more intense reflections in the wide angle region (centred at 4.2 and 3.5 Å in the PXRD pattern recorded at 90 °C) indicative of a higher degree of order within the columns.

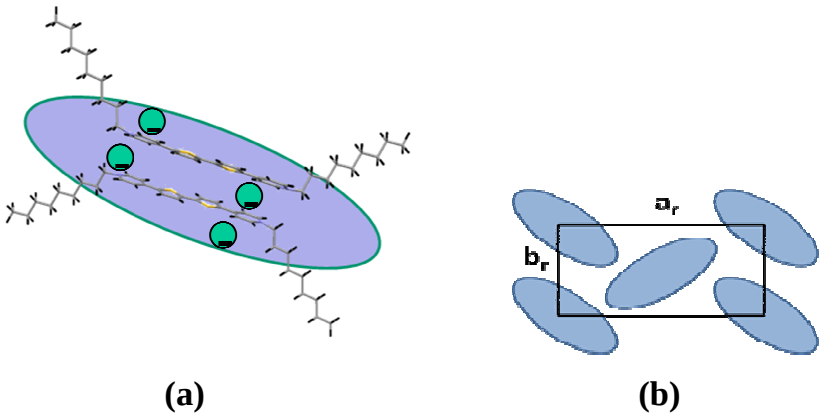

Fig. 4.5. Proposed model of dimerization of rod-like **9V(NTf$_2$)$_2$** molecules in the formation of disk-like aggregation (a) and schematic illustration of the Col$_r$ $P2_1/a$ mesophase.

The elongation of the alkyl chains from **9V(NTf$_2$)$_2$** to **10V(NTf$_2$)$_2$** and **11V(NTf$_2$)$_2$** induces an increase of mobility, enhancing the rod-shape side area, and therefore a different thermal behaviour. Indeed, compound **10V(NTf$_2$)$_2$** shows a highly disordered columnar rectangular mesophase in the first heating cycle (lattice parameters a = 60.2 Å and b = 22.6 Å) (Fig. 4.6a). The overall organization transforms into a lamellar liquid crystalline phase already in the first cycle at 125 °C on cooling from the isotropic state. The powder pattern shows diffractions due to the (001) and (002) planes in the small angle region, with a measured interplanar distance of 30.4 Å (Fig. 4.6b).

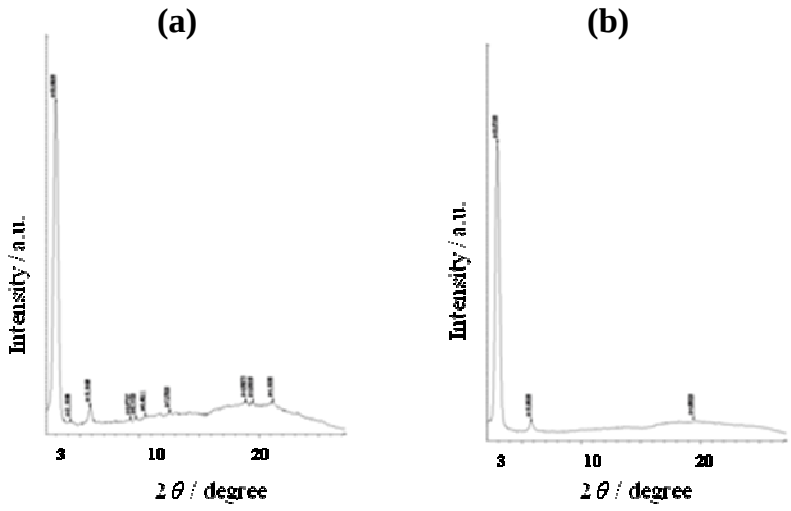

Fig. 4.6. Powder pattern of **10V(NTf$_2$)$_2$** recorded at 118 °C on heating in the first heating cycle (a) and at 125 °C on heating in the second heating cycle.

Therefore, the shape of the molecules switches from disk-like to rod-like with temperature and the transition between the two mesophase organization (columnar over calamitic and the opposite) is reproducible in all heating and cooling cycles. On the other hand, in the case of compound **11V(NTf$_2$)$_2$**, a disordered columnar rectangular mesophase is observed only in the first heating cycle (lattice parameters a = 51.4 Å and b = 41.3 Å) (Fig. 4.7a), while, when transformed into the lamellar liquid crystalline phase from the isotropic state (Fig. 4.7b), is definitively lost in all heating and cooling cycles.

In both cases, comparing the d values of about 30 and 33 Å with the length of the dications in **10V(NTf$_2$)$_2$** and **11V(NTf$_2$)$_2$**, respectively, calculated in their maximum elongation with all *trans* chains conformation of about 40 and 43 Å, combined with the POM observation, it is possible to propose an orthogonal lamellar mesophase of the SmA type, with high interdigitation between alkyl chains.

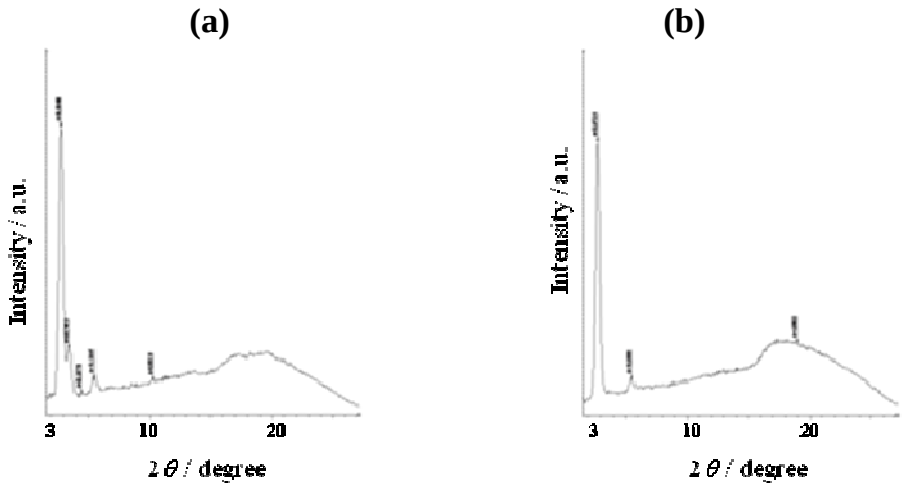

Fig. 4.7. Powder pattern of **11V(NTf$_2$)$_2$** recorded at 130 °C on heating in the first heating cycle (a) and at 130 °C on heating in the second heating cycle.

Fig. 4.8 summarizes the mesophase behaviour of the *m*V(NTf$_2$)$_2$ and highlights its strong dependence on the length of the alkyl chains in the positions *N*,*N'*of the pyridinium moiety. All of these compounds give rise to columnar rectangular mesophases in the first heating scan. However, the stability of this mesophase seems to decrease with the elongation of the chains (Fig. 4.8a). A reproducible

mesomorphism was obtained only from the 2nd heating scan and the columnar phase was definitely lost at this stage for **11V(NTf$_2$)$_2$** compound (Fig. 4.8b).

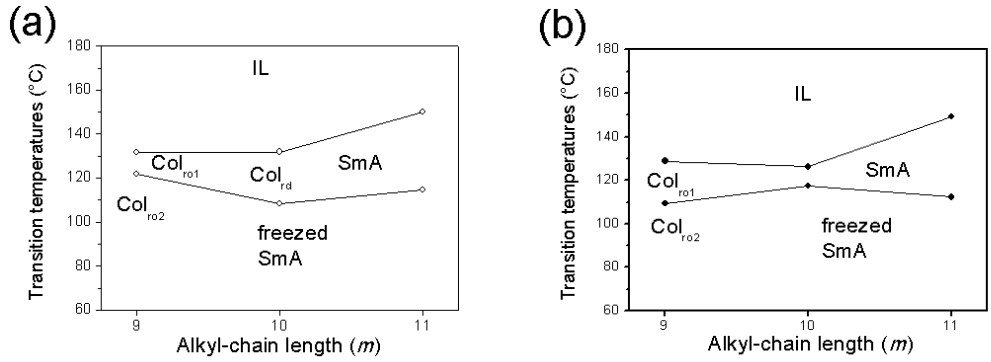

Fig. 4.8. Mesophase behaviour of compounds mV(NTf2)2 with m = 9-11 in (a) the second heating scan and (b) the second cooling scan.

4.4. Conclusions

We have designed and synthesized new thienoviologen derivatives which are able to self-assemble and form ordered mesophases. Despite the rod-like shape of the dications ***m*V^{2+}s** we observed that the compound containing bis(triflimide) anion **[*m*V(NTf$_2$)$_2$s]** self-assembled into columnar rectangular or smectic mesophases and that this behaviour was modulated by the alkyl-chain length. The role of the anion was crucial to obtain liquid-crystalline compounds, indeed, all the iodide precursors did not shown mesomorphism.

Thermal (DSC and POM analyses) and structural (XRD measurements) characterizations revealed that all compounds self-assembled in columnar rectangular phases in the first heating scan. On cooling (1st scan) instead, only **9V(NTf$_2$)$_2$** retained the columnar organization, while the others preferred a lamellar (smectic A) self-organization. Repetitive scans showed a well reproducible mesomorphism for all compounds. Notably, from the 2nd heating scan the columnar phase was definitely lost for **11V(NTf$_2$)$_2$** compound.

CHAPTER 5

Redox and spectroscopic properties of the thienoviologen mesogens

5.1. Introduction

The liquid-crystalline thienoviologens have been designed to be efficient electron-acceptor (*n*-type) functional materials for optoelectronic devices such as solar cells, electrochromic devices and light-emitting electrochemical cells. Self-assembling nanostructured molecular materials consisting of ionic and π-conjugated units form anisotropic ion-conductive pathways showing enhanced transport properties of the electronic charge carriers [96, 150] too. Recently, Kato et al. [97, 98] have presented a new class of electroactive nanostructured liquid crystals combining ionic and electronic moieties, demonstrating a reversible electrochromism in the smectic phase. We think that our compounds are very good *n*-type semiconducting liquid-crystals because their extended π-conjugation and their electron-acceptor character of viologen molecules. For this reasons we studied the redox properties in solution and in the liquid-crystalline phase. Because the redox properties in the solution phase are affected exclusively by the electroactive π-conjugated core of the molecules, herein we present the electrochemical and spectroelectrochemical properties for only one molecule 4,4'-(2,2'-bithiophene-5,5'-diyl)bis(1-decylpyridinium) triflimide 10V$(NTf_2)_2$, coupled by theoretical characterization performed at density functional theory (DFT) and time-dependent DFT levels of theory [151]. In addition, the electroactivity in the bulk states of the mesogens was studied either in the smectic phase or in the columnar phase. Because their semiconducting ordered materials nature, electronic conduction was also observed in the paramorphic solid phases of these materials that showed reversible and fast electrochromic responses. To our knowledge it is the first time that electrochromism is observed in the columnar

phases and in the paramorphic solid phases obtained on cooling from the corresponding mesophases.

5.2. Experimental and theoretical details

5.2.1. Materials

The thienoviologen compounds were synthesized as described in Chapter 4. Propylene carbonate (PC) was purchased from Sigma-Aldrich and was used after removing water by molecular sieves. Tetra-*n*-butylammonium perchlorate, TBAP (Fluka Chemika) was used as electrolyte without further purification.

5.2.2. Methods

Redox and spectroelectrochemical properties in solution phase.

The electrochemical behavior of the thienoviologen (1 mM) was studied by cyclic voltammetry (CV) experiments in a degassed electrolyte solution PC/0.1 M TBAP. The measurements were done at a platinum working electrode in a three-electrode cell, using a platinum auxiliary electrode, an Ag/AgCl reference electrode and a potentiostat configuration from AMEL s.r.l. (Mod. 7050). All the potentials were calibrated against the Fc/Fc^+ redox couple. Scan speed was 30 mV/s.

Spectroelectrochemistry was conducted as desribed in Chapter 2. The reference electrode was calibrated against the Fc/Fc^+ redox couple. The spectroelectrochemical cell was filled with a solution containing the thienoviologen (1 mM) in PC/0.1 M TBAP.

Electrochemical and spectroscopic measurements in the bulk phases.

To measure the transmittance through the liquid crystal cell we used the home-made optical line depicted in Scheme 5.1.

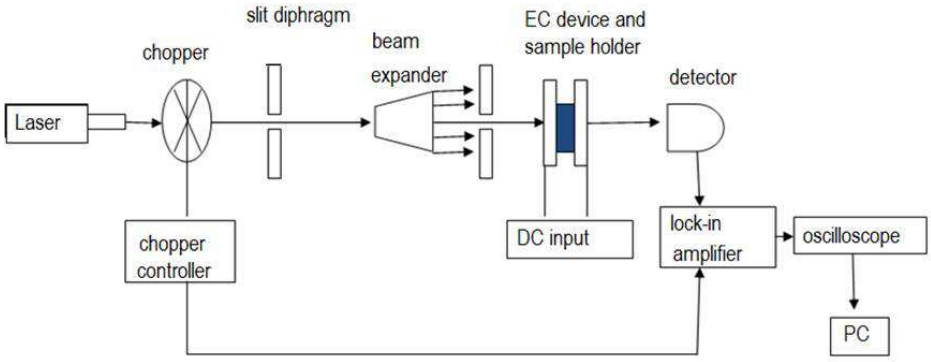

Scheme 5.1. Scheme of the optical line used for transmittance measurement

The beam of bright light emerging from a He-Ne laser (Melles Griot 05 LHR 106, wavelength 632.8 nm) passes through a chopper, whose rotation frequency controls the reference signal of the lock-in. The light leaves the chopper through a slit which avoids any reflection. The presence of a beam-expander, increasing the size of the beam, and a slit, reducing the size of the beam, produces a perfectly collimated beam of light, which reaches the liquid crystal cell located within a hot stage (Linkam LTS350 stage, TP94 System Controller). The light leaving the sample impinges on a photodiode (detector) that collects light and converts it into an electrical signal. The signal is then directed to a lock-in amplifier, sent to a reader, digital oscilloscope (Hewlett Packard 546001), and recorded on a PC. The software for recording and processing the optical data has been home made.

The measurements were carried out under atmospheric conditions. The liquid crystal cells comprised two glass plates coated with indium tin oxide (ITO) (the area of the electrode was 4 mm × 4 mm). The thickness of the cell was set at 5 μm by means of glass-spheres. The liquid crystals were capillary-filled into the cells in the isotropic states. The air dissolved in the liquid crystals was purged with argon in the isotropic state using a vacuum pump before the measurements. The transmittance curves were detected under application of potential steps modulated by the function generator (Amel 568 model programmable function generator). The transmittance was determined as the ratio of the intensity of the

transmitted light through the liquid crystal cell during the measurement to the intensity before the potential application.

The absorption spectra of the liquid-crystals films were recorded by an Horiba VS-140 spectrometer using a Linos LQX 1000 xenon fiber light source working in the 400-800 nm range. In order to keep the material phase under control, spectra were acquired with the liquid crystalline cell placed inside the Linkam hot stage. The incident light was propagated onto the sample by means of semirigid light guides placed above the Linkam viewing window and the transmitted light was detected by an optical fiber detector placed at the opposite side of the viewing window.

5.2.3. Computational details

All the calculations have been carried out using GAUSSIAN 03 code at density functional theory level [152]. The non-empirical PBE0 hybrid functional [121,122] has been adopted to perform geometry optimizations, in gas phase and in solvent, without symmetry constraints in combination with 6-31G′ basis set for all atoms. The computational effort has been reduced replacing the $–(CH_2)_9CH_3$ groups with less demanding ethyl groups. This substitution does not affect the spectral properties that are essentially due to the aromatic core [117,129]. In order to confirm proper convergence to equilibrium, vibrational frequency analysis has been done on the basis of analytical second derivatives of the Hamiltonian at the same level of theory. The di-cation species has been found to be more stable in a singlet spin state and has been treated with the restricted Kohn–Sham (RKS) formalism, while for the open-shell systems (cation species), unrestricted Kohn–Sham (UKS) calculations have been performed. No spin contamination has been found for the open shell system being the hS2i value equal to 0.77. The lowest 20 vertical excitation energies have been calculated by time-dependent density functional linear response theory (TDDFT) [125,126,131] on the PBE0/6-31G′ optimized geometries. Solvent effects on geometries optimizations and excitation energies, due to electrostatic interaction in polar solvent, have been introduced in the framework of the conductor-like approach (C-PCM) [153,154]. This approach provides results very close to those obtained by the original dielectric model for

high dielectric-constant solvents, but it is less prone to numerical errors arising from the small part of the solute electron cloud lying outside the cavity (escaped charge effects). Solvent shifts of excitation bands were evaluated by a recent nonequilibrium implementation [155] of the polarizable continuum model by using gas-phase structures.

5.3. Results and discussion

5.3.1. Redox and spectroelectrochemical properties in solution state

When a potential is applied to $10V(NTf_2)_2$, it can undergo reversible two-stage one electron reduction, with the formation of the stable radical cation and the neutral species or one stage two-electron reduction, with the consequent formation of only the corresponding neutral species. In general, it is not trial to decide a priori what kind of reduction reaction can occur, since some viologens undergo the first process while others the second one [61,62]. These two possible electrochemical behaviors depend on the value of the reduction potential as well as on the experimental conditions. It was previously noted that both the processes can occur without conformational changes during the redox process [61]. Cyclic voltammetry (Fig. 5.1) reveals one anodic peak (Ea = -1.07 V vs Fc/Fc^+) and one cathodic peak (Ec = -1.23 V vs Fc/Fc^+). Differently from what is generally observed for the cyclic voltammograms of compounds containing pyridinium moieties directly connected, that exhibit two anodic peaks and two cathodic peaks [61,62], here we are in presence of a single step two electron reduction (or two very closely spaced one electron reductions). The occurrence of a two electron step has already been observed for other extended viologens, where two pyridinium moieties were linked by a phenylene framework [61,62]. The same references report two closely spaced single step reductions in the case of pyridinium moieties separated by one thiophene ring. In our thienoviologen compound the pyridinium groups are separated by two thiophene rings, so it seems quite reasonable that inserting another thiophene ring, that is to say, increasing the separation between the pyridinium groups, the electrochemical behavior becomes that observed in Fig. 5.1. An increased spatial separation (and

then a decreased interaction) between the pyridinium moieties seems to make unstable the thienoviologe monocation ($10V^{+\cdot}$**)** that can undergo a dismutation reaction and evolve to the more stable $10V^{2+}$ dication and the $10V^{0}$ neutral forms. Another fact to be remarked is that the behavior is not completely reversible, suggesting that the oxidized species, $10V^{2+}$, is more stable than the di-reduced one, $10V^{0}$.

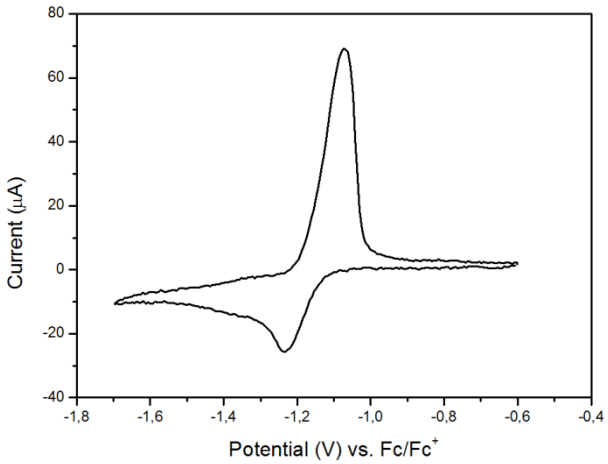

Fig. 5.1. Cyclic voltammogram of $10V(NTf_2)_2$ (1 mM) in PC containing 0.1 M TBAP. Scan rate = 30 mV/s.

Spectroelectrochemical experiments were used to evaluate the optical properties of $10V^{2+}$. As shown in Fig. 5.2, without applied potential (0.00 V) only a strong absorption band centered at 432 nm is present. After application of a potential (-1.20 V), resulting in the reduction of $10V^{2+}$, a new broadband centered at 662 nm appears whereas, the previous peak at 432 nm persists. During the electrochemical reduction the solution color changes from yellow to green. Increasing the applied voltage up to -1.60 V, the band at 662 nm grows in intensity and no significant absorption change in the visible spectrum is observed.

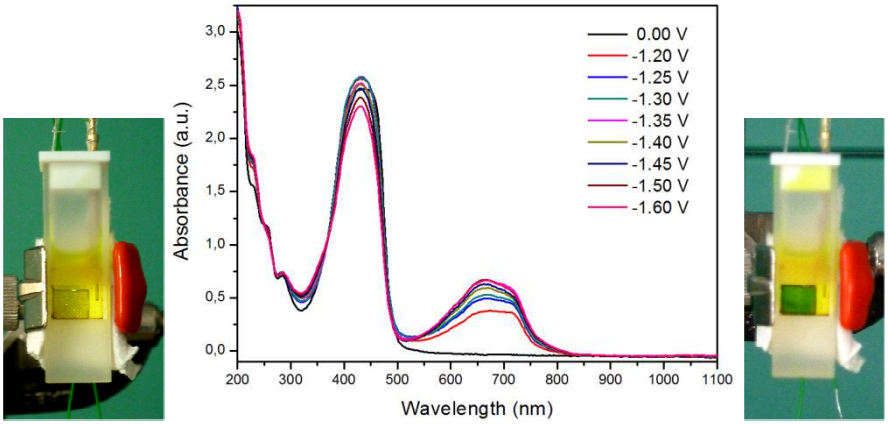

Fig. 5.2. Absorption spectra of $10V(NTf_2)_2$ (1 mM) in PC/ 0.1 M TBAP solution, from 0 V to -1.6 V vs Fc/Fc^+ and visual electrochromic response.

Going to high wavelength (from 900 to 1200 nm) no NIR absorption bands are registered. This spectral behavior is very similar even if we change the solvent (NMP, ε= 32.2). So, contrary to viologen and its derivate with a furan or monothiophene inter ring, we do not find NIR absorption peaks. In order to explain the observed experimental behavior we have undertaken a theoretical characterization of this system by using DFT and TDDFT previously employed for characterize similar systems [117]. As a first step of our work, we have fully optimized at DFT level the geometries of the three possible species in order to verify if significant conformational changes are induced by the redox processes. Starting from the optimized geometries, we have computed the excitation energies for the neutral and charged species. The results are reported in Table 1. From TDDFT computations the following spectral features are suggested: (i) the neutral species coming from a two-electron reduction should have a strong absorption maximum at 659 nm and with oscillator strength of 2.02 that is mainly due to an HOMO→ LUMO transition (71.8%). Two other peaks at 268 nm (f = 0.20) and at 208 nm (f = 0.15) are generated by transition from frontier orbitals to high energy unoccupied energy levels; (ii) the monocation radical show an HOMO→LUMOα transition (96.3%) at 1132 nm with an f value of 0.54 while the transition HOMO→LUMOβ (93.3%) generates an absorption band centered at 599 nm (f = 1.32); (iii) the dication shows a more complex behavior in the UV region but is mainly characterized by the presence of a HOMO→LUMO (70.6%) transition at 462 nm and with a large f value (1.73). Fig. 5.3 shows the energetic behavior of

the four Gouterman frontier orbitals and the HOMO and LUMO composition. It is worth to note that the HOMO–LUMO energy gap estimated from the onset position of the absorption spectrum of $10V^{2+}$ (2.53 eV) is in very good agreement with the time-dependent spectral simulation (2.68 eV). The agreement between the theoretical and experimental transition is quite good. In fact, the difference in the absorption maximum of the dication species is 30 nm (462 vs 432 nm), while for the neutral one is only 3 nm (659 vs 662 nm). On the basis of these considerations, the spectral behavior obtained in the presence of applied potentials can be assigned considering the presence of both the neutral and dication species. The absence in all the experimental spectra of the TDDFT predicted intervalence charge transfer (IV-CT) absorption band in the NIR region of $10V^{+\cdot}$ is probably due to the fast two-electron reduction as also indicated from the cyclic voltammogram.

Table 5.1. Computed vertical excitation energies, main configuration and oscillator strengths *f* for molecule $10V(NTf_2)_2$ in Propylene Carbonate (ε = 69.9).

	ΔE (eV, nm)	Main Configuration (%)	*F*	EXP
+2	2.68, 462	H→ L (70.6)	1.73	432
	4.65, 267	H-1 → L+1 (68.8)	0.12	
	4.96, 250	H-5 → L (62.2)	0.11	
	5.06, 245	H-2 →L+1(64.6)	0.13	
	5.81, 213	H-4 → L+1(43.0)	0.12	
+1	1.09, 1132	H-L α (96.3)	0.54	
	2.07, 599	H → L β (93.3)	1.32	
	4.62, 268	H-1 → L+1 (77.3)	0.10	
0	1.88, 659	H → L (71.8)	2.02	662
	4.63, 268	H-1 → L+3 (55.3)	0.20	
	5.95, 208	H → L+12 (63.1)	0.15	

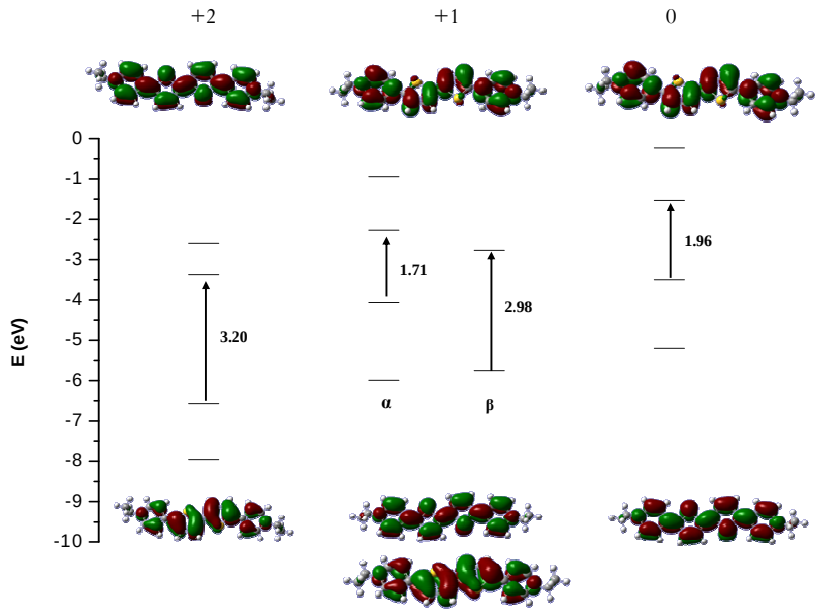

Fig. 5.3. Partial energetic diagram (eV) for the highest occupied and lowest virtual unoccupied molecular orbitals of molecule $10V(NTf_2)_2$ (neutral and cationic forms). The orbital compositions are reported for the most intense transitions.

5.3.2. Redox and spectroscopic properties in the bulk state

The redox behavior of the thienoviologen liquid crystals in the bulk states have been studied. The cell were filled by capillary action with the compounds in the isotropic state. When the samples were cooled in the columnar or Smectic A phases, the LC molecules spontaneously align parallel to the electrode surface. In those alignments, both the columns and the smectic layers were perpendicular to the electrode surfaces. The electric field was then applied in the direction of electronic and ion transport layers [97,98] (Fig.5.4).

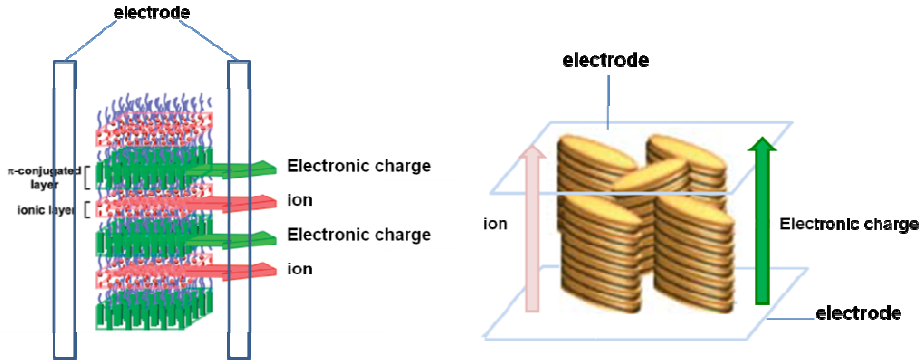

Fig. 5.4. Schematic illustration of a nanostructured smectic (a) and columanar (b) LC phase for the coupling of the ionic and electronic functions.

As described in Chapter 1, the frontier orbitals overlapping that characterizes the ordered semiconducting materials should lead to electronic bands having reasonable low Energy band gap (E_g) [156]. Indeed, the thin-film absorption spectrum of 9V$(NTf_2)_2$ in the columnar mesophase (Fig. 5.5) is broad and red-shifted with respect to the absorption spectrum in solution (Fig. 5.2).

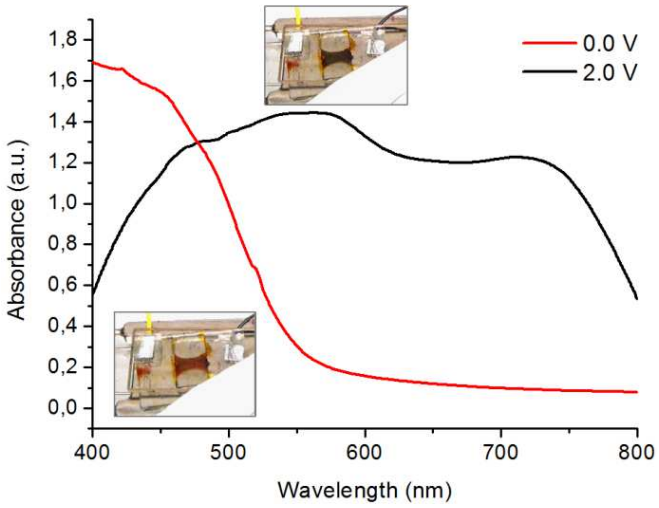

Fig 5.5. Absorption spectra of 9V$(NTf_2)_2$ in the Col_{ro} phase at 120 °C. The sample tickness is 5 μm.

When a DC voltage of about 2 V is applied to the cell, the color of the liquid crystal layers changed from red to dark and a wide band covering the entire visible region of the spectrum appeared (Fig. 5.5). The electron-acceptor nature of the thienoviologens suggests that the color change must be attributed to the formation of mono-reduced and bi-reduced species.

The response behavior was measured by monitoring the transmitted light intensity of a He-Ne laser (λ = 632.8 nm) through the samples as previously described (see Methods).

Semiconducting liquid crystals show an efficient electrochromic response in presence of both a good overlapping LUMOs orbitals of the large π-conjugated system, that allow a fast electronic (or holes) hopping via π–π interactions between sites [81,118], and an electrolyte solution [102]. The formation of an electrical double layer at the electrode surface due to the ions of the electrolyte prevent the electrode polarization that otherwise limits the electronic charge

injection. Electrolyte solution can be avoided if the semiconducting liquid crystals incorporate ionic groups [97,98], because an electrical double layer is rapidly generated by the fast moving counterions, under an electric field.

In our case the reduction process occurs because the electrons, injected from the cathode, flow through the highly delocalizated π-system of the molecules. This process is favored by the self-assembling of the molecules in columnar or smectic layers, perpendicular to the electrode surfaces (planar orientation). At the same time the triflimide anions migrate toward the anode.

Fig. 5.6 shows the responses of the transmittance for thienoviologen compounds in the columnar and smectic phase as a function of the application time of double-potential steps between 0 and 1.5 V. The electrochromic responses of the compounds in both mesophases are completely reversible even if appreciable difference can be observed comparing the kinetic curves of $9V(NTf_2)_2$ (Fig. 5.6a) with those of $11V(NTf_2)_2$ (Fig. 5.6 b).

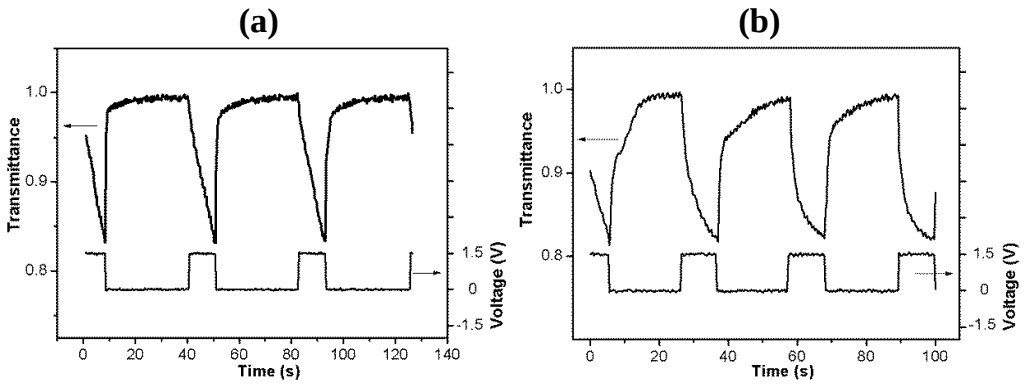

Fig. 5.6. Response of the transmittance of $9V(NTf_2)_2$ in the Col_{ro} phase at 120 °C (a) and of $11V(NTf_2)_2$ in the SmA phase at 145 °C (b) under the application of the double potential step sequences between 0 V (30 s) and 1.5 V (10 s). The sample thickness is 5 μm.

As reported in Table 5.2, similar coloration times (calculated as the time needed to achieve 90% of the maximum transmittance change) of about 8-9 s were observed for both the phases. The bleaching times instead, are very different and reveal the different way in which the electronic transport occurs in the two phases. Indeed, as largely reported in literature, in the smectic phase the extent of

frontier orbital overlap is lower [73] with respected to that occurring in the columnar phase where orientational ordered parameters are larger [76].

Table 5.2. Transmittance change (Δ%T) and switching times for the liquid crystalline phases.

Compound	T (°C)	Phase	Operating voltage (V)	Δ%T	τ_c (s)	τ_b (s)
$9V(NTf_2)_2$	120	$Col_{ro\ 1}$	1.5	15	8	3
	80	$Col_{ro\ 2}$	2.5	10	8	20
$11V(NTf_2)_2$	145	SmA	1.5	18	9	14
	80	Freezed SmA	2.5	8	9	25

τ_c = coloration time, τ_b = bleaching time, Col_{ro} = Columnar rectangular order phase; SmA = Smectic A phase

We have also demonstrated that the thienoviologens exhibited an electrochromic response in more viscous ordered phase formed on cooling (paramorphosis). In amorphous solid state of organic semiconductor organized on cooling from highly ordered smectic phase Vlachos et al. [157] measured the same high carrier mobilities of those in liquid crystalline phase. Similarly, we observed the electrochromism and thus electronic conduction, down to room temperature in the columnar ordered and freezed smectic A phases. The kinetic curves of the thienoviologen compounds at 80 °C in the columnar and freezed smectic A phases are reported in Fig. 5.7 a and b, respectively. It is possible to observe clearly that also in this conditions, the bleaching process and thus the electronic conduction in the smectic phase is slower than that in the columnar.

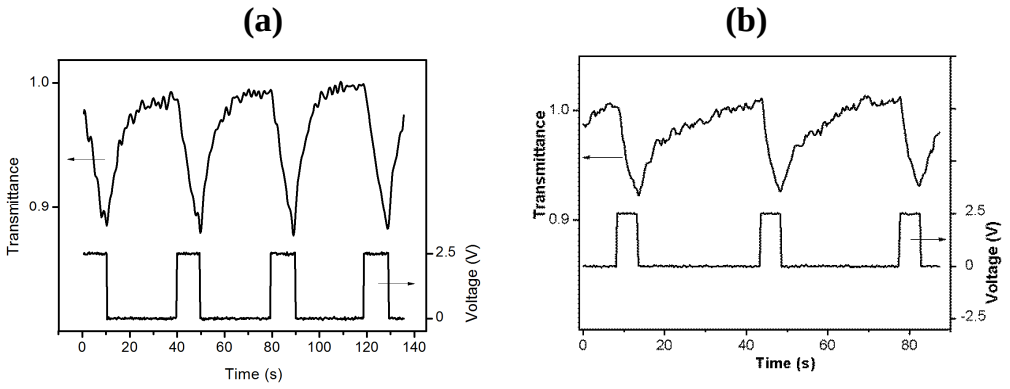

Fig. 5.7. Response of the transmittance of $9V(NTf_2)_2$ (a) and $11V(NTf_2)_2$ (b) at 80 °C in the paramorphic phase under the application of the double potential step sequences between 0 V (30 s) and 2.5 V (10 s). The sample thickness is 5 μm.

5.4. Conclusions

The study of the redox properties in solution of the new synthesized thienoviologen mesogens showed that these molecules, undergo a one-step two-electron reduction. It is possible that the generated mono-cation radical species has a very short lifetime, and gets converted to the more stable dication and neutral forms.

Moreover, an efficient electrochromic response was observed in the liquid-crystalline phase of these compounds. The electrochemical reduction caused the switch of the colour of the thin film materials from red to dark. The shorter response times for the bleaching process observed in the columnar phase with respect to the smectic one, should reflect a larger overlap between the frontier molecular orbitals in the columnar phase.

CHAPTER 6

Novel electrochromic plastic film containing a thienoviologen derivative

6.1. Introduction

Viologens are a class of electrochromic (EC) molecules largely used as coloring cathodic materials in device such as electronic papers [58,59], smart windows and displays [26,29,30, 34-37,51,57]. In chapter 5, the redox properties in the solution state of the thienoviologen were studied, revealing an interesting electrochromic response in the visible region. The EC solution switched from yellow to green when a moderate potential (~ 1.2 V) is applied. These results indicate that this molecule is a potent candidate for application in EC displays. It was demonstrated that a desirable electrochromic device (ECD) should be complementary [159], which means that a device composed of one anodic and one cathodic coloring material undergoes a simultaneous coloring or bleaching process. A complementary device offers the benefit of increasing the coloration efficiency to enhance the colored/bleached contrast and also to promote cycling stability by preventing undesirable side reactions between the electrolyte and counter electrode [160]. For this reasons we have prepared a new complementary EC system composed of the thienoviologen as cathodic material and ferrocene (Fc) as anodic molecule both dissolved in a thermoplastic polymeric matrix (Scheme 6.1). The performance of the ECD were investigated by cyclic voltammetry, UV-vis-NIR spectroscopy and EC switching studies.

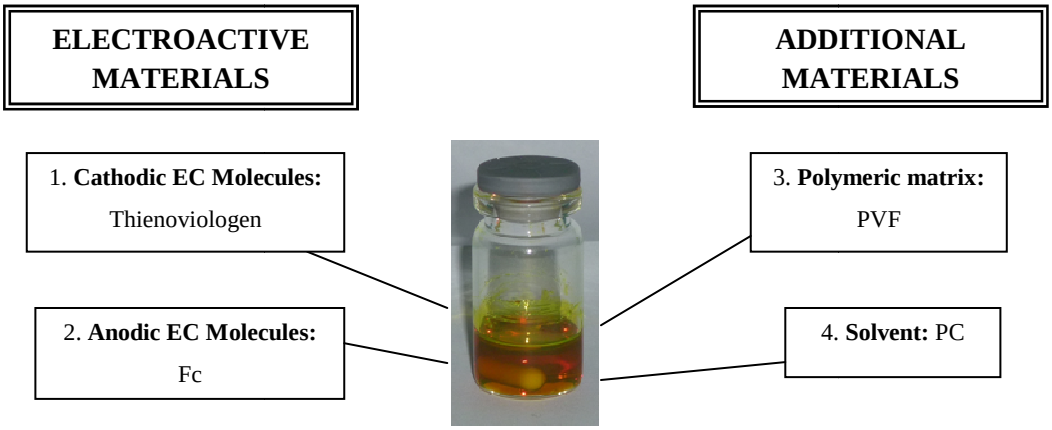

Scheme 6.1.

6.2. Experimental

6.2.1. Materials

The thienoviologen compound $10V(NTf_2)_2$ was synthesized as previously described in Chapter 3. Ferrocene was purchased from Sigma-Aldrich and used without further purification. Propylene carbonate (PC) was purchased from Sigma-Aldrich and was used after removing water by molecular sieves. Tetra-*n*-butylammonium perchlorate, TBAP (Fluka Chemika) was used as an electrolyte without further purification. Poly (vinyl formal), PVF given from Sigma-Aldrich was used as a thermolplastic polymer for the EC films.

6.2.2. Methods

The EC mixtures composed of PVF (35 wt %), of thienoviologen (2 wt %), of Ferrocene (0.8 wt %), TBAP (2.5 wt %) and PC (59.7 wt %) was warmed to a temperature of 150 °C for about 1 hour.

The EC cell was assembled by drop casting of the hot EC mixture sandwiched between two parallel ITO-coated glass support (supplied by Visiontek Systems Ltd. with a sheet resistance of 27 ohm/sq and a thickness of 1 mm) creating an active area of 2 x 2 cm^2. The thickness was set at 60 µm by a plastic spacer. Finally, the device was sealed with an epoxy resin.

Cyclic voltammetry was performed on the EC cell with an Amel Instruments 7050 model potentiostat. UV-Vis-NIR spectra were recorded with a Thermo Scientific GENESYS 10S UV-Vis spectrophotometer. Electrochromic Switching Studies were performed with a Jasco V-550 UV-Vis spectrophotometer. In our experimental setup the cells were powered by two electrodes fixed to the opposite extremes of the cell. The potential difference were supplied by means of an Amel 2049 model potentiostat and an Amel 568 model programmable function generator. Measurements were performed at 25 °C.

6.3. Results and discussion

6.3.1. Cyclic voltammetry

The electrochemical behavior of the EC plastic film was studied by cyclic voltammetry (CV) performed between -2.0 and +0.8 V. The cyclic voltammograms depicted in Fig. 6.1, shows clearly the oxidative and reductive character of the complementary system. The typical reversible anodic peak of Ferrocene appears at the half-wave potential ($E_{1/2}$) of 0.02 V while, the two reduction peaks at -1.21 (reversible) and at -1.42 V (irreversible) can be ascribable at the thienoviologen compound. The irreversibility of the second reduction peak could be due to the rapid evolution of the neutral species to the radical cationic. Despite the redox behavior observed in the solution phase (described in the Chapter 5) where a single step two electron reduction (or two very closely spaced one electron reductions) occurred, here, we are in presence of a two-stage one electron reduction of the thienoviologen. In addition, while in the solution experimental condition the more stable species were the neutral and di-cationic, in this semi-solid medium (plastic film) the stability of the mono-reduced species appears evident.

Although in the literature there are not similar studies that could help us in the comprehension of this phenomenon, we think that the high viscosity of the medium, and the presence of the anodic species can affect the electrochemical behavior of this viologen compound. In order to confirm the stability of the radical cationic thienoviologen in this system, we have performed spectroelectrochromic and kinetic studies.

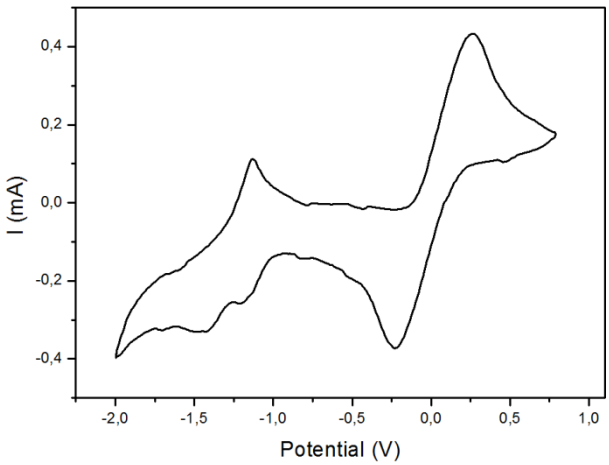

Fig. 6.1. Cyclic voltammogram of the EC plastic film in a two-electrodes cell. Scan rate 50 mV/s

6.3.2. Spectroelectrochromic behavior

The electronic spectra of the film sandwicted in a two-electrode cell under increasing applied voltages and its coloration change were reported in Fig. 6.2. From 0 V up to 1.0 V the film is yellow and only a strong absorption band (λ_{onset} = 530 nm) due to π-π^* transition of the thienoviologen dication appears in the spectrum. As a potential of 1.10 V is applied it is possible to observe a weak band centered at 725 nm due to the radical cation thienoviologen. Increasing the voltages up to 1.25 V this band grow in intensity and a new band at 644 nm appears. According to the cyclic voltammogram 1.25 V is the onset of the second reduction peak, so the band at 644 nm is due to neutral species. At higher voltages only one broad band with its maximum at 664 nm is present. Probably beacause the great stability of the mono-reduct product, under this wide band there are the band either of the neutral or the radical cationic species.

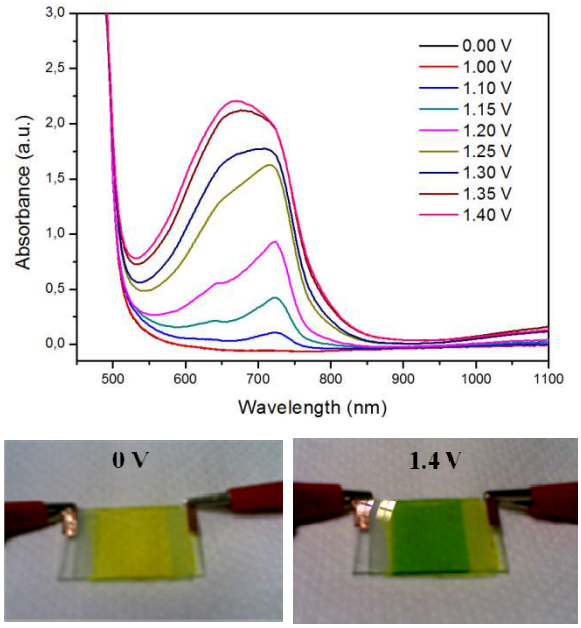

Fig. 6.2. Electronic spectra of the film (top) and its electrochromic response in a two-electrode cell (bottom). The thickness of the film was 60 μm.

6.3.3. Electrochromic switching studies

The switching kinetics of the ECD were calculated by chronoabsorptometry at the two wavelengths of maximum absorption: 644 nm and 725 nm. Increasing potentials were applied at the device up to reach the maximum optical contrast (Δ%T) and the kinetic curves were reported in Fig. 6.3. Although at the two monitored wavelengths the device was transparent in the bleaching state (T_b > 90 %), the Δ%T values (see Table 6.1) was not as high as for others viologen-based ECDs [142,143,145].

Table 6.1 reported also the coloration times (τ_c) that were calculated as the time needed to achieve 90% of the maximum transmittance change (Δ%T) in a single switching cycle. The response times for the coloration at both wavelengths were around 8 s, while for the decoloration (τ_b) were approximately 24 - 28 s. Despite to other devices in which cathodic and anodic molecules are dispersed in polimeric matrix [145,158] no optical memory was observed.

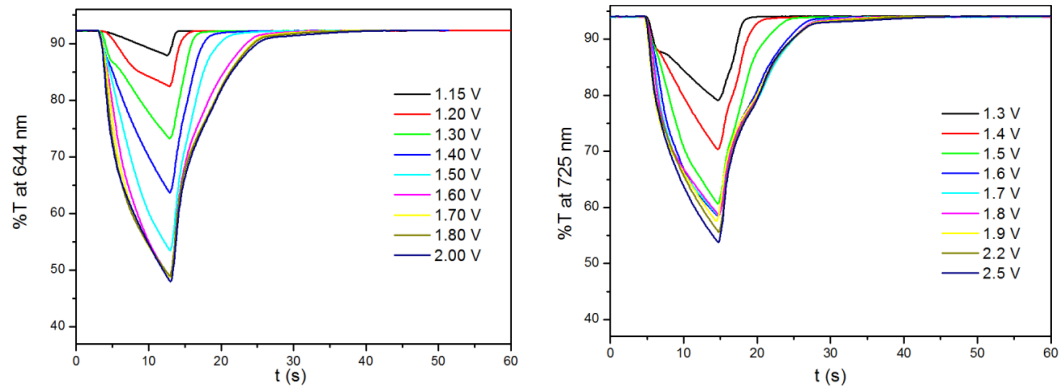

Fig. 6.3. Kinetic curves obtained by switching the ECD at different voltages and monitoring the %T at 644 nm and 725 nm.

The coloration efficiency CE values calculated for a 2 x 2 cm^2 ECD at the two wavelengths monitored were reported in Table 1. Although there are not thienoviologen-based ECD in the literature, this device exhibited a modest CE compared to those reported in the literature for viologen-containing EC device [145].

Table 6.1. Response times for the coloration (τ_c) and bleaching (τ_b) and CE of the EC film measured at 644 and 725 nm.

Wavelength (nm)	Operating Voltage (V)	Δ%T	τ_c (s)	τ_b (s)	CE (cm^2/C)
644	2.0	44.4	7.8	24.5	34.94
725	2.5	40.3	7.8	28.1	31.43

Another important parameter for the complete characterization of an ECD is its stability. The transmittance was monitored at 644 nm during repeated redox stepping experiments. In Fig. 6.4 has reported the attenuation of the optical contrast (Δ%T) of the device switched between 1.8 V (applied for 10 s) and 0 V with a delay time between two neighboring switches of 40 s for many consecutive operational cycles. It is possible to observe a considerable loss (~34%) of the contrast after 2000 switching cycles. During the next 4000 operational cycles, the EC system lost the 56.4% of the initial contrast that decreased to 18.3%. The Δ%T attenuation was monitored up to 10000th cycle, where its value was 16 %.

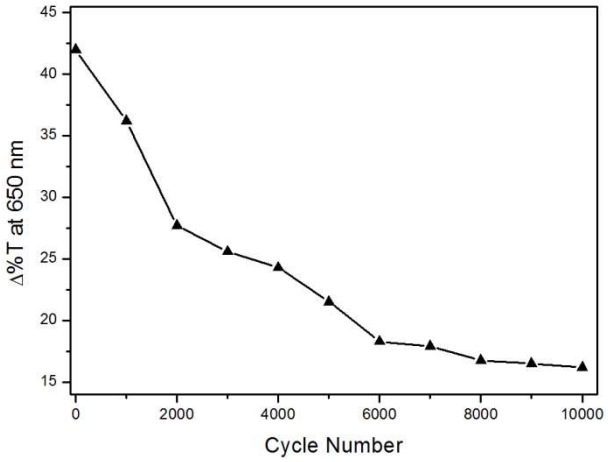

Fig. 6.4. Variation of the optical contrast (Δ%T) during 10000 switching cycles. Pulse amplitude: 1.8 V. Pulse length: 10 s. Waiting time between neighboring cycles: 40 s

6.4. Conclusions

We presented a new electrochromic plastic film based on a thienoviologen derivative as cathodic coloring material. The film showed a color switch from yellow to green. Despite the electrochemical studies in solution phase, here we observed by cyclic voltammetry and UV-vis spectroscopy the presence of the radical cationic species. This device has shown fast response times but moderate optical contrasts and coloration efficiency values in comparison with similar devices. The low redox stability is a considerable limit for its potential technological applications.

SUMMARY AND OUTLOOK

Two important classes of organic semiconductor materials for optoelectronics were prepared and fully characterized. Our attention was pointed to small molecular semiconductors because, compared with conjugated polymers, they offer several intrinsic advantages. Their monodisperse nature allows to improve a wide range of properties such as molecular functionality, rigidity, stacking, strong intermolecular (π–π) interactions, and most importantly well-defined structure and high purity [5].

First of all, we focused on materials able to absorb in the near-infrared (NIR) of the solar spectrum. Attenuation in the NIR is desirable since about one half of the total solar energy spectrum falls in this region. NIR Electrochromic devices could be useful for environmental control in buildings [20]. Materials based on triarylamine moieties seem to be very promising for NIR applications [16-22], because the intervalence charge transfer (IV-CT) absorption band produced by their radical cations [15]. Therefore, a new triarylamine derivative: *N*,*N*'-Bis(4-heptanoylamidophenyl)-*N*,*N*'-di(4-methoxyphenyl)-1,4-phenylendiamine (TPPAHM) was designed and synthesized. As reported in Chapter 2, compared to its analogous unsubstituted *N*,*N*,*N*',*N*'-Tetraphenyl-1,4-phenylendiamine (TPPA), the TPPAHM exhibited many advantages. Indeed, the incorporation of specific electron donating substituents at the *para* position of phenyl groups improved its electrochemical stability (preventing any coupling reaction), lowered the oxidation potentials, and red-shifted the NIR absorption, as demonstrated by cyclic voltammetry and spectroelectrochemistry.

To better understand the oxidation mechanism of triarylamine derivatives, the experimental investigation was supported with theoretical studied. DFT first principles computations revealed that the triarylamine radical cations have a delocalized intervalence (IV) state in which the unpaired electron is fully delocalized over the whole molecules. Consequently, the two oxidation processes

occur with the involvement of the delocalized HOMO orbital that releases an electron in the first ionization, while in the second, the electron is given by the SOMO orbital created in the first oxidation process. Before these results, in many previous publications [45,138-140] it was supposed that a two-steps one-electron oxidation occurred with the removal of the electrons from the two nitrogens. Thus, these results can open a new theory on the oxidation of the triarylamines with multiple redox centers.

Complementary electrochromic solution based on TPPAHM or TPPA as anodic molecules and ethyl viologen (EV^{2+}) as cathodic molecule, were characterized. The blue-coloration of the mono-reduced viologen with the strong absorption of the triarylamine radical cations, allowed to modulate a wide range of the solar radiation (Chapter 3). The electrochromic switching studies revealed that the redox stability of the EV^{2+}/TPPAHM system is better that those based on TPPA. Owing to its good solubility and high electrochemical stability, the EV^{2+}/TPPAHM system was mixed with a thermoplastic polymer by warming. The electrochromic gel prepared showed a fast coloration time to reach very good optical contrast and appreciable coloration efficiency compared with other similar viologen-based gel. No optical memory was observed in this device in which its colored state bleach rapidly upon removing the external bias because the electrochromes can freely diffuse and exchange electrons (self-erasing mechanism) [36, 44]. The gel was also sandwiched between two conductive plastic substrates and its electrochromic response indicate its potential applications in flexible electronics.

The other class of organic molecular semiconductor investigated was the extended viologen liquid crystals. Most of the liquid crystalline semiconductors studied up to now are of p-type [24], but new liquid crystals with electron-acceptor character have to be synthesized for optoelectronic device such as bulk heterojunction solar cells. With the aim to contribute significantly to this research field we designed and synthesized a new family of mesogens with a π-conjugated core composed of bi-thiophene group incorporated between two pyridium moieties. This molecules known as thienoviologens have shown a very interesting and unexpected mesomorphic behavior that was largely discussed in Chapter 4.

Despite their rod-like shape, these molecules self-assembled in columnar mesophases other than the expected lamellar (smectic A) one. Interestingly, this behavior was modulated by the alkyl-chain length (9, 10, 11, carbon atoms). Moreover, the role of the anion was crucial to disclose the liquid crystalline nature of the thienoviologens dications. Indeed, all the iodide precursors did not shown mesomorphism.

The electron-acceptor character of these compounds, extensively studied in solution phase, combined to their liquid crystalline properties, led to excellent n-type semiconducting properties in the bulk phases (Chapter 5). The solution-phase cyclic voltammetry revealed for these compounds a single step two-electron reduction, due to a large spatial separation (and then a weak interaction) between the two redox centres (nitrogens of pyridium units).

The spectroelectrochemistry showed the electrochromic behavior of these compounds. The agreement of the experimental electronic spectra with those simulated confirmed the instability of the mono-reduced species that probably evolved to the more stable dication and the neutral forms upon a dismutation reaction.

The redox behavior in the liquid crystalline bulk state was also investigated. An efficient electrochromic response was observed either in the columnar or in the smectic phases. The electrochemical reduction caused a colour switch of the thin film from red to dark. The bleaching process in the columnar phase was faster than in the smectic, because the electronic transport is favored in the columnar phase.

As reported in Chapter 6, the electrochromic behavior of the thienoviologen was also tested in a thermoplastic polymer matrix in which it was dispersed with a counter electrode (ferrocene). In contrast to the solution-phase electrochemical studies, here we were able to detect the presence of the radical cationic species by cyclic voltammetry and UV-vis spectroscopy. This device has shown fast response times but moderate optical contrasts and coloration efficiency values in comparison with similar devices.

Finally, thienoviologens are well-known for their high fluorescence quantum yield in solution [62,65]. Thus, the combination of fluorescence and

supramolecular organization within high ordered mesophases is of fundamental interest for application such as OLEDs [166]. Preliminary studies (here not reported), revealed fluorescence quantum yields in solution (dichloromethane) for our compounds of ~ 60%, completely in agreement with the literature data obtained for similar thienoviologens [62,65]. Photophysical measurements were done also on the thin liquid-crystalline films. High quantum yields were also observed in the bulk phases of this materials. Moreover, the fluorescence intensity was shown to be modulated either in intensity or in frequency by the application of a dc voltage. This phenomenon that to our knowledge is new, was called "Electric Field Enhanced Fluorescence". Interestingly, we have observed that the kinetic behavior of the fluorescence and electrochromic response are very similar, indicating that both phenomena depends by the same electrochemical reduced species.

Finally, the fast response times for the emission and the quenching of the fluorescence observed upon double potential steps sequence, indicate a very easily fluorescence modulation in these multifunctional materials that can be used as active components in optical modulators.

REFERENCES

[1] C. K. Chiang et al., Phys. Rev. Lett. 39 (1977) 1098.

[2] H. Dong et al., Chem. Soc. Rev. 41 (2012) 1754.

[3] R.S Forrest, M.E. Thomson, Chem. Rev. 107 (2007) 923.

[4] H. Dong, C. Wang, W. Hu, Chem. Commun. 46 (2010) 5211.

[5] A. Mishra, P. Bäuerle, Angew. Chem. Int. Ed. 51 (2012) 2020.

[6] Y. Shirota, J. Mater. Chem. 15 (2005) 75.

[7] Y. Song et al., J. Am. Chem. Soc. 128 (2006) 15940.

[8] A.Mishra, M. K. R. Fischer, P. Bäuerle, Angew. Chem. Int. Ed. 48 (2009) 2474.

[9] J. Roncali, P. Leriche and A. Cravino, Adv. Mater. 19 (2007) 2045.

[10] Z. Ning, H. Tian, Chem. Comm. (2009) 5483.

[11] C. Lambert, G. Nö1l, Angew. Chem. Int. Ed. 37 (1998) 2107.

[12] C. Lambert, G. Nö1l, J. Am. Soc. Chem. 121 (1999) 8434.

[13] V. Coropceanu, M. Malagoli, J.M. André, J. L. Brédas, J. Am. Soc. Chem. 124 (2002) 10519

[14] V. Coropceanu, C. Lambert b, G. Nö1l, J.L. Brédas, Chem. Phys. Lett. 373 (2003) 153

[15] A.V. Szeghalmi et al., J. Am. Chem. Soc. 126 (2004) 7834.

[16] S.J. Yeh, et al., Electrochem. Comm. 5 (2003) 373.

[17] K.Y. Chiu, et al., J. Electroanal. Chem. 578 (2005) 283.

[18] G.S. Liou, S.H. Hsiao, M. Ishida, M. Kakimoto, Y. Imai, J Polym Sci Part A: Polym Chem 40 (2002) 2810.

[19] G.S. Liou, Y.K. Fang, Dyes and Pigments 74 (2007) 273.

[20] H.J. Yen, G.S. Liou, Chem. Mater. 21 (2009) 4062.

[21] H.J. Yen, H.Y. Lin, G.-S. Liou, Chem. Mater. 23 (2011) 1874.

[22] H.J. Yen, K.Y. Lin, G.-S. Liou. J. Mater. Chem. 21 (2011) 6230.

[23] C. J. Brabec, N. S. Sariciftci, and J. C. Hummelen, Adv. Funct. Mater. 11 (2001) 15.

[24] Y. Shimizu, K. Oikawa, K. Nakayamac, D. Guillon, J. Mater. Chem. 17 (2007) 4223.

[25] W. Pisula et al., Macromol. Rapid Commun. 30 (2009) 1179.

[26] P. M. S. Monk, R. J. Mortimer, D. R. Rosseinsky, Electrochromism and Electrochromic Devices, Cambridge University Press, Cambridge, UK, 2007.

[27] J.R. Platt, J. Chem. Phys. 34 (1961) 862.

[28] S.K. Deb, Appl.Opt.8 (1969) 192.
[29] R. J. Mortimer, A. L. Dyer, J. R. Reynolds, Dispaly 27 (2006) 2.
[30] P.M.S. Monk, R.J. Mortimer, D.R. Rosseinsky, Electrochromism: Fundamentals and Applications, VCH, Weinheim, 1995.
[31] C.G. Granqvist, Handbook of Inorganic Electrochromic Materials, Elsevier, Amsterdam, 1995.
[32] M. Green, Chem. Ind. (1996) 641
[33] N. Leventis,, ninth ed. Electrochromic Devices, in McGraw-Hill Encyclopedia of Science and Technology, 6, McGraw-Hill, New York, 2002. pp. 254–257.
[34] R.J. Mortimer, Chem. Soc. Rev. 26 (1997) 147.
[35] R.J. Mortimer, Electrochim. Acta 44 (1999) 2971.
[36] D.R. Rosseinsky, R.J. Mortimer, Adv. Mater. 13 (2001) 783.
[37] N.M. Rowley, R.J. Mortimer, Sci. Prog. 85 (2002) 243.
[38] R.J. Mortimer, N.M. Rowley, Metal complexes as dyes for optical data storage and electrochromic materials in: J.A. McCleverty, T.J. Meyer, M.D. Ward (Eds.), Comprehensive Coordination Chemistry - II: From Biology to Nanotechnology 9.2, Elsevier, Oxford, 2004 pp. 581–619.
[39] R.D. Rauh, Electrochim. Acta 44 (1999) 3165.
[40] Z.C. Wu et al., Science 305 (2004) 1273.
[41] R.S. Berns, F.W. Billmeyer, M. Saltzman, M. Billmeyer, principles of color technology, 3rd ed.; Wiley: New York, 2000.
[42] G. Wyszecki, W.S. Stiles, Color Science; Wiley: New York, 1982.
[43] A.A. Argun et al., Chem. Mater,16 (2004) 4401.
[44] P. M. Beaujuge, J.R. Reynolds, Chem. Rev. 110 (2010) 268.
[45] T.D. Selby, K.Y. Kim, S.C. Blackstock, Chem. Mater. 14 (2002) 1685.
[46] Y. Liu, H. Ma, A. K.Y. Jen, Chem. Mater. 11 (1999) 27.
[47] H. Li et al., Chem. Mater. 14 (2002) 4484.
[48] E.W. Forsythe, M.A. Abkowitz, Y. Gao, J. Phys. Chem. B. 104 (2000) 3948.
[49] S.E. Bailey, J.I. Zink, S.F. Nelsen, J. Am. Chem. Soc. 125 (2003) 5939.
[50] M. Robin, P. Day, Adv. Inorg. Radiochem. 10 (1967) 247.
[51] P.M.S. Monk, N.M. Hodgkinson, R.D. Partridge, Dyes and Pigments 43 (1999) 241.
[52] F. Ito, T. Nagamura, J. Photochem. Photobiol. C. 8 (2007) 174.
[53] B. Han, et al., Top. Curr. Chem. 287 (2009) 181.
[54] S. Fukuzumi, Eur. J. Inorg. Chem. (2008) 1351.
[55] W. Sliwa, B. Bachowska, T. Girek, Curr. Org. Chem. 11 (2007) 497.

[56] BG. White, Trans. Faraday Soc. 65 (1969) 2000.
[57] P.M.S. Monk, The Viologens: Physicochemical Properties, Synthesis and Applications of the Salts of 4,4' Bipyridine; John Wiley & Sons: New York, 1998.
[58] D. Cummins, et al., J. Phys. Chem. B 104 (2000) 11449.
[59] M. Grätzel, Nature 409 (2001) 575.
[60] S. Durben,. T. Baumgartner, Angew. Chem. Int. Ed. 50 (2011) 7948.
[61] W. W. Porter III, T. P. Vaid, A. L. Rheingold, J. Am. Chem. Soc. 127 (2005) 16559.
[62] K. Takahashi, et al., J. Chem. Soc. Chem. Commun. (1992), 62
[63] C. J. Kelley, et al., Heterocycl. Chem. 38 (2001) 11.
[64] M. Valasek, et al., J. Org. Chem. 70 (2005) 405.
[65] R. Nakajima, H. Iida, T. Hara, Bull. Chem. Soc. Jpn. 63 (1990) 636.
[66] W.M. Albers, G.W. Canters, J. Reedijk, Tetrahedron 51 (1995) 3895.
[67] J.W. Happ, J.A. Ferguson, D.G. Whitten, J. Org. Chem. 37 (1972) 1485.
[68] T. S. Arrhenius, et al., Proc. Natl. Acad. Sci. U.S.A. 83 (1986) 5355.
[69] M. Nanasawa, M. Miwa, M. Hirai, T. Kuwabara, J. Org. Chem. 65 (2000) 593.
[70] S. Hunig and H. Berneth, Top. Curr. Chern. 92 (1980) 1.
[71] W. M. Albers et al., Bioelectrochemistry and Bioenergetics 42 (1997) 25.
[72] J. Tant, et al., J. Phys. Chem. B 109 (2005) 20315.
[73] S. Sergeyev, W. Pisula, Y. H. Geerts, Chem. Soc. Rev. 36 (2007) 1902.
[74] V. de Cupere, Langmuir 22 (2006) 7798.
[75] A. J. J. M. van Breemen, J. Am. Chem. Soc. 128 (2006) 2336.
[76] D. Demus, J. Goodby, G. W. Gray, H.-W. Spiess, V. Vill, ‘‘Handbook of Liquid Crystals’’, Wiley VCH, Weinheim 1998.
[77] G. W. Gray, J. W. G. Goodby, ‘‘Smectic Liquid Crystals- Textures and Structures’’, Leonard Hill, Glasgow 1984.
[78] J. Wu, W. Pisula, K. Müllen, Chem. Rev. 107 (2007) 718.
[79] Y. Shimizu, J. Mater. Chem. 17 (2007) 4223.
[80] Electronic Materials: the Oligomer Approach, ed. G. Wegner and K. Müllen, Wiley-VCH, Weinheim, 1998.
[81] M. O'Neill, S. Kelly, Adv. Mater. 23 (2011) 566.
[82] S. Laschat, et al. Angew. Chem. Int. Ed., 46 (2007) 4832.
[83] X. Crispin et al., J. Am. Chem. Soc. 126 (2004) 11889.
[84] J. Cornil, J.P. Calbert, J. L. Bredas, J. Am. Chem. Soc. 123 (2001) 1250.
[85] K. Kohary et al., Phys. Status Solidi B 241 (2004) 76.
[86] V. Lemaur et al., J. Am. Chem. Soc. 126 (2004) 3271.

[87] P. M. Borsenberger, L. Pautmeier, H. Bässler, J. Chem. Phys. 94 (1991) 5447
[88] V. Coropceanu et al., Chem. Rev. 107 (2007) 926 .
[89] (a) R.J. Kline, M.D. McGehee, Polym. Rev. 46 (2006) 27.
[90] H. Sirringhaus, Adv. Mater. 17 (2005) 2411.
[91] N. Tessler , Y. Preezant , N. Rappaport, Y. Roichman, Adv. Mater. 21 (2009) 2741 .
[92] J.F. Chang et al., Phys. Rev. B 76 (2007)
[93] R.A. Marcus, Rev. Mod. Phys. 65 (1993) 599.
[94] P.F. Barbara, T.J. Meyer, M.A. Ratner, J. Phys. Chem. 100 (1996) 13148.
[95] X. Feng et al., Nat. Mater. 8 (2009) 421.
[96] T. Kato et al., Angew. Chem. Int. Ed 45 (2006) 38.
[97] S. Yazaki, M. Funahashi, T. Kato J. Am. Chem. Soc. 130 (2008) 13206.
[98] S. Yazaki et al. J. Am. Chem. Soc. 132 (2010) 7702.
[99] H. Shimura et al., J. Am. Chem. Soc. 130 (2008) 1759.
[100] H. Shimura et al., Adv. Mater. 21 (2009) 1591.
[101] C.V. Hoven,. A. Garcia, G.C. Bazan, T. Q. Nguyen, Adv. Mater. 20 (2008**)** 3793.
[102] K. Tanabe, T. Yasuda, M. Yoshio, T. Kato, Org. Lett. 9 (2007) 4271.
[103] I. Aprahamian et al., Angew. Chem., Int. Ed. 46 (2007) 4675.
[104] H. C. Chang et al., J. Mater. Chem. 17 (2007) 4136.
[105] I. Tabushi, K. Yamamura, K. Kominami, J. Am. Chem. Soc. 108 (1986) 6409.
[106] S. Asaftei et al., J. Mater. Chem. 22 (2012) 14426.
[107] K. Yamamura, Tetrahedron Lett. 28 (1987) 6475.
[108] T. Hatazawa, R. H. Terrill, R. W. Murray, Anal. Chem. 68 (1996) 597.
[109] Y. Haramoto, et al., Liq. Cryst. 19 (1995) 319.
[110] P.K. Bhowmik, et al., Liq. Cryst., 30 (2003) 1433.
[111] P.K. Bhowmik, S. Han, I.K. Nedeltchev, J.J. Cebe, Mol. Cryst. Liq. Cryst., 419 (2004) 27.
[112] P.K. Bhowmik, H. Han, J.J. Cebe, I.K. Nedeltchev, Polymer Prepr. 43 (2002) 1385.
[113] K. Binnemans, Chem. Rev. 105 (2005) 4148.
[114] K.V. Axenov, S. Laschat, Materials 4 (2011) 206.
[115] V. Causin, G. Saielli, J. Mater. Chem. 19 (2009) 9153.
[116] P. H. J. Kouwer , T. M. Swager, J. Am. Chem. Soc. 129 (2007) 14042.
[117] B.C. De Simone et al., Theor. Chem. Acc. 131 (2012) 1215.
[118] M. O'Neill, S. Kelly, Adv. Mater. 15 (2003) 1135
[119] J. Cornil et al., Thin Solid Films 363 (2000) 72 .
[120] R. Ahlrichs, et al., Chem. Phys. Lett. 162 (1989) 165.

[121] M. Ernzerhof, G.E. Scuseria, J. Chem. Phys. 110 (1999) 5029
[122] C. Adamo, V. Barone, J. Chem. Phys. 110 (1999) 6158
[123] A. Schaefer, H. Horn, R. Ahlrichs, J. Chem. Phys. 97 **(**1992) 2571
[124] K. Eichkorn, F. Weigend, O. Treutler, R. Ahlrichs, Theor. Chem. Acc. 97 **(**1997) 119
[125] R. Bauersnschmitt, R. Ahlrichs, Chem. Phys. Lett. 256 (1996) 454.
[126] M.E. Casida (1995) In: Chong DP (ed) Recent advances in density functional methods Part I. Word Scientific, Singapore.
[127] A.D. Quartarolo, N. Russo N, E. Sicilia, Chem. Eur. J. 12 (2006) 6797.
[128] A.D. Quartarolo, E. Sicilia, N. Russo, J. Chem. Theory Comput. 5 (2009) 1849.
[129] A.D. Quartarolo, I. Lanzo, E. Sicilia, N. Russo, Phys. Chem. Chem. Phys. 11 (2009) 4586.
[130] I. Lanzo, A.D. Quartarolo, N. Russo, E. Sicilia, Photochem. Photobiol. Sci 8 (2009) 386.
[131] D. Jacquemin, B. Mennucci, C. Adamo, Phys. Chem. Chem. Phys. 13 (2011) 16987.
[132] A. Klamt, V. Jonas, J. Chem. Phys. 105 (1996) 9972.
[133] A. Klamt J. Phys. Chem. 100 (1996) 3349.
[134] M. Renz, K. Thellacker, C. Lambert, M. Kaupp, J. Am. Chem. Soc. 131 (2009) 16292.
[135] O. Yurchenko et al., J. Phys. Chem. B 116 (2012) 30.
[136] C. Lambert, G. Nöll, J. Am. Chem. Soc. 121 (1999) 8434.
[137] I. Seguy et al., J. Appl. Phys. 89 (2001) 5442.
[138] W.H. Chen, K.L. Wang, D.J. Liaw, K.R.Lee, J.Y. Lai, Macromolecules 43 (2010) 2236.
[139] J.V. Grazulevicius, P. Strohriegl, J. Pielichowski, K. Pielichowski, Prog Polym Sci 28 (2003) 1297.
[140] A. Ito, H. Ino, K. Tanaka, K. Kanemoto,T. Kato, Org. Chem. 67 (2002) 491.
[141] H.Y. Wu , et al., J. Polym. Sci Part A: Polym. Chem. 48 (2010) 3913.
[142] G. Chidichimo et al., Chem. Mater. 19 (2007) 353.
[143] G. Chidichimo et al., J. Phys. Chem. C 114 (2010) 16700.
[144] K.C. Ho, Y.W. Fang, Y.C. Hsu, L.C. Chen, Solid State Ionics 165 (2003) 279.
[145] C. Pozo-Gonzalo, et al., Sol. Energy Mater. Sol. Cells, 93 (2009) 2093.
[146] T. Komura, et al., Electrochim. Acta 46 (2001) 3579.
[147] K. Takahashi, Jpn. Patent 668277, Sony Corp, Japan, Pubbl. 23.03.1993.

[148] J. Hock, A.M.W. Cargill Thompson, J.A McCleverty, M.D. Ward, J. Chem. Soc., Dalton Trans. 22 (1996) 4257.
[149] I. Dierking, Textures of Liquid Crystals, 2003, Wiley-VCH Verlag, Weinheim.
[150] T. Kato, T. Yasuda, Y. Kamikawa, M. Yoshio, Chem. Commm. (2009) 729.
[151] M.E. Alberto et al., Chem. Phys. Lett. 552 (2012) 141.
[152] M.J. Frisch et al., GAUSSIAN 03, Revision B.04, Gaussian, Inc., Pittsburgh, PA, 2003.
[153] V. Barone, M. Cossi, J. Phys. Chem. A, 102 (1998) 1995.
[154] M. Cossi, N. Rega, G. Scalmani, V. Barone, J. Comput. Chem. 24 (2003) 669.
[155] M. Cossi, V. Barone, J. Chem. Phys. 115 (2001) 4708.
[156] J. Hanna, Opto-electron. Rev. 13 (2005) 259.
[157] P. Vlachos et al. Chem. Comm. (2005) 2921.
[158] N. Kobayashi, S. Miura, M. Nishimura, Y. Goh, Electrochim. Acta, 53 (2007) 1643.
[159] H. Hamada et al., Displays 4 (1983) 221.
[160] T.H. Kuo, C.Y. Hsu, K.M. Lee, K.C. Ho, Sol. Energy Mater. Sol. Cells, 93 (2009) 1755.
[161] M. Sommer, S.M. Lindner, M. Thelakkat, Adv. Funct. Mater. 17 (2007) 1493.
[162] E.T. Seo et al., J. Am. Chem. Soc. 88 (1966) 3498.
[163] W.H. Bruning, R.F. Nelson, L.S. Marcoux, R.N. Adams, J. Phys. Chem. 71 (1967) 3055.
[164] K. Choi, S.J. Yoo, Y.E. Sung, R. Zentel, Chem. Mater. 18 (2006) 5823.
[165] O. Yurchenko, J. Heinze S. Ludwigs, Chem. Phys. Chem. 11 (2010) 1637
[166] S.A. Bening et al. Liq. Cryst. 28 (2001) 1105.
[167] http://www.epapercentral.com/epaper-technologies-guide